Development of Sustainable Thermoplastic Elastomers

A Dissertation

Presented to the Faculty of

Department of Chemical & Biomolecular Engineering

University of Houston

In Partial Fulfillment

of the Requirements for the Degree

Doctor of Philosophy

in

Chemical Engineering

by

Shu Wang

May 2015

Development of Sustainable Thermoplastic Elastomers

_____
Shu Wang

Approved:

_____
Chair of the Committee
Megan L. Robertson, Assistant Professor,
Chemical & Biomolecular Engineering

Committee Members:

_____
Ramanan Krishnamoorti, Professor,
Chemical & Biomolecular Engineering

_____
Jacinta C. Conrad, Assistant Professor,
Chemical & Biomolecular Engineering

_____
Haleh Ardebili, Assistant Professor,
Mechanical Engineering

_____
Yan Yao, Assistant Professor,
Electrical & Computer Engineering

_____
Suresh K. Khator, Associate Dean,
Cullen College of Engineering

_____
Michael P. Harold, Professor and Chair,
Chemical & Biomolecular Engineering

Acknowledgements

I would like to thank my advisor, Prof. Megan L. Robertson for her guidance and encouragement during the course of this work. Her expertise and knowledge, as well as the spirit of hard working have greatly influenced me over the last five years. I truly appreciate her patience, enthusiasm and guidance.

I also thank Prof. Ramanan Krishnamoorti, Prof. Jacinta C. Conrad, Prof. Yan Yao and Prof. Haleh Ardebili for serving as my committee members. I appreciate their time and effort on my dissertation and defense. I would specially thank Dr. Krishnamoorti and Dr.Conrad, who have also been my committee members for my qualifying exam and proposal defense. Their excellent insights and beneficial discussion in this study have helped me a lot throughout the whole journey of my PhD study.

I would like to express my deep thanks to Dr. Charles Anderson, and Dr. Rigoberto Advincula for their assistance in experiments. I would also like to express my sincere appreciation to Sameer Vajjala Kesava and Prof. Enrique D. Gomez for their time and dedication to the TEM measurements, and Dr. Eric Cochran for the SAXS program which helped a lot in the morphology identification. I also want to acknowledge National Science Foundation for support of this research project.

I would also like to thank my former and current group members in our lab for their assistance and encouragement over the years: Avantika Singh, Vivek Yadav, Guozhen Yang, Brian Rohde, Kim Mai Le, Sheli Mauck, Wenyue Ding, and Tyler Cooksey. I am so grateful that I have had wonderful labmates and I cherish our friendship.

I would also like to express my deep appreciation to my friends in chemical engineering department: Yi Li, Kai He, Ye Li, Jinsu Kim, Chinedu Umeasiegbu, and

Rahul Pandey. We have spent a lot of wonderful time together and I wish we will continue to be good friends for the rest of my life.

Last but not the least, I would like to express my deepest appreciation to my family for their support and encouragement. I thank my parents, YuLin Wang and Mingqiong Yu, my brother, Wei Wang, my parents-in-law, Cuizhen Ma, and Shaowei Hong, as they have always been there for me. My deepest thanks go to my husband, Chuan Hong and my daughter, Gracie. I am so beloved to have them in my life.

Development of Sustainable Thermoplastic Elastomers

An Abstract

of a

Dissertation

Presented to the Faculty of

Department of Chemical & Biomolecular Engineering

University of Houston

In Partial Fulfillment

of the Requirements for the Degree

Doctor of Philosophy

in

Chemical Engineering

by

Shu Wang

May 2015

Abstract

Sustainable poly(styrene-*b*-(lauryl-*co*-stearyl acrylate)-*b*-styrene) (SAS) triblock copolymers containing a rubbery midblock derived from fatty acids were designed with targeted properties appropriate for thermoplastic elastomer applications. Well-defined polymers with desired compositions and controlled molecular weight distributions were successfully synthesized using reversible addition fragmentation chain transfer (RAFT) polymerization. SAS exhibited elastomeric behavior at room temperature and were processable above the order-disorder transition (ODT) temperature. The alkyl side-chain length of the polyacrylates (as well as the related midblock composition of SAS) was utilized as a convenient parameter for tuning the physical properties of SAS, including the melting temperature and viscosity of the midblock polyacrylate, melt viscosity of SAS above the ODT, and tensile properties.

The thermodynamic interactions between the components of SAS, polyacrylates and polystyrene, were explored through determination of the Flory-Huggins interaction parameter, χ, through cloud point measurements on binary polymer blends and measurement of the ODT of the triblock copolymers. It was shown that χ was independent of the length of the alkyl side-chain of the polyacrylates, in the limit of large alkyl side-chains (i.e., more than 10 carbon atoms), in stark contrast to theoretical predictions using group contribution methods and solubility parameter theory.

The morphology of SAS was probed by transmission electron microscopy, showing the presence of spherical polystyrene domains in the polyacrylate matrix, as well as small angle X-ray scattering, indicating the presence of randomly oriented grains upon compression molding. Large amplitude oscillatory shear was employed at a temperature

below ODT to align the randomly oriented grains. The predominant orientation was determined to be hexagonally close-packed spherical domains with the {0001} planes parallel to the shear plane, with a small population of face-centered cubic spherical domains with the $\{1\bar{1}0\}$ planes parallel to the shear plane.

Fully sustainable triblock copolymers with midblocks derived from fatty acids and endblocks derived from salicylic acid were also successfully synthesized with RAFT polymerization. The properties of the resulting poly(acetylsalicylic ethyl methacrylate-*b*-lauryl methacrylate-*b*-acetylsalicylic ethyl methacrylate) (ALA) triblock copolymers were examined for their utility as thermoplastic elastomers. Poly(acetylsalicylic ethyl methacrylate) was found to be a suitable replacement for polystyrene, with a glass transition temperature above room temperature. The morphology and mechanical properties of ALA were comparable to that observed in the partially sustainable SAS triblock copolymers.

Table of Contents

List of Figures

List of Tables

Chapter 1

Introduction

Polymers are macromolecules composed of many repeated units and are ubiquitous in every level of life, such as packaging, toys, clothing, rubber tires, cushions, insulation, fabrics, coatings, pressure sensitive adhesives, cosmetics, etc. [1]. Since the 20^{th} century, crude oil has been a vital source for a wide range of raw materials for the manufacturing of polymers. However, due to the awareness of the depletion of fossil sources and the environmental pollution such as global warming and acid rain from fossil manufacturing, there has been increasing desire to derive polymers from sustainable sources [2-5].

Sustainable sources, including plant oils [6, 7], plant sugars [8], terpenes [9], polysaccharides [10], rosins [11], and lignin [12] have been explored as the building materials for a variety of classes of polymeric materials, including thermoplastic elastomers [13, 14], thermoset resins [15], pressure sensitive adhesives [16, 17], brushes [18] and shape memory materials [19].

Vegetable oils and their fatty acids are a particularly attractive source, due to their low toxicity, biodegradability, availability, relatively low price, and ease of functionalization [7, 20, 21]. The carbon-carbon double bonds on the triglyceride structure are amenable to a variety of functionalization chemistries that can lead to subsequent polymerization. Vegetable oils are often epoxidized through a reaction with performic acid [22], or alternatively through a lipase-catalyzed process [23], resulting in the synthesis of epoxy resins [24]. Epoxidized vegetable oils have also been converted to polyols for polyurethanes [25]. Epoxidized oils can be acrylated through a ring-opening

reaction with acrylic acid, leading to polyacrylates [26]. Vegetable oils can be functionalized with cyclic structures, and then polymerized through ring-opening metathesis polymerization (ROMP) [27]. The carboxylic acid end-group of a fatty acid can be converted to a hydroxyl end-group [28, 29] and subsequently converted to an acrylate or methacrylate group [30], appropriate for radical polymerization techniques.

Of particular interest to this study is the derivation of sustainable thermoplastic elastomers (TPEs). Combining the processing advantages of thermoplastics with the flexibility and extensibility of elastomeric materials, TPEs have found versatile applications in industry, including electronics, clothing, adhesives, and automotive components [31]. One of the most common classes of TPEs is composed of linear ABA triblock copolymers. Styrene-based linear ABA triblock copolymers, such as poly(styrene-*b*-butadiene-*b*-styrene) (SBS) or poly(styrene-*b*-isoprene-*b*-styrene) (SIS), are among the most important and widely used TPEs. Based on the considerations of incompatibility and viscosity which affect both processibility and efficiency of phase separation in the melt, the molecular weight of the PS blocks is generally in the range of 10 to 15 kg/mol, and the PB or PI blocks have molecular weights from 50 to 70 kg/mol [31]. The PS volume fraction is about 20~30%, at which the equilibrium morphology of the SBS/SIS TPEs is PS spheres or cylinders dispersed in the rubbery PB or PI matrix. And the PB or PI mid-blocks form bridges connecting the spheres/cylinders. The resulting arrangement is physical crosslinking of the polymers (Figure 1.1). The PS domains prevent diffusion of the chains once the structure is formed. Chemically crosslinked polymers can not be recycled because the crosslinks connect all of the polymer chains together, making it impossible for the material to flow. In contrast,

crosslinks in TPEs are reversible. When the material is heated, the structure transforms to a disordered phase, allowing the material to be processed. As the triblock copolymer cools down, the microphase separated structure will be re-formed, and the elastomeric behavior is recovered.

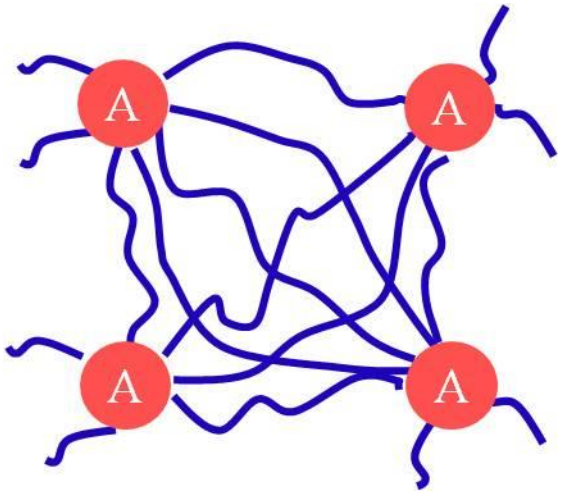

Figure 1.1: Phase structure of styrene based ABA TPEs. Spheres representing PS domains and red lines representing PB or PI matrix (Reproduced from Ref [31]).

SBS and SIS polymers have tensile strengths up to about 30 MPa and elongation at break of up to 800%, resembling vulcanized rubbers (Figure 1.2) [31].

A major drawback of SBS/SIS TPEs is the limited oxidative stability and UV resistance owing to the unsaturated carbon double bonds of the mid-block in the polymer [32, 33]. In order to overcome this shortage, several researchers used saturated poly(alkyl acrylate) as the mid-block to substitute polydiene. Although the mechanical properties were not comparable to styrenic TPEs, the stability and application as pressure-sensitive adhesives, which require softer matrix phases, were revealed to be enhanced [34, 35].

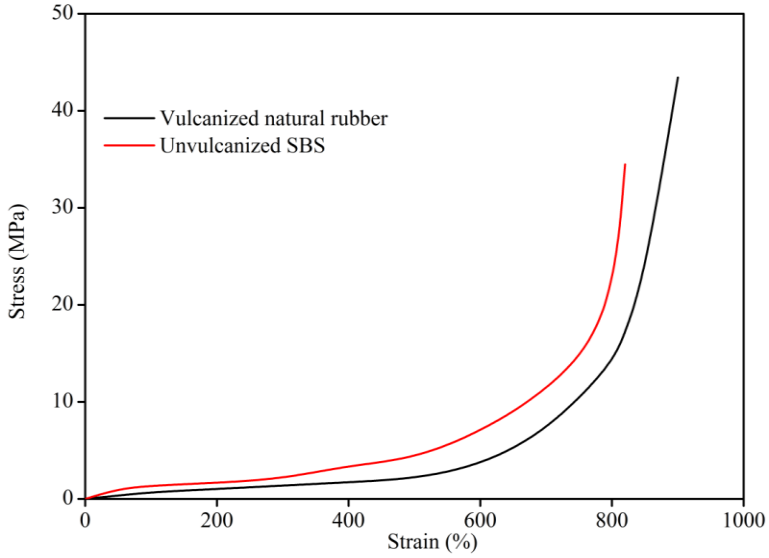

Figure 1.2: Stress-strain properties of TPEs (Reproduced from Ref. [31])

The main criteria in selecting building materials for ABA type TPEs are the glass transition temperatures of the two components and the incompatibility [31]. Block A must be a glassy/hard polymer at the usage temperature (usually room temperature) but amorphous and rubbery at higher temperatures (for processing the material) and block B must be an amorphous/rubbery polymer at both the usage and higher temperatures [31].

Polymers containing long acrylic and aliphatic side-chains or backbones with cyclobutyl, cyclopentyl or long alkyl groups, such as long chain *n*-alkyl (meth)acrylates [34] and decalactone [36, 37] derived from fatty acids, and menthide [38, 39] derived from essential oils. In this dissertation, polymers derived from fatty acids are examined as the soft midblock of these TPEs, offering a number of advantages including low glass transition temperatures [40-42] and long alkyl side chains which are highly hydrophobic and provide a greater resistance to degradation [43, 44].

There have been very few studies in literature regarding sustainable glassy endblocks for TPEs, including α-methylene-γ-butyrolactone (MBL) found in tulips [45,

46], lactide [38, 39, 47-49], rosin acid [14], and methacrylated vanillin [50]. In this dissertation, salicylic acid is explored as a source for the hard, glassy end-blocks of the TPEs. Salicylic acid is a signal chemical in plants and can be found in many fruits, vegetables and food product [51-53]. The hydroxyl and carboxylic acid groups on salicylic acid give access to functionalization to an acrylate (or methacrylate) group which is appropriate for radical polymerization [54]. The aromatic ring in the salicylic acid gives rigidity in the molecule and the resulting polymer is expected to have a high glass transition temperature which will be suitable as the hard endblock.

The application of triblock copolymers as TPEs requires careful control over their microstructure. Given that the phase behavior of triblock copolymers has been well-characterized [55-57], desired mechanical properties can be achieved by tuning the molecular composition and architecture. Though the effect of dispersity has been well documented [58-60], the most facile approach to achieving a desired microstructure in block copolymers is the implementation of controlled or living polymerization techniques to produce polymers with relatively narrow molecular weight distributions. Reversible addition-fragmentation chain transfer (RAFT) polymerization is a highly attractive candidate for polymerizing fatty acrylates, based on ease of implementation, tolerance to functional groups, mild conditions, and production of polymers with well controlled molecular weight distributions and architectures [61].

1.1. Block copolymers physics

Block copolymers (BCPs) consist of two or more chemically distinct polymer blocks which are linked by covalent bonds. BCPs are classified depending on the number and arrangement of the blocks. BCPs with two blocks are called diblock copolymers;

those with three blocks are triblock copolymers and those with more than three are multiblock copolymers. Based on how the blocks are arranged, they can be linear or star BCPs. Figure 1.3 presents the most common BCPs.

a) AAAAAA-BBBBB

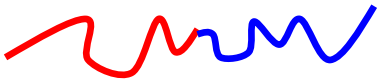

Linear AB diblock copolymer

b) AAAA-BBBB-CCCC

Liner ABC triblock copolymer (A and C could be same)

c) AAA-BBB-AAA-BBB-AAA

Linear ABABA multiblock copolymer

d) AAABBB-BBBAAA
BBBAAA

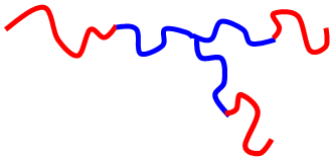

AB star block copolymer

Figure 1.3: Structures of common BCPs.

The thermodynamics of BCPs are described by the following parameters: the composition (overall volume fraction of each block) of the BCPs, the A-B segment-segment (Flory-Huggins) interaction parameter, χ, (or the related binary interaction energy density) and the overall degree of polymerization N [62]. For BCPs with incompatible A and B segments, the interaction parameter is positive and is generally proportional to 1/T. At equilibrium, BCPs will be arranged in configurations with minimum free energy. Increasing χ (or decreasing temperature) and N often leads to a reduction in A-B contacts. The individual blocks microphase separate to form separate

domains, given that macroscopic phase separation is prevented due to their covalent linkages.

The block copolymer phase diagram has been numerically determined using mean-field theory for diblock copolymers in weak, strong and intermediate segregation regime [63-65]. Later on, the theory was extended to symmetric triblock copolymers, asymmetric triblock copolymers and multiblock copolymers [66, 67]. Figure 1.4 presents the phase diagram for monodispersed symmetric ABA type triblock copolymer (N is the degree of polymerization of the diblock copolymers formed by snipping the triblock copolymers in half, f_A is the volume fraction of the endblocks A, and χ is the Flory-Huggins interaction parameter between segments A and B).

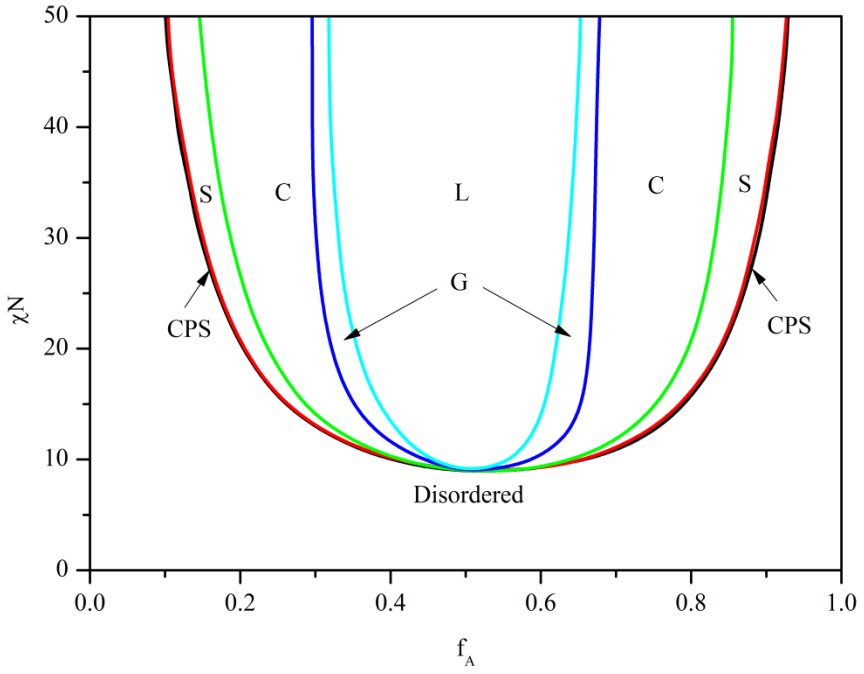

Figure 1.4: Phase diagram for symmetric ABA triblock copolymers. CPS: close packed spheres; S: body-centered cubic spheres; C: hexagonally packed cylinders; G: gyroid; L: lamellae. Plot modified from ref. [66, 67].

The idealized and most common morphologies for AB diblock copolymers and ABA symmetric triblock copolymers at equilibrium are shown in Figure 1.5 [59]. At very low A concentration, a spherical or cylindrical A phase disperses in a continuous B matrix. An alternating lamellae structure forms at about equal volume fractions. Further increasing A fraction results in a continuous A domain with cylindrical or spherical B phases dispersed.

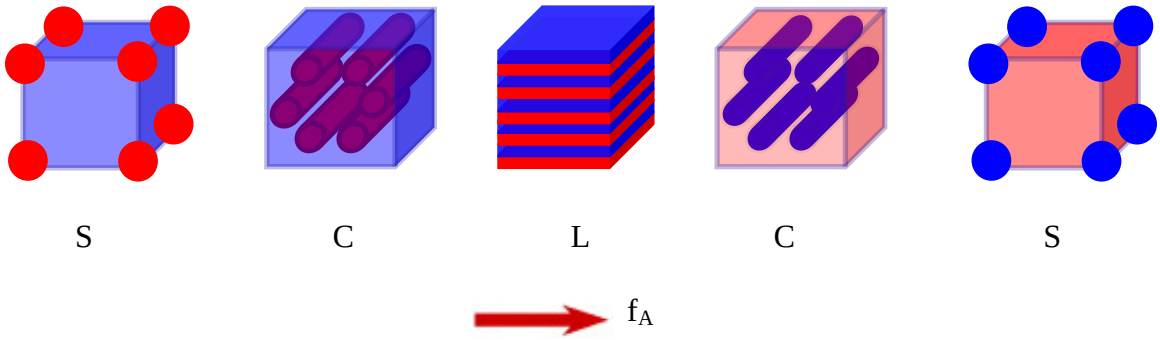

Figure 1.5: Morphology of ABA triblock copolymers at different compositions. (S) spheres, (C) hexagonally packed cylinders, (L) lamellae. The red and blue phases indicate A-rich and B-rich phases. Plot modified from ref. [59].

1.2. Flory-Huggins theory for binary polymer blends

The Flory-Huggins theory (FHT) for the free energy of mixing of two homopolymers A and B is given by

$$\frac{\Delta G_m}{kT} = \frac{\phi_A ln\phi_A}{v_{mon,A}N_{mon,A}} + \frac{\phi_B ln\phi_B}{v_{mon,B}N_{mon,B}} + \chi\frac{\phi_A\phi_B}{v_{ref}}, \qquad \text{(eq. 1.1)}$$

where ΔG_m is the free energy change on mixing per unit volume, k is the Boltzmann constant, T is the absolute temperature, ϕ_i is the volume fraction of each blend component (i=A or B), $v_{mon,i}$ is the volume of each monomer on chain i, v_{ref} is the reference volume (100 Å^3), $N_{mon,i}$ is the number of monomer repeat units in chain i, and χ is the Flory-Huggins interaction parameter [68, 69].

If we define

$$N_i = \frac{N_{mon,i} v_{mon,i}}{v_{ref}}, \quad \text{(eq. 1.2)}$$

and use weight-average degree of polymerization, N_w, as larger sized molecules will drive the phase separation of polymer blends, eq. 1.1 can be rewritten as

$$\frac{\Delta G_m v_{ref}}{kT} = \frac{\phi_A ln\phi_A}{N_{w,A}} + \frac{\phi_B ln\phi_B}{N_{w,B}} + \chi\phi_A\phi_B. \quad \text{(eq. 1.3)}$$

The first two terms in the right hand side of eq. 1.1 describe the contribution of the change in the combinatorial entropy upon mixing and the third term represents the enthalpic contribution. The interaction parameter χ defined in eq. 1.1 is dependent on the chemical microstructure and temperature, and the degree of polymerization and blend composition should not affect χ [68, 69]. However, studies have observed the dependence of χ on blend composition [70], chain architecture [71] and degree of polymerization [72].

χ obtained from binary blends is often linear function of 1/T,

$$\chi = \frac{A}{T} + B. \quad \text{(eq. 1.4)}$$

The binodal curve can be constructed by deriving expressions for the chemical potentials of each component in the blend using eq. 1.3 and equating the chemical potentials for each component in phases I and II:

$$ln\frac{\phi_A^I}{\phi_A^{II}} + (\phi_A^{II} - \phi_A^I)\left(1 - \frac{N_{w,A}}{N_{w,B}}\right) + \chi N_{w,A}[(1-\phi_A^I)^2 - (1-\phi_A^{II})^2] = 0 \quad \text{(eq. 1.5)}$$

and $$ln\frac{1-\phi_A^I}{1-\phi_A^{II}} + (\phi_A^I - \phi_A^{II})\left(1 - \frac{N_{w,B}}{N_{w,A}}\right) + \chi N_{w,B}[(\phi_A^I)^2 - (\phi_A^{II})^2] = 0. \quad \text{(eq. 1.6)}$$

Simultaneously solving equations 1.5 and 1.6 leads to the determination of ϕ_A^I and ϕ_A^{II} as a function of χ.

1.3. Shear alignment of BCPs

BCPs with well-resolved morphology are quite important in industry, however, spontaneously self-assembled nanostructures are randomly orientated and do not usually

exhibit long-range order, therefore the material is macroscopically isotropic. The application of external forces, i.e., shear [steady shear or large amplitude oscillatory shear (LAOS)] [73-75], electrical fields [76, 77], magnetic fields [78], or surface patterns [79] can lead to the desired alignment of the BCPs. Control of morphology is the key to manipulating the properties of the multi-component and multi-phase polymer systems.

Extensive studies have focused on the alignment of lamellae-forming systems through steady shear or LAOS [74, 80-87]. Three possible orientations have been identified as parallel, perpendicular and transverse, with regard to the shear flow direction [84], depending on the frequency, shear strain and temperature [74, 85-87].

In the case of cylindrical microstructured block copolymers, the predominant orientations are cylinders oriented parallel or perpendicular to the shear direction [73, 88-93]. However, some research has revealed that the transverse orientation is preferable when there are liquid crystal domains which also have a preference in the alignment [94, 95].

The shear alignment for spherical nanostructures is focused mainly on thin films and polymer micelle solutions. Body-centered cubic (BCC) phase is the most occurring structure for thin films and the predominant orientation mode is the close packed {111} plane parallel to the shear plane [75, 96-102].

Beside BCC phases, face-centered cubic (FCC) and hexagonally close-packed (HCP) phases have been extensively observed in polymer micelle solutions [103-106]. Shearing FCC micellar solution results in a coexistence of FCC and HCP phases, which was first suggested by McConnell et al., who examined the long range order in polymeric micellar crystals with steady shear [107]. The predominant mode of alignment is the

slippage of the closed packed {111} planes of FCC and {0001} planes from HCP along the shear direction. Stacked layers contain ABCABC planes of FCC and ABABAB planes of HCP. The resulting small angle x-ray scattering (SAXS) pattern possesses an inner set of six bright spots and higher order hexagonal patterns.

The preference of close packed or BCC phases in BCPs micelles was first studied by McConnell et al. [107, 108]. The micellar ordering structure is determined by the inter-micellar interaction potential. The key variable is the ratio of the coronal layer thickness (L) to the core radius (R_c) and smaller L/R_c prefers the close-packed structure while large L/R_c results in less dense BCC structure. The concentration of the micelle solution also affects the preference of structures. Hamley et al. studied the cubic phase in a poly(oxyethylene)-poly(oxybutylene) micelle solution and it was found that higher concentration preferred BCC and lower concentration favored FCC phases [109]. Temperature, packing density and number of arms in star polymer, and solvent selectivity also trigger the transformation between close packed and BCC phases [103, 104, 110, 111].

Relatively few studies have shown the occurrence of the close packed sphere (CPS) structures in polymer melts, though from theoretical predictions there is a narrow stable region on the phase diagram [63, 112]. An unaligned blend of poly(ethylene oxide)-*b*-poly(1,4-butadiene) (PEO-*b*-PB) and a PB homopolymer has been found to form FCC structures between the BCC phase and disordered phase, associated with packing frustration [113]. Huang et al. also demonstrated a very narrow temperature window for FCC in unaligned PEO-*b*-PB melts and proposed that the unimers an oligomeric micelles facilitated the stability of FCC lattice [114]. Imaizumi et al.

presented the formation of FCC in poly(1,3-cyclohexadiene)-b-poly(ethylene-*co*-but-1-ene)-b-poly(1,3-cyclohexadiene) triblock copolymer under the extensional flow field and thermal annealing but extensional flow alone resulted in low regularity [115, 116]. To our knowledge, no literature studies report the CPS phase in BCPs melts under large amplitude oscillatory shear and in this study we will demonstrate stable CPS of the sustainable triblock copolymers derived from fatty acids under LAOS.

1.4. Overview of this thesis

The specific aims of this research are as follows:

1. Establish synthetic techniques for triblock copolymer TPEs derived from fatty acids and salicylic acid, employing RAFT polymerization.

2. Characterize the thermodynamic interactions between the endblock and midblock of the TPEs, an essential step toward the design of multicomponent polymer systems.

3. Investigate the physical properties of the triblock copolymers for targeted application as TPEs, including the morphology, thermal properties, and mechanical properties.

4. Examine the effect of shear alignment on the morphology of triblock copolymer TPEs.

In the following chapters the dissertation is are organized as outlined below.

Chapter 2 describes the experimental methods used in this study. Detailed information on chemicals used, synthesis techniques and characterization procedures will be discussed.

Chapter 3 discusses the development of linear triblock copolymers with a random copolymer of lauryl acrylate and stearyl acrylate (i.e., polyacrylates, or PAs) as the midblock and polystyrene as the endblock. The morphology, thermal and mechanical properties of the triblock copolymers are characterized.

Chapter 4 investigates the effect of the chain length of the long side-chain poly(*n*-alkyl acrylate) on the thermodynamic interactions with polystyrene. Cloud point measurements on binary blends and characterization of the order-disorder transition of the triblock copolymers are employed.

Chapter 5 presents the alignment of the triblock copolymers under large amplitude oscillatory shear (LAOS), performed at temperatures lower than the order-disorder transition of the triblock copolymers.

Chapter 6 describes the development of fully sustainable triblock copolymers with a fatty acid-derived lauryl methacrylate midblock and end-blocks derived from salicylic acid, found in many plant-based sources. The morphology, thermal and mechanical properties of the triblock copolymers are characterized.

Chapter 7 gives a summary and conclusions of this research. An outlook of the challenges and future work is also discussed.

Chapter 2

Experimental Methods

This chapter describes synthesis and characterization methods for the development of sustainable triblock copolymers. Reversible addition fragmentation chain transfer (RAFT) polymerization was used for the preparation of poly(lauryl acrylate) (PLAc), poly(stearyl acrylate) (PSAc), poly(lauryl-*co*-stearyl acrylate) (PA), polystyrene (PS), poly(lauryl methacrylate) (PLMA), poly(acetylsalicylic ethyl methacrylate) (PASEMA), poly(styrene-*b*-(lauryl-*co*-stearyl acrylate)-*b*-styrene) (SAS), and poly(acetylsalicylic ethyl methacrylate-*b*-lauryl methacrylate-*b*- acetylsalicylic ethyl methacrylate) (ALA).

The structure of the polymers was characterized by proton nuclear magnetic resonance (^{1}H-NMR) and gel permeation chromatography (GPC). The thermal properties were measured by differential scanning calorimeter (DSC) and thermogravimetric analysis (TGA). The order-disorder transition temperature and viscosity were characterized with rheology. Shear alignment of the triblock copolymer was conducted with large amplitude oscillatory shear, employed on a rheometer. The mechanical properties of the triblock copolymers were characterized through tensile testing. The morphology was probed by small angle x-ray scattering (SAXS) and transmission electron microscopy (TEM). Specific details pertaining to the synthesis and characterization methods are presented here.

2.1. Polymer synthesis using reversible addition fragmentation chain transfer (RAFT) polymerization

This section details the synthesis of all polymer discussed in chapters 3-6 of this dissertation. All chemicals for the synthesis were purchased from Sigma-Aldrich unless otherwise noted.

RAFT polymerization, first published in 1998, is a controlled radical polymerization technique [117]. The generally accepted mechanism is shown in Scheme 2.1.

1) Initiation and propagation

2) Pre-equilibrium

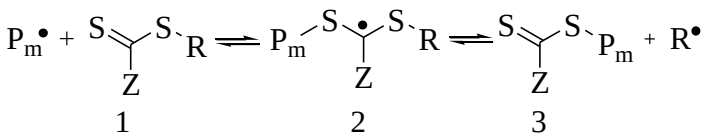

3) Reinitiation and propagation

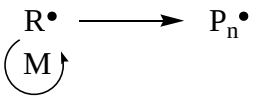

4) Main equilibrium

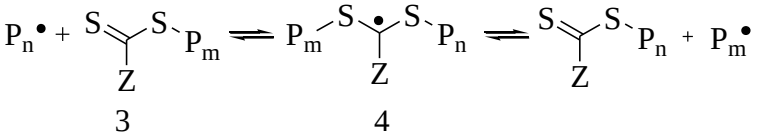

5) Termination

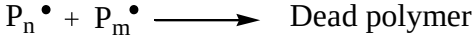

Scheme 2.1: Mechanism of RAFT Polymerization.

Chain transfer agent (CTA, 1) is essential in a RAFT system in which the Z group activates the thiocarbonyl bond (S=C) towards radical addition and R group will leave as

an active radical to reinitiate the growth of polymeric chains. After the initiation of the initiator and propagation with monomers, a propagating radical (P_m·) will be generated and then attach to 1, with the formation of an intermediate radical 2. A dormant polymeric thiocarbonylthio compound 3 and a radical (R·) will be produced by the fragmentation of the intermediate radical 2. The radical R· will react with monomers with the formation of a new propagating radical (P_n·). Rapid equilibrium between active P_n· and dormant 3 enables all chains to grow equally, thus the molecular weight increases linearly with conversion. Also, the low initiator concentration leads to low radical concentration so that the chance of termination is small, resulting in narrow molecular weight distributions, described by dispersity (*Đ)*, which is the ratio of weight average molecular weight (M_w) to number average molecular weight (M_n) [118].

With RAFT polymerization, block copolymers [119-122], star polymers [123-126], and complex molecular architectures [127] have successfully been built.

2.1.1. Synthesis of polyacrylate homopolymers and random copolymers

2.1.1.1. Synthesis of polyacrylate homopolymers and random copolymers using S*-1-dodecyl*-S*'-(α,α'-dimethyl-α"-acetic acid)trithiocarbonate*

Lauryl acrylate (LAc, 90%) was eluted through a silica gel (Fluka, 70–230 mesh) column to remove the monomethyl ether hydroquinone inhibitor. Stearyl acrylate (SAc, 97%) and 2,2′-azobis(2-methylpropionitrile) (AIBN, 98%) were recrystallized in ethanol (Koptec, 100%). LAc/SAc, AIBN, *S*-1-dodecyl-*S*'-(α,α'-dimethyl-α"-acetic acid)trithiocarbonate (DDMAT), and 1,4-dioxane (99.8%) were added at the predetermined molar ratio to a pressure vessel. After purging with argon for 20 min, the pressure vessel was sealed, immersed into a preheated oil bath at 70 °C and vigorously

stirred. The reaction scheme is shown in scheme 2.2. The polymerization was quenched by quick immersion of the pressure vessel into ice/water. Tetrahydrofuran (THF) was added to dissolve the product and the polymer was purified by precipitation into cold isopropyl alcohol. The precipitants were collected and dried under vacuum overnight at 40°C.

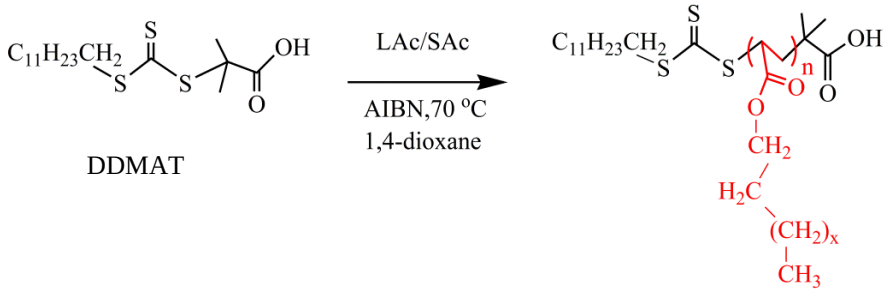

Scheme 2.2: Synthesis of PA using DDMAT.

2.1.1.2. Synthesis of polyacrylate homopolymers and random copolymers using 1,4-bis(thiobenzoylthiomethyl)benzene

A symmetric difunctional RAFT agent, 1,4-bis(thiobenzoylthiomethyl)benzene (BTBTMB), was synthesized according to ref. [128]. Poly(LAc-*co*-SAc) (or PA) was prepared using the similar procedure described section 2.1.1.1 except BTBTMB was used as the chain transfer agent (scheme 2.3). When x=9, it is poly(laury acrylate) (PLAc) homopolymer and when x=15, it is poly(stearyl acrylate) (PSAc) homopolymer. In the case of the random copolymer (PA), x is a combination of 9 and 15.

To investigate the polymerization kinetics of PLAc and PSAc homopolymers, a stock solution containing LAc or SAc, BTBTMB, AIBN (0.05 eq relative to BTBTMB) and 1,4-dioxane (99.8%) was prepared and separated into 5-8 pressure vessels in the glovebox. Once sealed, the vessels were taken out of the glovebox and heated at 70°C.

The reactions were quenched at a desired reaction time. The reaction conversion and molecular weight distribution were characterized using proton nuclear magnetic resonance (^{1}H-NMR) and gel permeation chromatography (GPC) respectively. To verify the composition of the statistical copolymer, PA, the same procedure was followed with a 50/50 mixture of LAc/SAc. The polymer was characterized with ^{1}H-NMR for the reaction conversion and LAc/SAc ratio in the copolymer, and GPC for the molecular weight distribution.

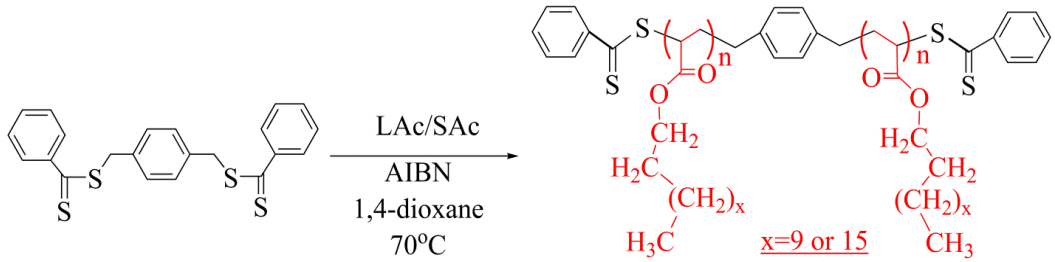

1,4-bis(thiobenzoylthiomethyl)benzene poly(LAc-*co*-SAc)

Scheme 2.3: Synthesis of PA using BTBTMB.

2.1.2. Synthesis of poly(styrene-b-(LAc-co-SAc)-b-styrene) triblock copolymers

Triblock copolymers SAS were synthesized in a two-step procedure (Scheme 2.4). The difunctional PA macro-chain transfer agent was first prepared as described in section 2.1.1.2. Styrene (99%) was purified with a basic aluminum oxide column to remove the 4-*tert*-butylcatechol inhibitor. Toluene (J.T. Baker, OmniSolv, HPLC grade) was purified using a SG Waters solvent purification system. PA was mixed with AIBN (0.05 eq relative to BTBTMB) and styrene in toluene in a pressure vessel. After purging with argon for 20 min, the pressure vessel was sealed, immersed into a preheated oil bath at 70°C and vigorously stirred for 2 days. The polymer was precipitated into cold methanol (BDH, ACS grade, 99.8%) twice and dried under vacuum overnight at 60°C.

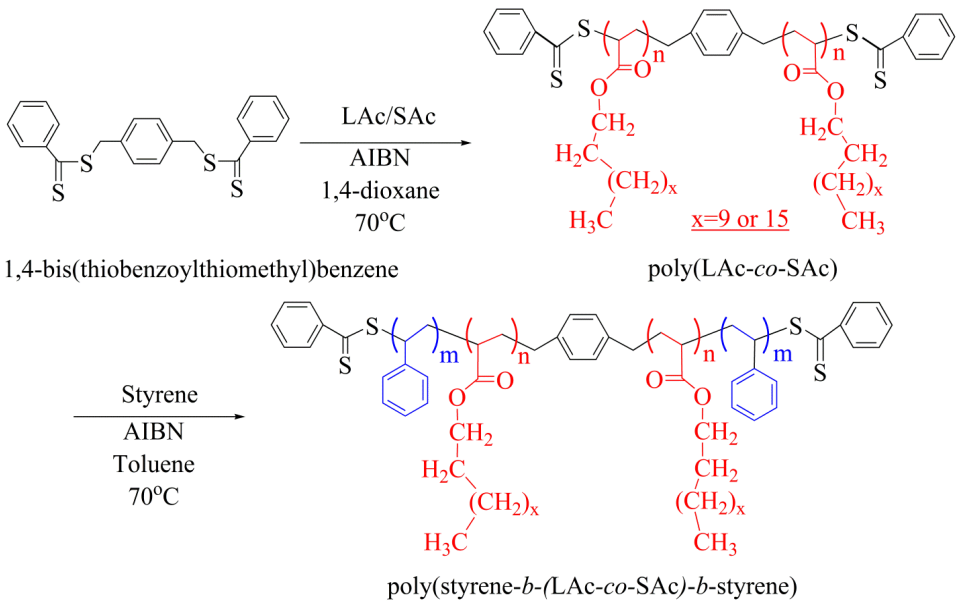

Scheme 2.4: Triblock copolymer synthesis using BTBTMB. Poly(LAc-*co*-SAc) (PA) is a random copolymer. For LAc, x=9, and for SAc, x=15.

One series of triblock copolymers were synthesized by a slightly modified procedure: polystyrene was first synthesized using dibenzyl trithiocarbonate as the RAFT agent, followed by chain extension with the acrylate monomers to form SAS triblock copolymers (Scheme 2.5).

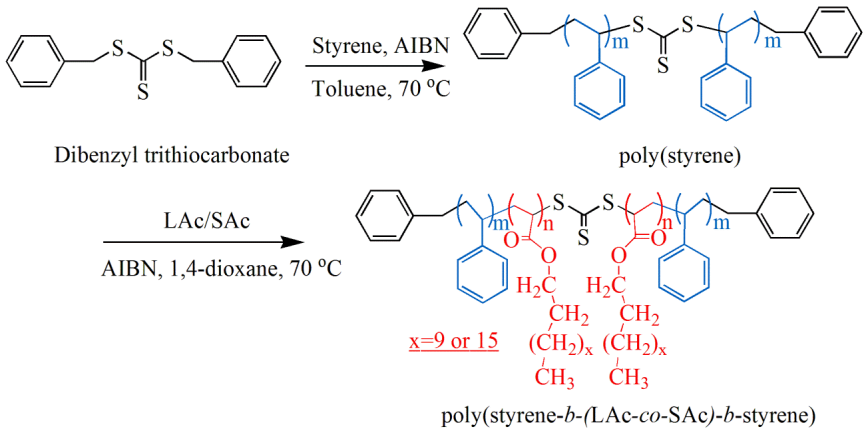

Scheme 2.5: Triblock copolymer synthesis using dibenzyl trithiocarbonate. Poly(LAc-*co*-SAc) (PA) is a random copolymer. For LAc, x=9, and for SAc, x=15.

2.1.3. Synthesis of poly(acetylsalicylic ethyl methacrylate-b-lauryl methacrylate-b-acetylsalicylic ethyl methacrylate) triblock copolymers

Acetylsalicylic ethyl methacrylate (ASEMA) was functionalized from acetylsalicylic acid. 2-hydroxyethyl methacrylate (HEMA) (stabilized, 97%) was passed through basic alumina column to remove the inhibitor. The reaction is shown in Scheme 2.6, following similar procedure as described in ref. [54].

Acetylsalicylic acid was dissolved in dichloromethane and oxalyl chloride was added to the above solution slowly under nitrogen flow. One drop of dimethylformamide was added and the solution was stirred at 0 ºC for overnight. Excessive oxalyl chloride and dichloromethane were removed using rotary evaporator. The resulting viscous liquid was re-dissolved in dichloromethane, and triethylamine and HEMA were added afterwards drop by drop under nitrogen flow. The solution was stirred at 0 ºC overnight, filtered to remove the white precipitant, washed with 5% sodium bicarbonate solution three times, dried over anhydrous sodium sulfate, and subsequently dried under vacuum. The yellow viscous liquid was further purified by silica gel chromatography (ethyl acetate/hexane: 4/6 (v/v)).

Poly(acetylsalicylic ethyl methacrylate-*b*-lauryl methacrylate-*b*- acetylsalicylic ethyl methacrylate) (ALA) was prepared in a two step RAFT polymerization using a difunctional RAFT agent, 1,4-bis(2-thiobenzoylthio)prop-2-yl)benzene (BTBTPB) (following ref. [128]). The selection of BTBTPB (structure shown in Scheme 2.7) as the CTA for LMA and ASEMA other than BTBTMB (structure shown in Scheme 2.4) lies in the fact that benzyl R group in BTBTMB is good for acrylate polymerization while a

tertiary R group is required for methacrylate polymerization [129]. The reaction scheme is presented in scheme 2.7.

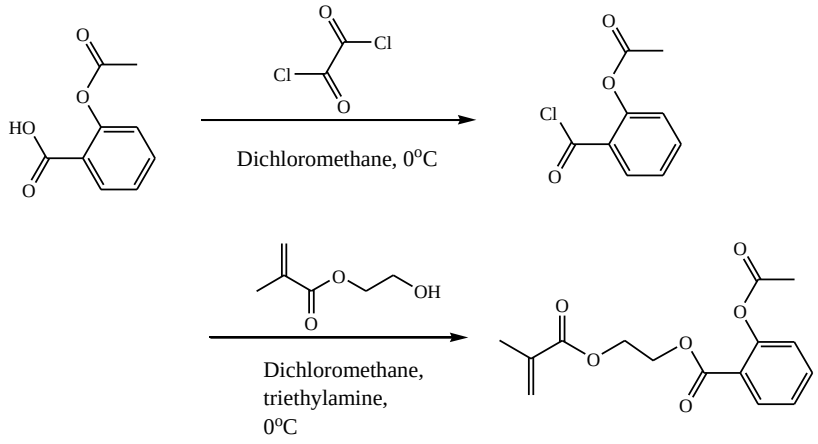

Scheme 2.6: Synthesis of acetylsalicylic ethyl methacrylate.

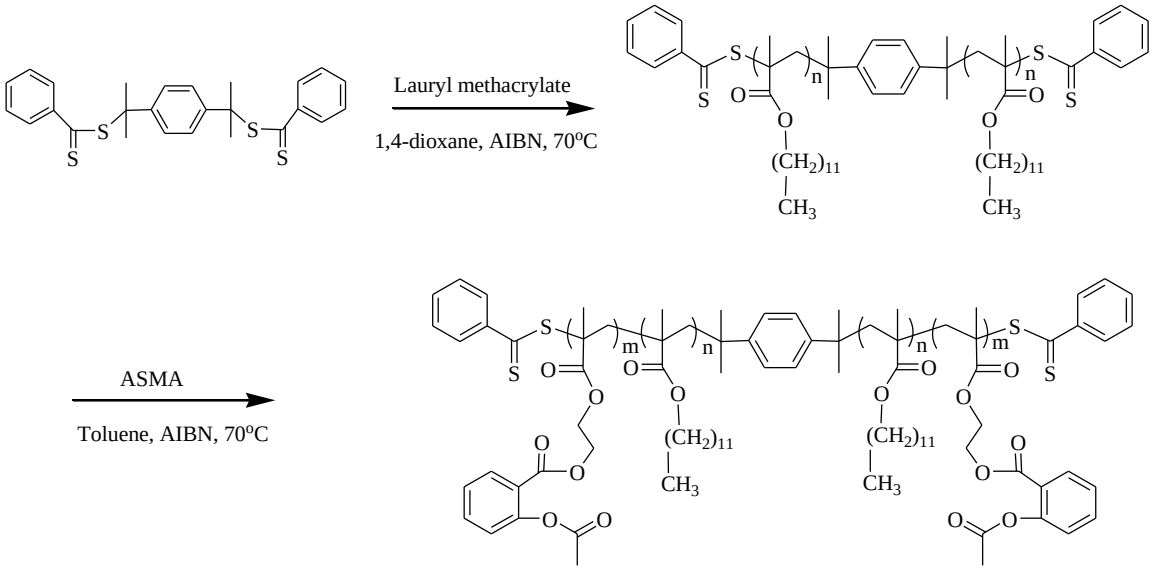

Scheme 2.7: Synthesis of ALA triblock copolymers

Poly(lauryl methacrylate) (PLMA) was first prepared in a pressure vessel with LMA, AIBN, BTBTPB and 1,4-dioxane. After purging with argon for 20 min the vessel was healed and immersed in a 70 °C oil bath. After 24 hours, the reaction was quenched by cooling with ice water. The solution was diluted with THF and precipitated in cold

isopropanol twice. The precipitant was collected and dried under vacuum at 40 °C overnight. PLMA was subsequently used as the macro-CTA to produce the triblock copolymer, ALA. PLMA was dissolved in toluene and ASEMA and AIBN were injected to the solution. The purged mixture was heated at 70 °C overnight and then the triblock copolymer was obtained by precipitating in cold methanol twice. ALA was dried under vacuum at 80 °C overnight.

2.2. Polymer characterization

2.2.1. Chemical analysis

Proton nuclear magnetic resonance (^{1}H-NMR) experiments were performed on a JEOL ECA-500 instrument using deuterated chloroform (99.8 atom % D) as the solvent. ^{1}H-NMR was utilized to determine the conversion, the relative proportions of meso and racemo dyads in the PLAc and PSAc homopolymers (evaluated following methods reported in refs. [40, 130]), the block ratio of the triblock copolymers and the composition (i.e., the fraction of LAc and SAc) in PA random copolymers (details will be discussed in Chapter 3 and 6).

Molecular weight and molecular weight distribution (including the dispersity, $Đ$) were measured by a Viscotek gel permeation chromatography (GPC) instrument using THF (OmniSolv, HPLC grade) as the mobile phase at 30°C. The flow rate was 1 mL/min and the injection volume was 100 µL. A triple detection system, including light scattering, a viscometer and refractometer, was employed to characterize the absolute molecular weight.

2.2.2. Thermal characterization

Melting temperature (T_m) and glass transition temperature (T_g) were characterized by a TA Instruments Q2000 differential scanning calorimeter (DSC), calibrated with an indium standard, with a nitrogen flow rate of 50 mL/min. The sample was placed in the calorimeter (using a Tzero Hermitic aluminum pan) and a heating-cooling-heating ramp was carried out at a rate of 10°C/min (the temperature range varied for different samples). The values of T_m and T_g were determined from the second heating.

2.2.3. Density

The densities of selected PAs (those that are amorphous at room temperature) were measured at room temperature (around 21°C) through the following protocol. A small portion of the polymer was placed on a glass slide and cooled with liquid nitrogen. The cold sample was fractured with a blade and quickly transferred to a vial containing a methanol/water mixture of known composition. The methanol/water content was adjusted to determine the composition range over which the polymer transitioned from being suspended in the solvent to sinking in the solvent. This range was narrowed until the density could be determined to 2 significant digits after the decimal point. The exact solvent mixture density was determined through weighing a known volume of the mixture (dispensed through a glass syringe) on an analytical balance (Mettler Toledo MS204S). For those polymers with melting temperature above room temperature, the polymer was solvent cast on a glass slide and cut with a knife after drying. The resulting densities were as follows: PLAc, 0.94 g/mL; PA copolymer with 76 wt % LAc, 0.94 g/mL; PA copolymer with 61 wt % LAc, 0.92 g/mL, PSAc, 0.92 g/mL.

2.2.4. Viscosity of PA and SAS

The viscosity of the PAs was characterized by a TA Instruments DHR-2 rheometer. Two experiments were conducted with a cone and plate geometry (40 mm diameter, cone angle 2.319°). Flow curves were obtained through measuring the viscosity at shear rates ranging from 100 to 10^{-4} s^{-1}, using the DHR-2 instrument's automatic steady state sensing. In select cases transient tests were also conducted in which the stress was held constant until steady state conditions (in both the shear rate and viscosity) were observed. This process was repeated for a variety of shear rates. The viscosity was determined by averaging the viscosity at the plateau.

The viscosity of the one series of triblock polymers synthesized using dibenzyl trithiocarbonate as the RAFT agent was also determined in the disordered state; the samples were placed between 25 mm parallel plates and heated in an electrically heated plates sample environment containing nitrogen gas. The measurements were taken at 150 °C (50 °C above the order–disorder transition temperature as determined by the rheometer, described in the Order-Disorder Transition section).

2.2.5. Thermal stability

The thermal degradation properties were probed by thermogravimetric analysis (TGA), using a TA Instruments Q500 analyzer. The sample was heated from 40°C to 600°C at a rate of 10°C/min in an argon environment (the balance argon purge flow was 40 mL/min and the sample purge flow was 60 mL/min).

2.2.6. Mechanical properties

Tensile testing was carried out with an Instron tensile tester with a 100 N load cell at a speed of 10 mm/min to obtain tensile strength and elongation at break of SAS and

ALA triblock copolymers at room temperature. Dog-bone-shaped testing bars (following ASTM D638, bar type 5, thickness 1.5 mm) were prepared by compression molding on a Carver Hotpress at an applied load of 4000 lbs at 210 °C. Pneumatic grips (maximum 2 kN) were used to affix the sample in the testing frame, at a compressed air pressure of 9 psi. Each measurement was repeated with 4–6 test specimens.

2.2.7. Order–disorder transition through rheology

Order–disorder transition temperatures (T_{ODT}) of SAS and ALA triblock copolymers were probed using the TA Instruments DHR-2 rheometer. The linear viscoelastic region was first determined in a strain sweep from 1% to 50% at a frequency of 10 rad/s. A frequency sweep was then completed (using a strain in the linear region) from 1 to 50 rad/s every 10 °C from 270 to 50 °C (200 to 20 °C for series 4 and 240 to 50 °C for ALA). The storage modulus (G') at a frequency of 10 rad/s was plotted versus temperature, and the sharp decrease in storage modulus indicated the T_{ODT}.

2.2.8. Morphology

The SAS and ALA triblock copolymers were prepared by compression molding on a Carver Hotpress at an applied load of 4000 lbs at 210 °C for 5 min prior to characterization with small-angle X-ray scattering (SAXS) and, in some cases, transmission electron microscopy (TEM). Additional SAXS experiments were conducted on shear-aligned triblock copolymers; the sample preparation is discussed in Section X.

SAXS experiments on SAS triblock copolymers were performed at the Advanced Photon Source (APS) at Argonne National Laboratories at Sector 5-ID-D beamline, maintained by the Dow–Northwestern–Dupont Collaborative Access Team (DND-CAT). The X-ray wavelength was 0.7293 Å, and the sample-to-detector distance was 4578 mm.

The scattering intensity was monitored by a Mar 165 mm diameter CCD detector with a resolution of 79 μm/pixel. The two-dimensional scattering patterns were azimuthally integrated to a one-dimensional profile of intensity versus scattering vector, $q = 4\pi \sin(\theta/2)/\lambda$ [θ is the scattering angle; λ is the wavelength].

The morphology of SAS and ALA triblock copolymers was probed using a Rigaku S-MAX 3000 SAXS instrument at the University of Houston, equipped with CMF optic incident beam (λ = 0.154 nm), 3 pinhole collimation, a 2-dimensional multiwire area detector with 1024 × 1024 pixels. The sample to detector distance was 3 m. The recorded scattered intensity distributions were integrated over the azimuthal angle and are presented as functions of the scattering vector.

Selected samples were characterized with TEM by our collaborators, Drs. Enrique Gomez and Sameer Vajjala Kesava at Pennsylvania State University. Sections of approximately 50 nm thicknesses were prepared for TEM experiments using a Leica EM UC6 microtome operating at 0 °C with a Leica EM FC6 cryo-attachment and a glass knife. Contrast between the polystyrene and polyacrylate domains was enhanced using 0.5 wt % (aq) RuO_4 vapor staining (5 min staining time). Imaging was done at the Materials Research Institute of the Pennsylvania State University on a JEOL 2010 LaB6 transmission electron microscope. Bright field images were recorded using a Gatan energy filter such that inelastic scattering is removed.

2.3. Determination of Flory-Huggins interaction parameter (χ)

Two methods were employed to characterize the Flory-Huggins interaction parameter (χ) between polystyrene and the polyacrylates: cloud point measurements and rheology. In this study, χ and N_i are calculated based on a reference volume (v_{ref}) of 100

Å^3, following ref. [131]. The choice of a constant reference volume (and one that is independent of monomer type) allows for the most direct comparison of χ parameters determined from blends containing polymers of varying molecular structure (and monomer volume). Furthermore, N_i is taken to be the weight-average degree of polymerization ($N_{w,i}$) in the determination of χ from cloud point measurements and number-average degree of polymerization ($N_{n,i}$) in the determination of χ from the order-disorder transition of triblock copolymers. In order to define χ and N_i based on v_{ref}, we will use

$$N_{w,i} = \frac{v_{mon,i}N_{mon,i}}{v_{ref}} = \frac{M_{mon,i}}{\rho_i N_A}\frac{M_{w,i}}{M_{mon,i}}\frac{1}{v_{ref}} = \frac{M_{w,i}}{\rho_i N_A v_{ref}} \quad \text{(eq. 2.1)}$$

and

$$N_{n,i} = \frac{v_{mon,i}N_{mon,i}}{v_{ref}} = \frac{M_{mon,i}}{\rho_i N_A}\frac{M_{n,i}}{M_{mon,i}}\frac{1}{v_{ref}} = \frac{M_{n,i}}{\rho_i N_A v_{ref}}, \quad \text{(eq. 2.2)}$$

where $M_{mon,i}$ is the molecular weight of a monomer repeat unit, $v_{mon,i}$ is the volume of a monomer repeat unit, $N_{mon,i}$ is the number of monomer repeat units on the polymer chain, $M_{w,i}$ is the polymer weight-average molecular weight, $M_{n,i}$ is the polymer number-average molecular weight, ρ_i is the polymer density, and N_A is Avogadro's number.

2.3.1. Cloud point measurements

Films consisting of PS/PLAc (or PS/PSAc) blends were cast from dichloromethane solutions at room temperature on microscope slides. The films were allowed to air dry and were subsequently dried in a vacuum oven at 150 °C for 4 hours. The sample was covered by a second slide and sealed using 3M Scotch-Weld Epoxy Adhesive to avoid the thermal degradation of the polymers at elevated temperatures. The cloud point temperatures were determined through observing the optical character of the sample in a microscope (Olympus BX51TRF) equipped with a heating cell (Instec

HCS302-01). The sample temperature was calibrated with a thermocouple and a calibration curve was constructed relating the sample temperature to the reported heating cell temperature. The sample was first heated to a temperature at which the blend was transparent, indicating the two polymers were miscible, and the sample was then cooled down slowly by 1 °C increment, and stabilized at each temperature for 2 mins before observation of the sample with the microscope. The temperature at which the sample started to become opaque was identified as the cloud point temperature. The accuracy of the cloud point temperature is estimated to be within ±1 °C for all experiments based on repeat measurements of the same sample. Experiments conducted upon heating to identify the location of the phase boundary were consistent with the results obtained upon cooling (observed difference was ≤ 2 °C). The relationship of χ and T was constructed by comparing the cloud point temperature and theoretical binodal curve predicted from the Flory-Huggins theory (as described in chapter 1).

2.3.2. Rheology

The order–disorder transition temperatures (T_{ODT}) of SAS triblock copolymers were probed using a TA Instruments DHR-2 rheometer as described in section 2.2.7. Multiple measurements were performed on the same sample to determine the error of the measurement, which was within ±1 °C.

From the theoretical phase diagram for symmetric triblock copolymers, the χN value can be determined from the curve separating ordered phase and disordered phase. N could be calculated based on the molecular weight of the triblock copolymer. Thus χ is derived. The relationship between T and χ could be constructed. Four series of triblock copolymers were examined with different midblock composition.

2.4. Shear alignment of SAS triblock copolymers

Large amplitude oscillatory shear (LAOS) was performed using the TA Instruments DHR-2 rheometer. The sample disk with a diameter of 25 mm and thickness of 1.2 mm was prepared by compression molding on a Carver Hotpress at an applied load of 4000 lbs at 240 °C. The sample disk was mounted to the 25 mm parallel plates with a gap of 1 mm (Figure 2.1). Two different alignment temperatures, 210 °C and 180 °C, were studied to investigate the influence of temperature on the alignment. Different oscillatory frequencies (1 rad/s, 10 rad/s, and 100 rad/s) were also utilized to examine the effect of frequency on the alignment. After LAOS at a strain of 100% for 3 hrs, the sample was cooled down to room temperature and removed from the rheometer. Three samples were cut from the disk (detailed in Figure 2.1) and examined with SAXS using the Rigaku instrument (refer to section X for details). The incident beam was in the shear gradient direction (refer to Figure 2.1).

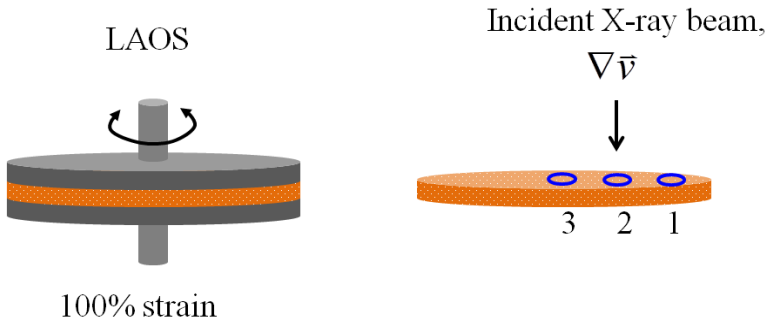

Figure 2.1: Setup of LAOS and sample positions for SAXS measurement. X ray beam in the velocity gradient direction and three samples measured by SAXS.

For selected samples aligned using a frequency of 1 rad/s at 180 °C, SAXS measurements were taken at five different positions along the disc radius. The strain imposed at the location of each measurement has been calculated to be of 16%, 32%,

48%, 64% and 80%. Measurements were obtained in the velocity gradient, velocity, and vorticity directions (refer to Figure 2.2).

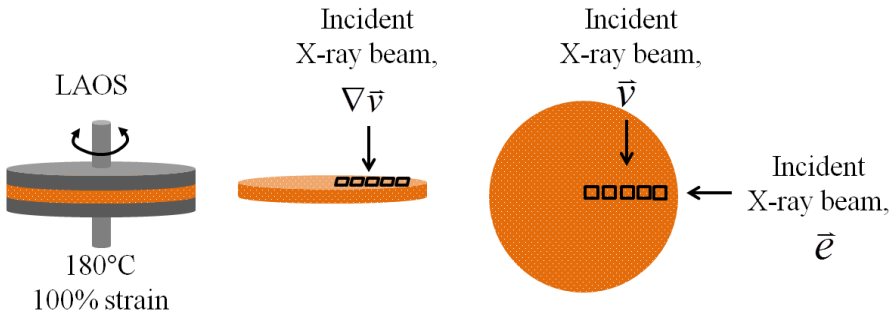

Figure 2.2: Setup of LAOS and sample positions for SAXS measurement. X ray beam in three direction and five samples measured by SAXS.

The 2D SAXS patterns were analyzed using 1) a home-built program provided by Dr. Eric Cochran (Iowa State University) and 2) the Scatter program designed by Forster et al., [132, 133] to identify the structure and orientation of the grains.

2.5. Characteristics of polymers in this study

Five series of SAS triblock copolymer were studied and the nomenclature SASX-Y-Z refers to triblock copolymer series X (1-5), with weight % of LAc in the mid-block of Y%, and PS volume % of Z%. In series 1-4, the polymer molecular weight is held constant (within experimental error). The characteristics for SAS are summarized in Table 2.1.

Table 2.1: Characteristics of SAS triblock copolymers in this study

	Mid-block [PA]			SAS triblock copolymers		
Name	M_n (kg/mol)[b]	$Đ$	wt% LAc[a]	M_n (kg/mol)	$Đ$	ϕ_{PS} at room temp.[b]
SAS1-100-23	81.9	1.28	100	108.9	1.68	0.23
SAS1-76-23	80.7	1.31	76	107.5	1.69	0.23
SAS1-61-24	81.6	1.24	61	109.7	1.65	0.24
SAS2-100-23	57.3	1.26	100	76.2	1.67	0.23
SAS2-76-24	58.2	1.30	76	78.4	1.65	0.24
SAS2-61-23	56.8	1.28	61	75.7	1.61	0.23
SAS3-100-17	57.3	1.26	100	70.4	1.44	0.17
SAS3-76-18	58.2	1.30	76	72.3	1.43	0.18
SAS3-61-18	56.8	1.28	61	70.7	1.42	0.18
SAS4-100-18[c]	39.2[f]	NA[g]	100	48.7	1.38	0.18
SAS4-73-18[c]	39.5[f]	NA[g]	73	49.0	1.42	0.18
SAS4-62-18[c]	38.8[f]	NA[g]	62	48.3	1.44	0.18
SAS5-0-24	59.7	1.26	0	81.1	1.38	0.24
SAS5-0-21	36.9	1.20	0	47.7	1.42	0.21
SAS5-0-17	59.7	1.26	0	73.2	1.44	0.17
SAS5-0-14	59.7	1.26	0	70.7	1.38	0.14
SAS5-0-12	59.7	1.26	0	69.0	1.44	0.12

[a]wt% LAc was calculated based on NMR.
[b]vol% PS was calculated based on measured polyacrylate densities (procedure described in Experimental Methods) and the PS density of 1.04 g/cm^3 reported in ref. [134].
[c]Series 4 polymers were synthesized through chain extension from PS with M_n = 9.5 kg/mol, Đ = 1.13.
[f]Calculated by subtracting M_n of the PS end-blocks from the M_n of the triblock copolymer.
[g]Not available.

The homopolymers used in the cloud point measurements described in chapter 4 are listed in Table 2.2. The polymers studied in chapter 6 are presented in Table 2.3.

Table 2.2: Characteristics of PLAc, PSAc and PS in cloud point measurements

Name	M_n (kg/mol)	M_w (kg/mol)	$Đ$	N_w[a] (at room temp.)
PS	3.1	3.4	1.11	55.7
PLAc	3.8	4.4	1.15	77.0
PSAc	2.5	2.6	1.05	46.6

[a]N_w is the weight-average degree of polymerization (based on a reference volume of 100 $Å^3$ and using the room temperature densities of the polymers).

Table 2.3: Characteristics of polymers described in Chapter 6

Name	M_n	$Đ$	ϕ_{PASEMA}
PLMA	87.6	1.21	0
PASEMA	30.4	1.24	1
ALA triblock copolymer	130.5	1.60	0.283

Chapter 3

Development of Poly(styrene-*b*-(lauryl acrylate-*co*-stearyl acrylate)-*b*-styrene) Triblock Copolymers

In this chapter, we discuss the synthesis and physical properties of poly(styrene-*b*-(lauryl acrylate-*co*-stearyl acrylate)-*b*-styrene) (SAS) triblock copolymers, which act as TPEs and contain mid-blocks derived from vegetable oils such as soybean oil and palm kernel oil. We have chosen to focus on a copolymer of lauryl acrylate (LAc) and stearyl acrylate (SAc) as the mid-block of the triblock copolymers as these monomers offer a number of advantages, including low glass transition temperatures [40, 41] and long alkyl side chains which are highly hydrophobic and provide a greater resistance to degradation [43, 44]. Additionally, we hypothesize that varying the length of the side chains on the polyacrylate mid-block (through varying the LAc to SAc ratio) will allow us to tune the physical properties of the triblock copolymer. The synthesis, morphology, and thermal and mechanical properties of these triblock copolymers are investigated.

3.1. Synthesis and characterization of PA homopolymers and random copolymers

3.1.1. Synthesis of PA using DDMAT

The ^{1}H NMR spectrum of PA is shown in Figure 3.1. The peaks at 4.0, 2.25, 1.87, 1.59, 1.26, and 0.87 ppm indicate the incorporation of the acrylate monomers and the peak at 3.3 ppm indicates the functional group of CTA was maintained after polymerization, allowing for subsequent chain extension. For PLAc, the theoretical ratio of peak area at 1.26 ppm to peak area at 0.87 ppm is 18:3, and for PSAc, the theoretical ratio is 30:3. In the copolymer, the LAc/SAc ratio is calculated from the ratio of these

two peak areas using

$$x_{LAc} = \frac{10-R}{4}, \quad \text{(eq. 3.1)}$$

$$x_{SAc} = \frac{R-6}{4}, \quad \text{(eq. 3.2)}$$

and $$wt\ \%\ LAc = \frac{x_{LAc}\times 240.38}{x_{LAc}\times 240.38 + x_{SAc}\times 324.54}\times 100, \quad \text{(eq. 3.3)}$$

where x_{LAc} and x_{SAc} are the mole fractions of LAc and SAc repeat units, respectively, and R is peak area b divided by peak area a in the NMR spectra. The wt% LAc calculated with this method was very close to the feed concentration.

The effect of AIBN level on the Đ was studied at AIBN levels of 1eq (molar ratio to DDMAT), 0.1eq and 0.05eq for both SA (100eq) (Table 3.1) and LA (100eq) (Table 3.2). The reaction time was 24 hr. It can be seen from Table 3.1 and Table 3.2 that lower AIBN level resulted in lower Đ and when the AIBN level was 0.05eq, the Đs were less than 1.2. In the following sections, AIBN level of 0.05eq was used to ensure narrow molecular weight distributions.

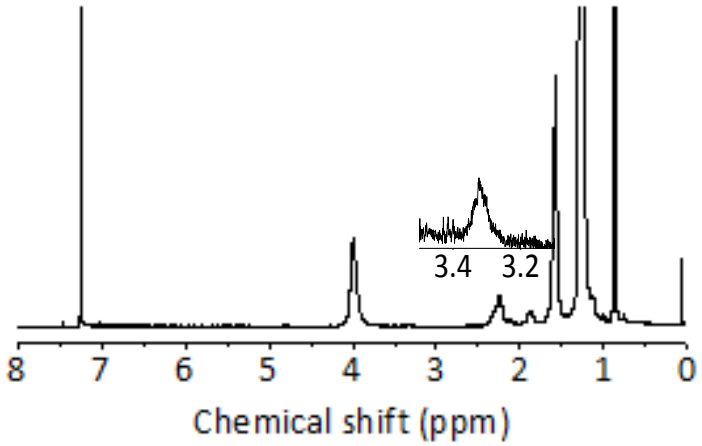

Figure 3.1: ^{1}H-NMR data obtained from PA using DDMAT.

Table 3.1: Effect of AIBN level on Đ of PSAc

AIBN	Mn (kg/mol)	Conversion	Đ
1eq	14.7	45%	1.41
0.1eq	15.6	48%	1.34
0.05eq	14.2	44%	1.19

Table 3.2: Effect of AIBN level on Đ of PLAc

AIBN	Mn (kg/mol)	Conversion	Đ
1eq	16.7	69%	1.30
0.1eq	17.6	73%	1.26
0.05eq	18.4	76%	1.19

PAs were synthesized at different monomer ratios, 100/0, 75/25, 50/50, 25/75 and 0/100. The degrees of crystallinity were calculated as the ratio between the enthalpy of fusion of the sample and the 100% crystalline polymer using references ΔH_{ref}(PLAc)=215 J/g for PLAc and ΔH_{ref}(PSAc)=218 J/g for PSAc [135]. T_m and degree of crystallinity (x) are summarized in Table 3.3.

Table 3.3: T_m and degree of crystallinity of PA at different SAc/LAc ratios

SA/LA ratio	M_n (kg/mol)	Melting point (°C)	Degree of crystallinity
100/0	39.9	54.7	41.3%
76/24	38.9	43.2	29.5%
52/48	43.2	28.36	20.1%
24/76	41.1	11.98	19.7%
0/100	44.0	2.21	19.5%

T_m of PA is also shown in Figure 3.2. The T_m values decrease linearly as the LAc fraction increases and are consistent with ref. [136].

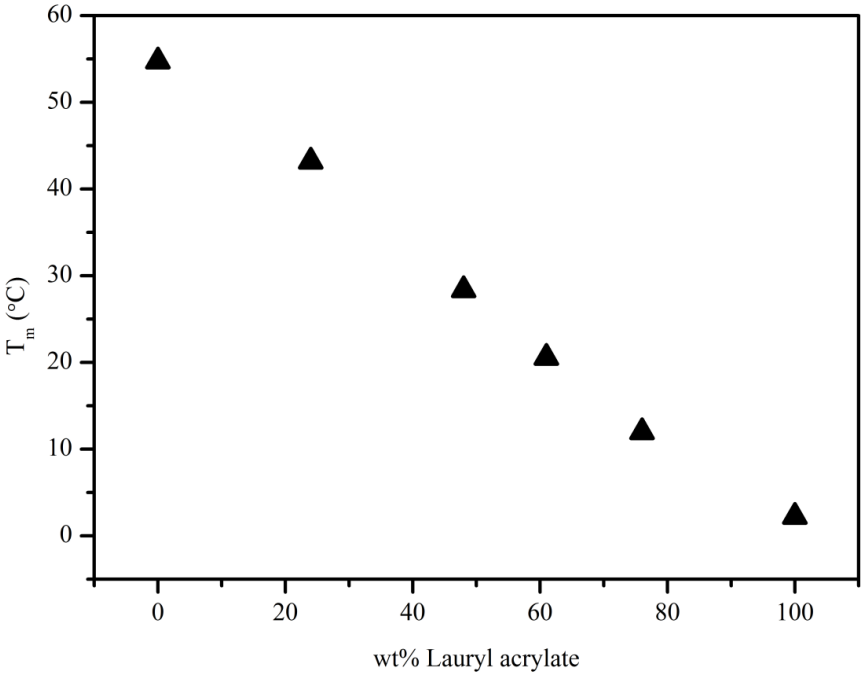

Figure 3.2: Melting temperatures (T_m) of PA.

The presence of side-chain crystallinity and the melting and crystallization behavior of poly(alkyl acrylates) with long side-chains have been previously reported [135-137], which is consistent with our study. The T_g for PLAc and PSAc have been reported in literature to be -65°C and -110°C, respectively. In order to measure the T_g of PLAc and PSAc, the crystallization needed to be suppressed. PLAc and PSAc were quenched in liquid nitrogen and transferred to the DSC to be subject to a heating ramp at a rate of 10°C to 100°C. The DSC results are shown in Figure 3.3. The T_g was absent from both of them. Attempt was also made to measure T_g of PLAc using rheometer by cooling the sample down from room temperature to -120°C. Storage and loss moduli and tanδ were recorded (Figure 3.4) and the T_g was not able to be measured. In TPEs

applications, the T_m of the soft segment should be less than the usage temperature (usually room temperature) [31], thus a LAc fraction higher than 60% is needed.

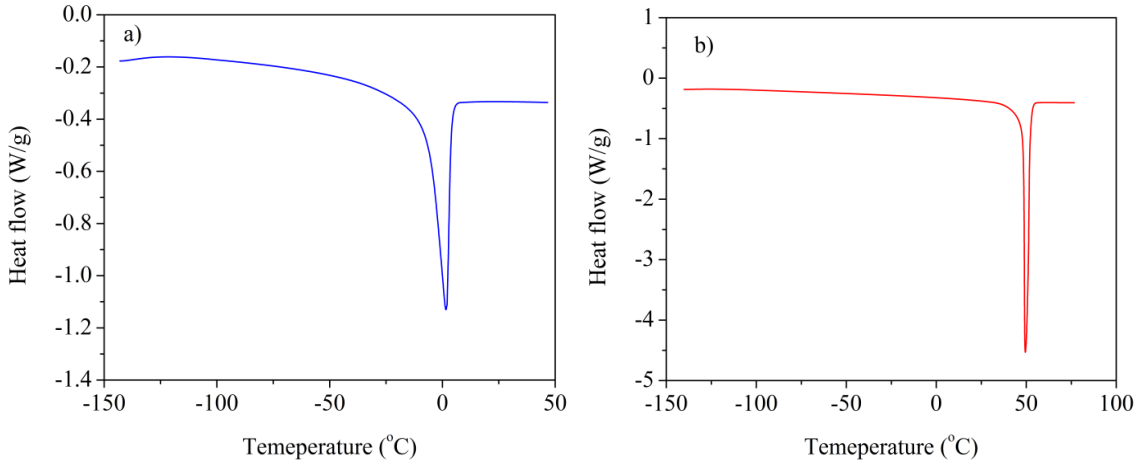

Figure 3.3: DSC measurement for (a) PLAc and (b) PSAc.

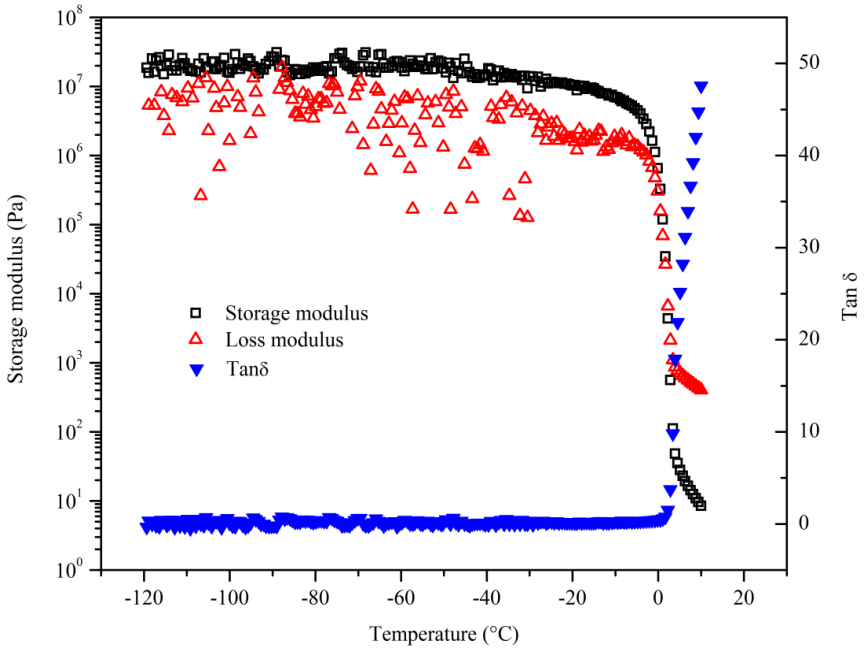

Figure 3.4: Measurement of T_g by rheometer for PLAc.

3.1.2. Synthesis of PA using BTBTMB

Random copolymers of PA were prepared using a difunctional RAFT chain transfer agent-BTBTMB and the composition of PA was chosen as 100/0, 75/25 and 60/40 (weight ratio of LAc to SAc).

The NMR spectrum of PA is shown in Figure 3.5. The peaks at 4.0, 2.25, 1.87, 1.59, 1.26, and 0.87 ppm indicate the incorporation of the acrylate monomers, and the three peaks from 7.3 to 8.0 ppm (inset of Figure 3.5) show the presence of the functional groups on the RAFT agent (BTBTMB) after polymerization, allowing for subsequent chain extension to synthesize triblock copolymers.

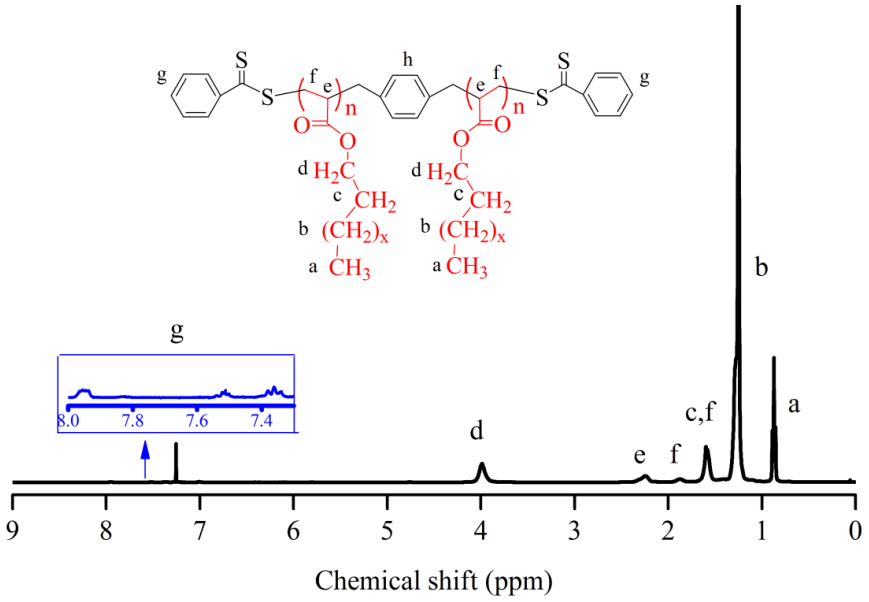

Figure 3.5: ^{1}H-NMR data obtained from PA.

The kinetics of polymerization of LAc and SAc were monitored by measuring the M_n and Đ of the polymer as a function of reaction conversion, shown in Figure 3.6. The M_n of PLAc (Figure 3.6a) and PSAc (Figure 3.6b) increase linearly with the monomer conversion, indicating the controlled behavior of the RAFT polymerization [118]. The Đ

is relatively low, around 1.3. The slightly higher Đs as compared to that obtained for other monomers such as *tert*-butyl acrylate [138] can be attributed to the higher rate of termination in polyacrylates with long side-chain lengths [139, 140]. Similar results have been observed in the literature for LAc [141].

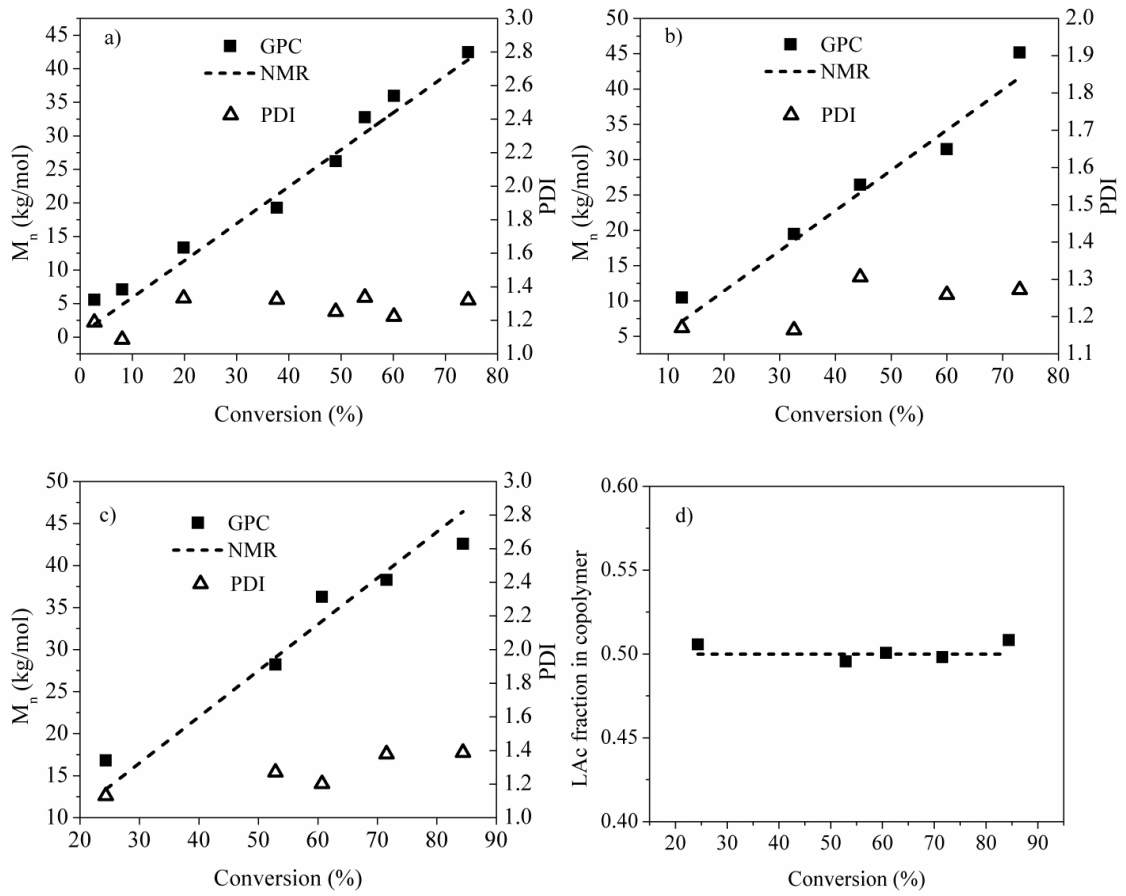

Figure 3.6: M_n and *Đ* as a function of monomer conversion for the RAFT polymerization of a) LAc, b) SAc, and c) a 50/50 feed mixture of LAc/SAc. The weight fraction of LAc in the copolymer from c) is shown in d).

A copolymer of LAc and SAc was also monitored in order to measure the polymer composition as a function of monomer conversion. Figure 3.6c shows the M_n and Đ as a function of monomer conversion for a 50/50 feed mixture of LAc/SAc. The NMR M_n values are calculated by multiplying the target molecular weight by the conversion determined by NMR. The LAc/SAc ratio in the copolymer was determined by

^{1}H-NMR, revealing that the LAc/SAc ratio is consistent throughout the reaction, without any detectable composition drift (Figure 3.6d, the dashed line indicates the feed composition). Previous studies have also reported a lack of composition drift and reactivity ratios close to 1 for polyacrylate copolymers with varying side-chain lengths [142, 143].

The viscosity of the PA random copolymers at 30 °C is plotted as a function of copolymer composition in Figure 3.7 and the complete viscosity as a function of shear rate data are presented in Figure 3.8.

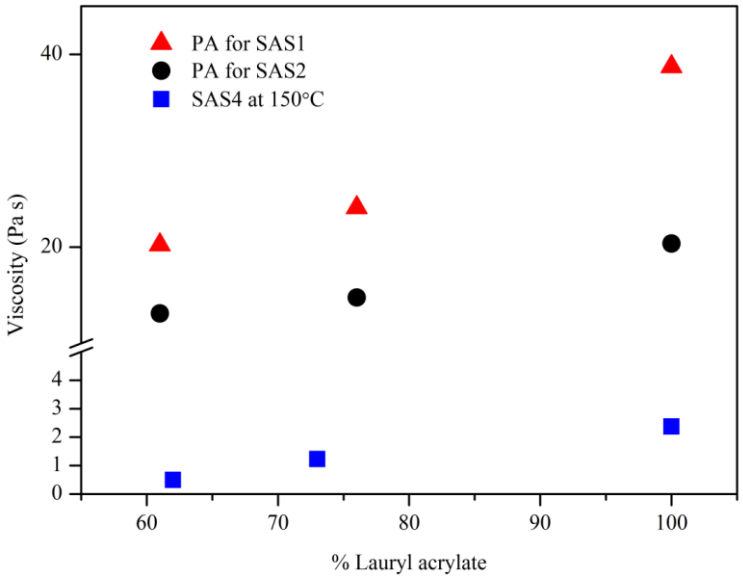

Figure 3.7: Viscosity of PA at 30 °C.

The increase in viscosity as the LAc content increases likely results from differences in the glass transition temperature (T_g) of the random copolymers [40, 41]. Additionally, increasing the side-chain length (which also reduces the number of monomer repeat units as the mid-block molecular weight is held constant within a series)

is expected to reduce the hydrodynamic volume of the polymer, also reducing the viscosity.

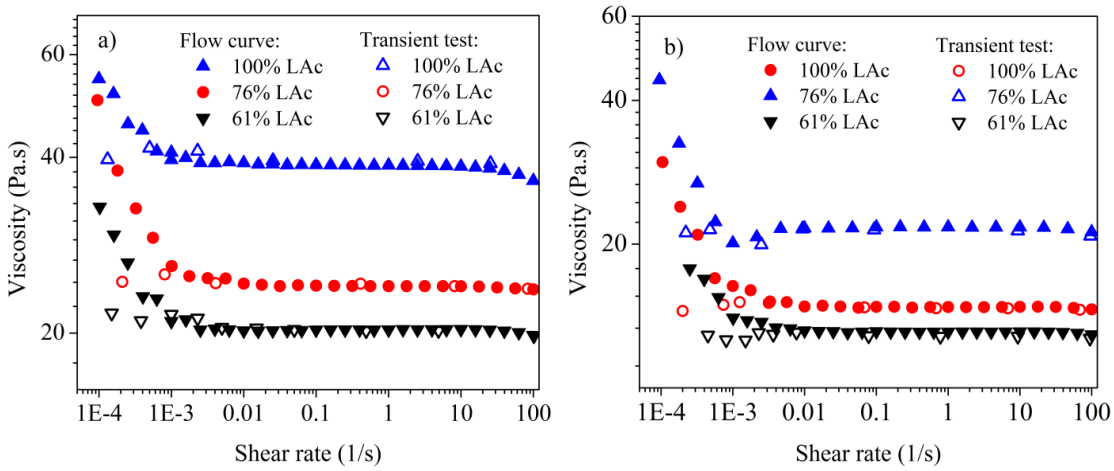

Figure 3.8: Viscosity of PA as a function of shear rate using two test set-ups: flow curve (closed symbol) and transient test (open symbol), both at 30°C. a) PA with M_n of 81 kg/mol, b) PA with M_n of 57 kg/mol.

The shear rate-dependence of the viscosity in the PA copolymers (Figure 3.8) show unusual behavior at low shear rates. In the flow curves (obtained by sweeping through various shear rates, allowing the instrument to sense the steady-state conditions), an increase in viscosity is observed at low shear rates. However, when a transient test was conducted (in which the stress was held constant for a long period of time to manually ensure that the steady-state shear rate and viscosity were attained at each stress value) this upturn disappeared (Figure 3.8). The difficulty in reaching steady-state conditions in these polymers may indicate the presence of structural rearrangement or alignment of the polymer chains under non-steady state conditions. Additionally, the upturn in viscosity at low shear rates was observed in the PA polymer containing 61% LAc at 25 °C even when the transient test was conducted (Figure 3.9). This behavior may be the result of the

proximity to the crystallization temperature in this polymer (determined to be 19 °C using DSC analysis).

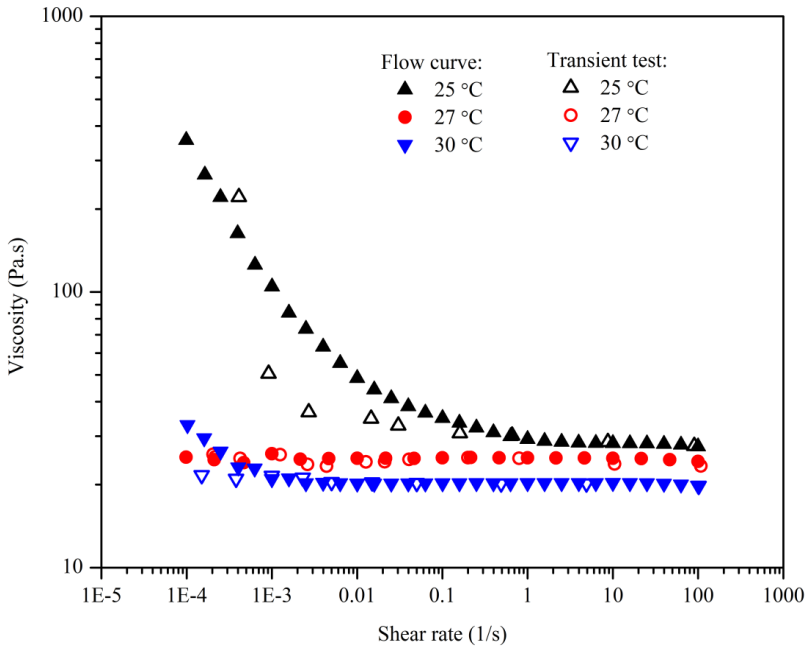

Figure 3.9: Viscosity of PA (61 wt% LAc, M_n=81.6 kg/mol, Đ=1.24) at different test temperatures and two sets of tests.

3.2. Synthesis and characterization of SAS

The ^{1}H-NMR obtained for SAS triblock copolymers was shown in Figure 3.7. Compared to Figure 3.6, the peaks at 6.3-7.2 ppm indicate the incorporation of polystyrene block and also, the functional groups from the RAFT agent were retained (inset of Figure 3.10).

Four series of SAS triblock copolymers were synthesized, in which the midblock composition (SAc/LAc ratio) was varied to study the impact of the midblock composition on the ultimate macroscopic properties of the triblock copolymer (Series 1-4 in Table 2.1 in chapter 2). In each series the polymer molecular weight is held constant while the midblock composition is varied. Representative GPC data are shown in Figure 3.11 for

SAS2-100-23 (and the PA random copolymer that was chain extended with styrene to form this triblock copolymer).

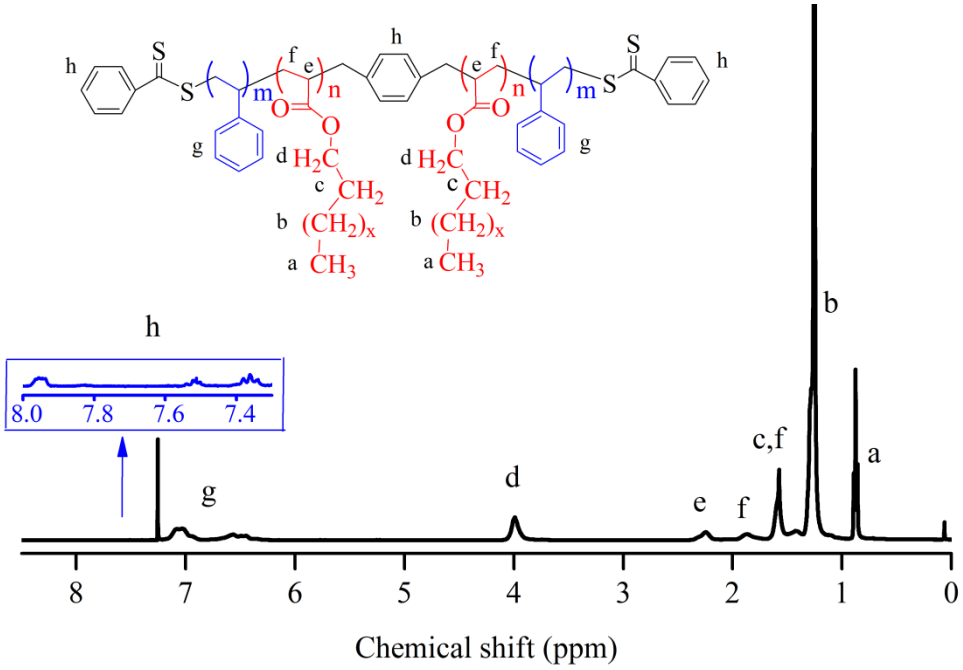

Figure 3.10: ^{1}H-NMR obtained for SAS triblock copolymers.

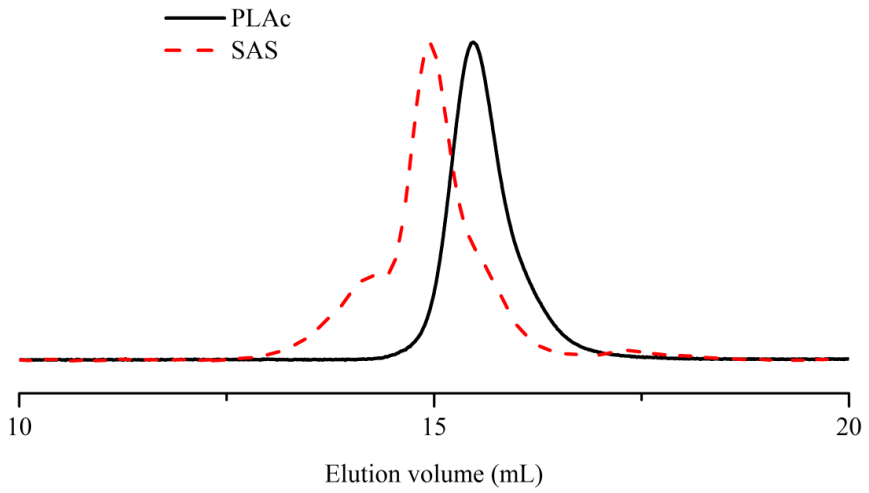

Figure 3.11: GPC traces for PLAc and SAS2-100-23.

There is a distinct shift to the left in the data when comparing the PA random copolymer and triblock copolymer. The GPC data for the triblock copolymers show

trimodal distributions. The shoulder to the right of the primary peak may indicate the presence of PA random copolymers that were not chain extended or diblock copolymer. The trimodal nature of the GPC data are also similar to that observed in ref. [144], in which the largest size mode (to the left of the primary peak) was attributed to chain branching.

Thermal stability of PA and SAS triblock copolymers

TGA data obtained from PS and PA are shown in Figure 3.12a. There is little difference between them, and therefore we anticipated that the triblock copolymers would exhibit similar thermal degradation behavior. TGA data obtained from the SAS triblock copolymers are shown in Figure 3.12b. All triblock copolymers are quite stable up to 320ºC, indicating that the polymers can be processed at elevated temperatures without degradation.

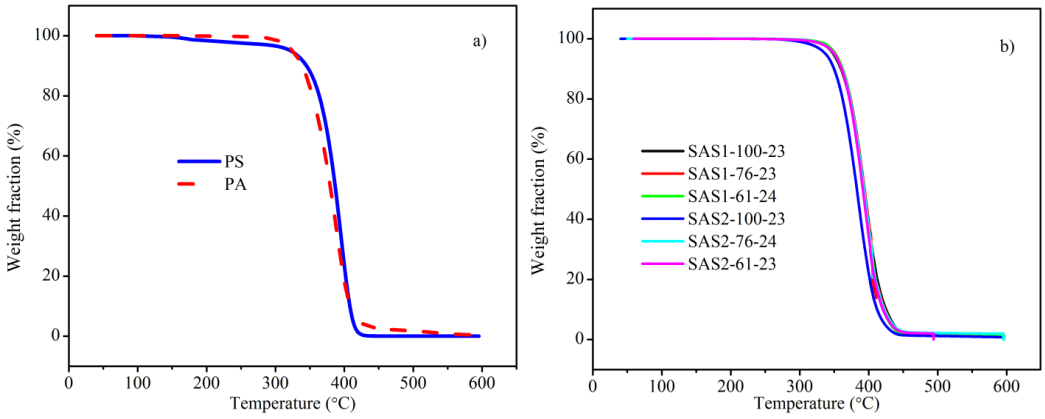

Figure 3.12: TGA data obtained from (a) PS (blue, solid line) and PA (red, dotted line) and (b) SAS triblock copolymers.

Morphology of SAS triblock copolymers

The morphology of the SAS triblock copolymers was investigated by both SAXS and TEM. The integrated 1D SAXS profiles are shown in Figure 3.13 for

series 1 and 2. The six polymers shown in Figure 3.13 exhibit similar features in the SAXS profiles. The 2D SAXS data for these polymers (Figure 3.14) show isotropic rings, indicating the random orientation of the grains during compression molding.

Broad scattering peaks are observed in Figure 3.13, with the presence of higher order peaks. The loci of the higher order peaks are not consistent with any single known microstructure. Co-existing structures may be possible in these polymers; however, the broadness of the primary peak makes it difficult to resolve the coexistence. The morphology after compression molding may not be at equilibrium. The structure of the SAS triblock copolymers will be further elucidated in chapter 5 with shear alignment.

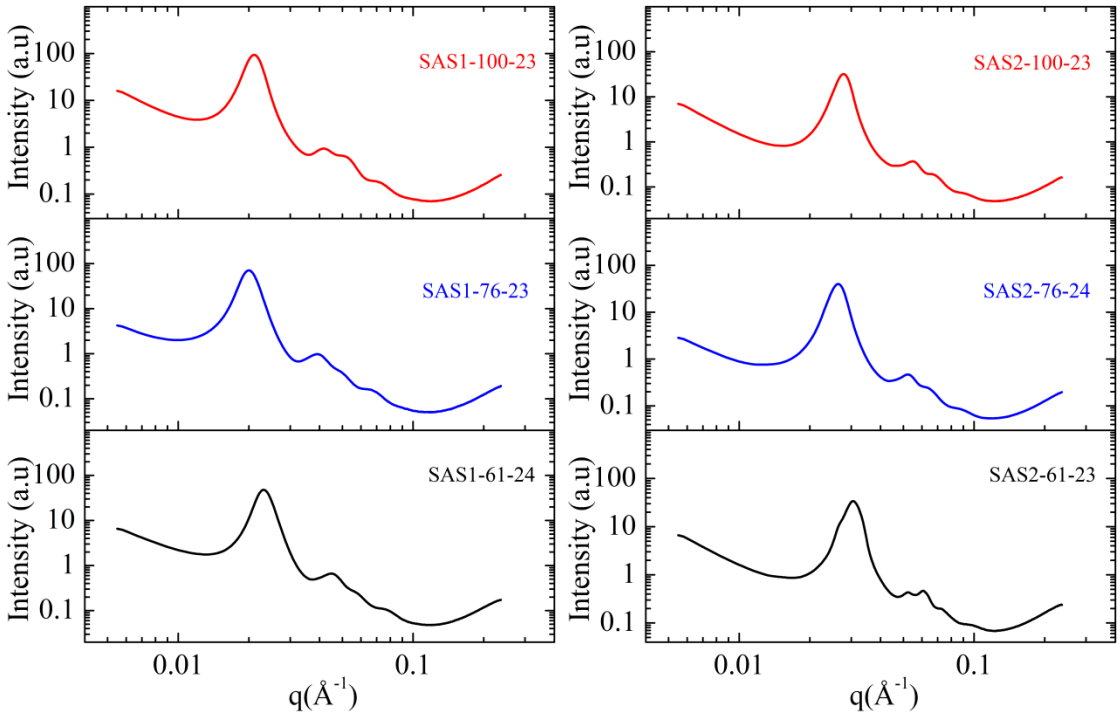

Figure 3.13: 1D SAXS profiles for SAS triblock copolymers at room temperature.

A representative TEM micrograph for SAS1-100-23 is shown in Figure 3.15a (Fourier transform of image shown in Figure 3.16a) where the dark regions correspond to PS domains because of RuO_4 staining. The micrograph in Figure 3.15a suggests a poorly

ordered spherical morphology. The lack of long range order is consistent with the broad peaks that are observed in the SAXS data. The micrograph in Figure 3.15a is similar to that in a publication by Mahanthappa and coworkers [145], where the microstructure was surmised to be influenced by crystallization of the triblock copolymer matrix. In our study, however, we prepared sections at 0 ^{o}C, in the vicinity of the T_m of the matrix of SAS1-100-23 (2 ^{o}C), and imaged the sections at 25 ^{o}C (above the T_m). Thus, we expect that crystallization of the matrix to have a minimal effect on the microstructure.

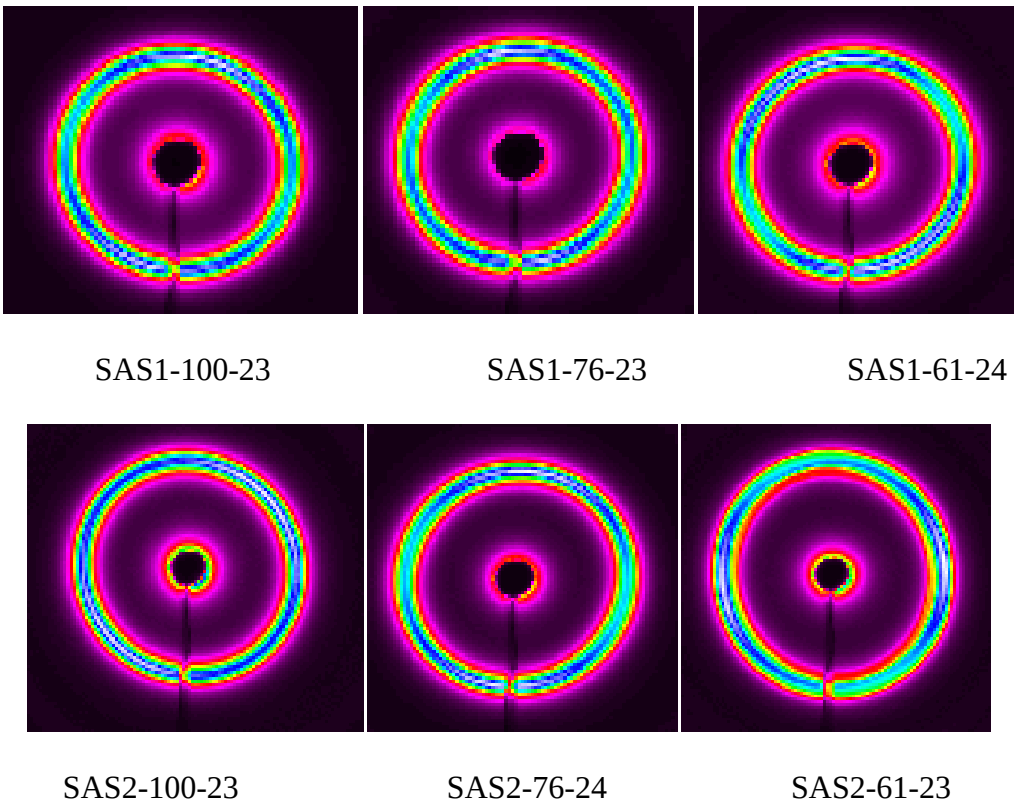

Figure 3.14: 2D SAXS plots for selected triblock copolymers.

A slightly different scenario as compared to the other samples is observed in the SAXS data obtained for SAS2-61-23. The 2D SAXS data (Figure 3.13) indicates the highest degree of anisotropy as compared to the other samples. TEM data was also

obtained on SAS2-61-23, shown in Figure 3.15b (Fourier transform of image shown in Figure 3.16b). A poorly ordered microphase separated morphology is also observed in Figure 3.15b, although in this case there appears to be connectivity between some of the PS spherical domains.

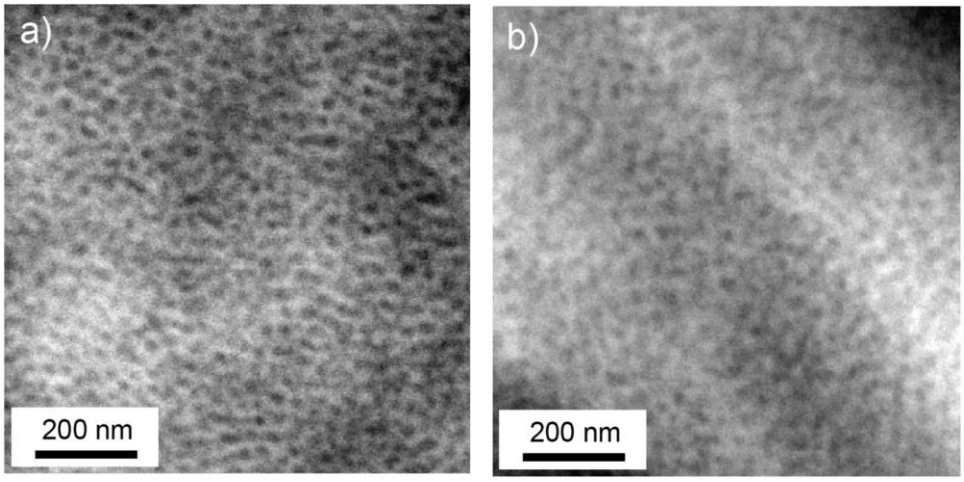

Figure 3.15: TEM micrographs obtained from a) SAS1-100-23 and b) SAS2-61-23.

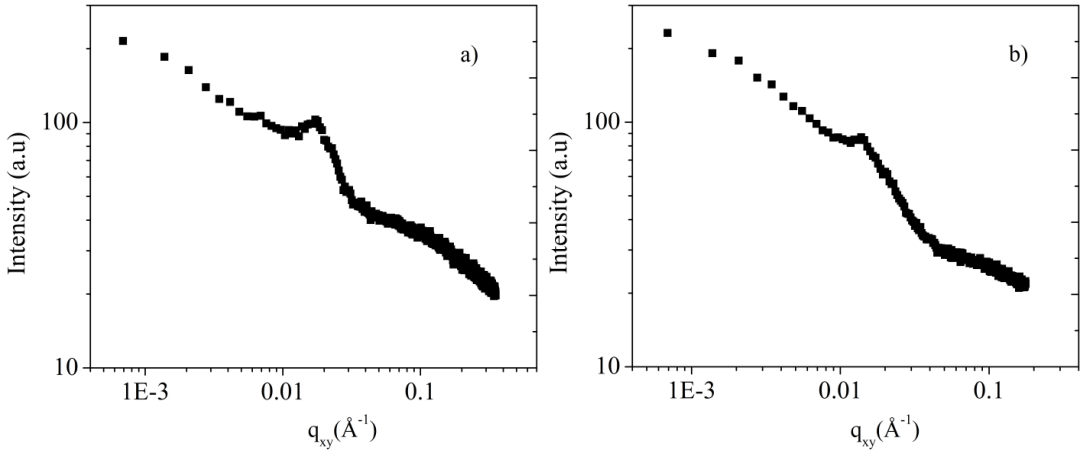

Figure 3.16: Fourier transforms of TEM image of a) SAS1-100-23 and b) SAS2-61-23.

To lend further evidence to the presence of a disordered spherical structure in which some of the spheres are connected, SAS1-100-23 and SAS2-61-23 were viewed in

an optical microscope through crossed polarizers; birefringence was not observed (note that the grain size and refractive indices of the polymers will influence the efficacy of this method for detecting anisotropic structures). Cylindrical or spherical microstructures are highly desirable for TPE applications, as they provide physical crosslinking and elastomeric behavior resulting from bridged PA chains connecting distinct glassy PS domains [31]. It is important to note that the data shown in Figures 3.13 and 3.15 are not necessarily representative of an equilibrium structure (the processing temperature of the polymers was in the vicinity of the T_{ODT}), yet are very relevant to understanding of the mechanical testing data as the same processing conditions were used for morphological and mechanical testing studies.

Order-disorder transition of SAS triblock copolymers

The order-disorder transition temperatures (T_{ODT}) of SAS triblock copolymers are summarized in Figure 3.17. Within each series, when the molecular weight of the triblock copolymer and styrene content are kept constant, but the ratio of LAc/SAc in the mid-block is varied, there is negligible effect on the T_{ODT} (i.e., compare each series in Figure 3.16 in which the color of the data points is held constant, and the symbols are varying). Note that the polymers in Series 4 have the smallest deviations in molecular weight and PS fraction (Table 3.4), due to the alternative synthetic scheme employed (Scheme 2.5). Importantly, in SAS triblock copolymers we are potentially able to tune the physical properties of the triblock copolymer without varying the T_{ODT}. The T_{ODT} is important for TPE applications as it affects the temperature at which the materials must be processed in the melt state. In series 1, the T_{ODT} is in the vicinity of the T_g of PS end-blocks. As the molecular weight of the triblock copolymer is increased, two distinct transitions emerge

and the T_{ODT} and T_g can be independently characterized. Comparing series 2 and 3, the mid-block molecular weights are similar to one another, but the two series contain polymers with different PSt fractions. A higher PS fraction results in a higher T_{ODT}, as observed in Figure 3.17. For series 1, the T_{ODT} was too high to be determined (an upper temperature limit of 280°C was chosen to avoid degradation of the polymer).

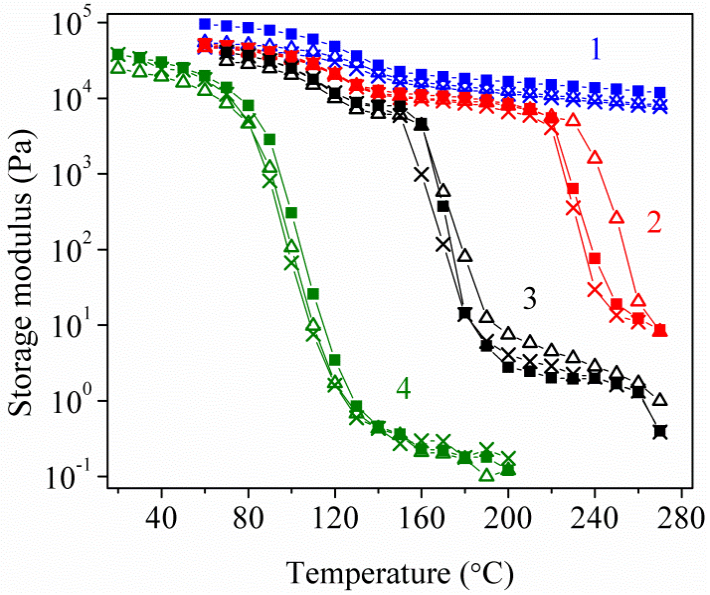

Figure 3.17: Storage modulus as a function of temperature of SAS triblock copolymers. In series 1-3: 100 wt% LAc (×), 76 wt% LAc (Δ), 61 wt% LAc (■). In series 4: 100 wt% LAc (×), 73 wt% LAc (Δ), 62 wt% LAc (■).

It is quite unexpected that the T_{ODT} would be independent of the mid-block composition. And detailed discuss regarding the thermodynamic interactions between PS and PA is the subject of Chapter 4.

Mechanical Properties of SAS Triblock Copolymers

Tensile testing data obtained from SAS triblock copolymers (series 1 and 2) are shown in Figure 3.18.

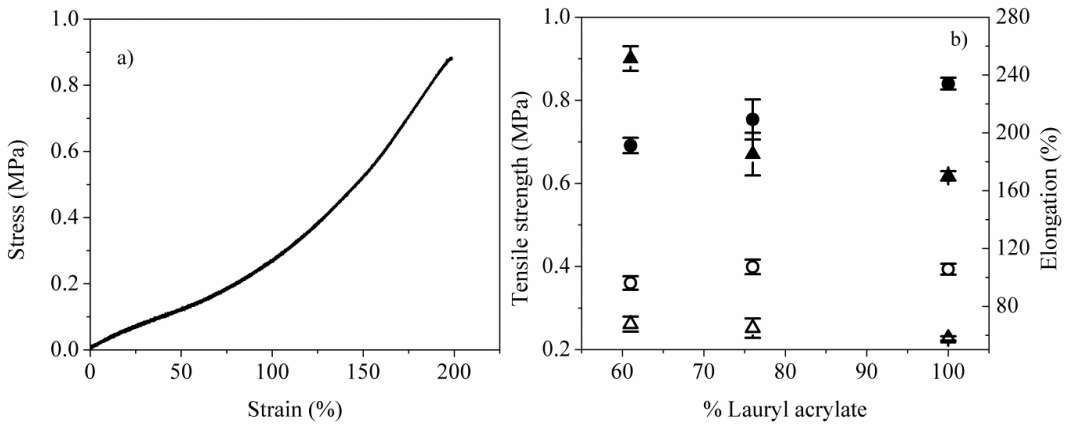

Figure 3.18: a) A representative stress-strain curve of SAS. b) Tensile stress and elongation at break of SAS: Series 1 tensile strength (▲) and elongation (●) and Series 2 tensile strength (Δ) and elongation (○).

The tensile strength and elongation at break are much lower than commercial SBS triblock copolymers [31]. It is known that the mechanical properties of TPEs are highly dependent on the molecular weight between entanglements (M_e) of the mid-block [31]. In order to obtain high tensile strength, the soft matrix needs to be entangled, requiring M_n of the mid-block to be 2-3 times larger than M_e (the exact relationship between the critical molecular weight, M_c, and M_e depends on the polymer structure [146]). In the commercial SBS and SIS triblock copolymers, the M_e for poly(butadiene) and poly(isoprene) are 1.7 kg/mol and 6.1 kg/mol, respectively [147, 148]. However, polyacrylates have higher M_e's and as the alkyl chain length increases, M_e increases substantially, resulting in lower tensile strengths (Table 3.5). The M_e for poly(lauryl methacrylate) has been reported to be 225 kg/mol [34], and we anticipate the M_e for PLAc to be similarly large.

Table 3.5: Mechanical properties of poly(*n*-alykl acrylate)-based TPEs

End-block	Mid-block	M_e (kg/mol)	M_n (kg/mol)	σ_b (MPa)	ε_b (%)
poly(styrene)	poly(butadiene)	1.7[147]	13.7-63.4-13.7[31]	25.0[31]	900[31]
poly(styrene)	poly(isoprene)	6.1[148]	13.7-63.4-13.7[31]	32.0[31]	1150[31]
poly(methyl methacrylate)	poly(*n*-propylacrylate)	16	10-50-10	14.0	660[149]
poly(methyl methacrylate)	poly(*n*-butyl acrylate)	28	10-50-10	12.5	540[150]
poly(methyl methacrylate)	poly(isooctylacrylate)	59	10-50-10	6.5	320[150]
poly(methyl methacrylate)	poly(lauryl methacrylate)	225	10-48-10	3	75[34]

For an entangled polymer, the M_e could be calculated from the rubbery plateau modulus (G_N) using [1]

$$M_e = \frac{\rho RT}{G_N}. \qquad \text{(eq. 3.4)}$$

We have synthesized 3 high molecular weight PLAc polymers in order to characterize the M_e (up to M_n = 170 kg/mol). In all cases, no rubbery plateau in the storage modulus was observed and the rheology data were consistent with an unentangled polymer (Figure 3.19, data were obtained from 0 to 50 °C and shifted to a reference temperature of 0 °C.). Therefore, we can conclude that the SAS triblock copolymers summarized in Table 3.4 will contain PA mid-blocks that are unentangled.

The unentangled matrices in the SAS triblock copolymers result in lower tensile strengths as compared to SBS or SIS TPEs. Though this may be a disadvantage for some TPE applications, many recent articles in literature have focused on the use of polyacrylates for TPEs due to their hydrophobicity and soft matrix [34, 149]. A soft

matrix may be an advantage in pressure sensitive adhesives or applications employing oil-extended TPEs.

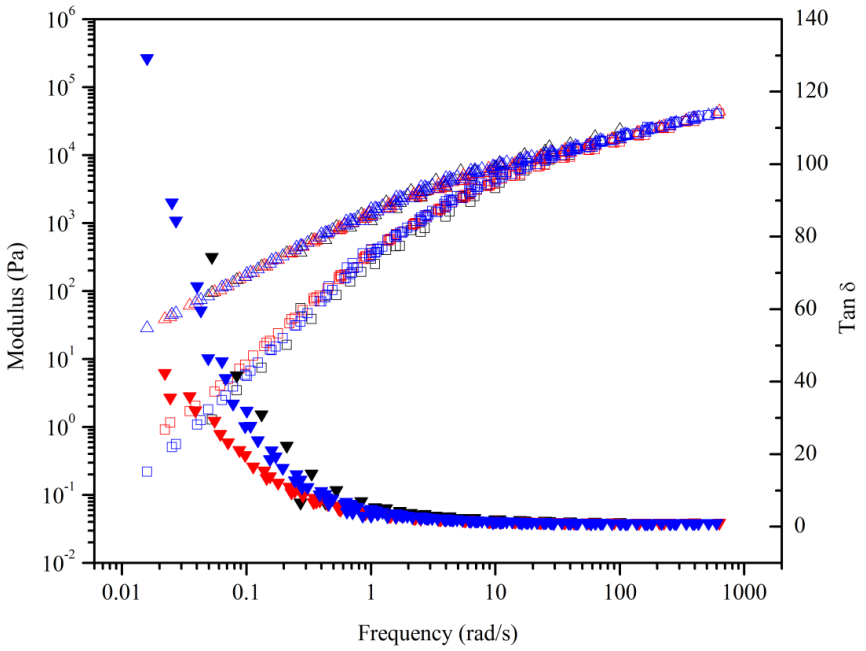

Figure 3.19: Master curves for storage modulus (□), loss modulus (Δ), and tan δ (▼) for three PLAc samples. Black: M_n=84 kg/mol, Đ=1.36; Red: M_n=130 kg/mol, Đ=2.05; Blue: M_n=170 kg/mol, Đ=1.55.

In some cases, the mid-block composition can be used to manipulate the SAS triblock copolymer mechanical properties. In series 1, as the LAc fraction increases, the ultimate tensile stress decreases whereas the elongation at break increases (Figure 3.18). Thus, in this higher molecular weight series, it is possible to tune the mechanical properties of the triblock copolymers by changing the side chain length of the mid-block. In contrast, in series 2 the SAS triblock copolymer mechanical properties did not appear to be affected by the mid-block composition.

3.3. Concluding remarks

In this study, we established the synthetic strategy for fatty acid-derived long chain acrylates using RAFT polymerization with a difunctional RAFT chain transfer agent. The polymerizations of the fatty acid-derived acrylate monomers were well-controlled with a linear increase of molecular weight as a function of monomer conversion and relatively low values of the Đ (around 1.3).

Four series of poly(styrene-*b*-(lauryl acrylate-*co*-stearyl acrylate)-*b*-styrene) (SAS) triblock copolymers were synthesized. The SAS triblock copolymers exhibited microphase separation, likely a spherical morphology without strong long range order, as indicated by SAXS and TEM. The physical properties of the polymers can be readily tuned by varying the acrylate mid-block composition, including the melting temperature, viscosity, and triblock copolymer tensile properties. Mechanical testing reveals the thermoplastic elastomeric behavior of the triblock copolymers. The acrylate mid-block composition does not affect the order-disorder transition temperature of the triblock copolymer. This indicates that the acrylate composition can be used as a tool to manipulate the physical properties of the triblock copolymers without affecting the order-disorder transition temperature, or processing temperature, of the TPEs.

Chapter 4

Thermodynamic Interactions between Polystyrene and Long Alkyl Side Chain Polyacrylates

The development of structured multicomponent materials, including block copolymers and blends, requires knowledge of the thermodynamic interactions governing their self-assembly. The thermodynamics of polymer blends and block copolymers are described by the following parameters: the composition of the block copolymer or blend, the Flory-Huggins interaction parameter, χ, (or the related binary interaction energy density) and the number of repeat units of each component i in the blend or block copolymer (N_i) [62].

The length of the side-chain of short-chain poly(*n*-alkyl acrylates) and poly(*n*-alkyl methacrylates) has been demonstrated to greatly influence their interactions with other polymers. Previous studies have characterized the χ parameter between polystyrene and various short-chain poly(*n*-alkyl acrylates) using a variety of experimental techniques: cloud-point measurements or miscibility studies of blends [151, 152], the domain spacing of block copolymer melts [153], melt titration [154], and swelling experiments on interpenetrating networks [155]. A wider body of literature exists for the measurement of the χ parameter between polystyrene and various short-chain poly(*n*-alkyl methacrylates), particularly for mixtures of polystyrene and poly(methyl methacrylate), employing cloud-point measurements or miscibility studies of blends [156-158], small-angle neutron scattering [159, 160], neutron reflectivity [161, 162], solution behavior [163], PVT experiments [157], melt titration [154], and swelling experiments on crosslinked

polymers [164]. Furthermore, molecular dynamics simulations have been employed [165, 166].

Few studies have directly examined the influence of the side-chain length on the thermodynamic interactions between polystyrene and poly(*n*-alkyl acrylates) or poly(*n*-alkyl methacrylates), especially for large *n*. Two key studies have demonstrated that the solubility parameter of poly(*n*-alkyl acrylates) and poly(*n*-alkyl methacrylates) decreases with increasing alkyl chain length (*n*) for relatively short side-chain lengths (up to $n = 10$) [151, 167]. Systematic experimental measurements of the binary interaction energy density (which is directly related to the χ parameter) with increasing *n* were not in agreement with that predicted from the solubility parameters [151]. Importantly, experimental measurements indicated that the binary interaction energy density increases only slightly when *n* increases from $n = 4$ to 10, in stark disagreement with the predictions from the solubility parameters [151]. To our knowledge, no previous studies have examined the thermodynamic interactions between polystyrene and long-chain poly(*n*-alkyl acrylates) or poly(*n*-alkyl methacrylates) (i.e., when *n* is greater than 10).

In Chapter 3, we have demonstrated that varying the midblock composition didn't change the order-disorder transition temperature of the SAS triblock copolymers with similar molecular weight and volume fraction of end PS block. In this Chapter, we will investigate the thermodynamic interactions between PS and PA and the effect of the side chain length of the acrylate on the thermodynamic interactions.

Two experimental methods were employed to characterize the χ parameter: cloud point measurements on binary blends and determination of the order-disorder transition

temperature of triblock copolymers. The values of $\chi(T)$ determined from both methods are compared, and the alkyl side-chain length-dependence of the χ parameter is examined.

4.1. Temperature-dependence of the volume of a monomer repeat unit ($v_{mon,i}$)

The room temperature volume of a monomer repeat unit, $v_{mon,i}^{o}$, can be calculated as $v_{mon,i}^{o} = \frac{M_{mon,i}}{\rho_i N_A}$. At elevated temperatures, $v_{mon,i}$ will be affected by the thermal expansion of the polymer, which can be calculated using the following equation:

$$v_{mon,i}(T) = v_{mon,i}^{o}[1 + \alpha_i(T - T^o)], \quad \text{(eq. 4.1)}$$

where α_i is the volumetric thermal expansion coefficient, T^o is room temperature, and T is the temperature of interest. The volumetric thermal expansion coefficient of PS has been reported to be 2.16×10^{-4} K^{-1} and 5.13×10^{-4} K^{-1} for the glassy and rubbery states, respectively [168]. For PLAc, PSAc, and poly(LAc-*co*-SAc), there are no reported values to follow, however, Rogers et al. have studied the thermal expansion coefficients of a series of poly(*n*-alkyl methacrylates) [169]. For PLAc and poly(LAc-*co*-SAc), the polymer is in a rubbery amorphous state at room temperature (the melting temperature, T_m, and the glass transition temperature, T_g, are below room temperature); the value of the thermal expansion coefficient is taken as that of poly(lauryl methacrylate) in the rubbery state (6.8×10^{-4} K^{-1}) [169].

For the PSAc homopolymer, which has a T_m of around 50 °C, the thermal expansion coefficients in the semi-crystalline and amorphous states were taken to be those of poly(stearyl methacrylate) (PSMA) in the semi-crystalline (4.0×10^{-4} K^{-1}) and amorphous (6.2×10^{-4} K^{-1}) states, respectively [169]. Additionally, there is a drastic increase in the specific volume during the melting transition. PSMA exhibited a 4.8%

increase in specific volume upon melting [169], and this same increase in specific volume upon melting was applied to PSAc in our study.

For all polymers employed in this study, the temperature-dependent values of $v_{mon,i}$ were used to calculate the temperature-dependent volume fraction (ϕ_i) and N_i of each component in the blend or block copolymer. As the polymers utilized in this study have similar temperature-dependencies of $v_{mon,i}$, the values of ϕ_i did not vary significantly with temperature.

4.2. Determination of the χ parameter from cloud point measurements in binary blends

Cloud point experiments were conducted on binary blends of PS and polyacrylate homopolymers. The homopolymer characteristics are summarized in Table 2.2 in chapter 2.

Figure 4.1 shows a representative ^{1}H-NMR data obtained from poly(stearyl acrylate). The % meso and racemo dyads were determined for PLAc and PSAc homopolymers, following the method described in refs. [40, 130]. The following are relevant proton peak locations: meso-methylene (1.47 and 1.88 ppm), racemo-methylene (1.57 ppm), and methyne (2.25 ppm). The % meso content was calculated by dividing the peak area at 1.88 ppm by the peak area at 2.25 ppm, chosen for their lack of overlap with other peaks in the spectrum. The % racemo content was calculated by subtracting the % meso content from 100%. The results are shown in Table 4.1 and we can conclude that PLAc and PSAc have very similar tacticity and the effect of tacticity difference on the thermodynamic interactions could be neglected.

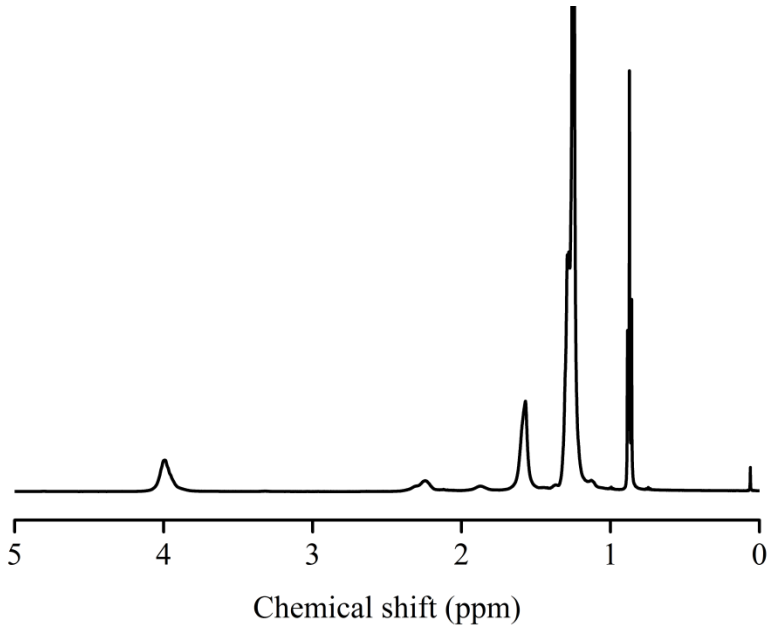

Figure 4.1: Representative ^{1}H-NMR data obtained from poly(stearyl acrylate).

Table 4.1: % meso and racemo dyads in PLAc and PSAc

Polymer	% meso dyads	% racemo dyads
PLAc	39	61
PSAc	36	64

The temperature at which the blend transitioned from transparent to opaque (i.e., the cloud point temperature, T_{cp}) was determined using an optical microscope and the results are shown in Figure 4.2. The blend characteristics are summarized in Tables 4.2 and 4.3.

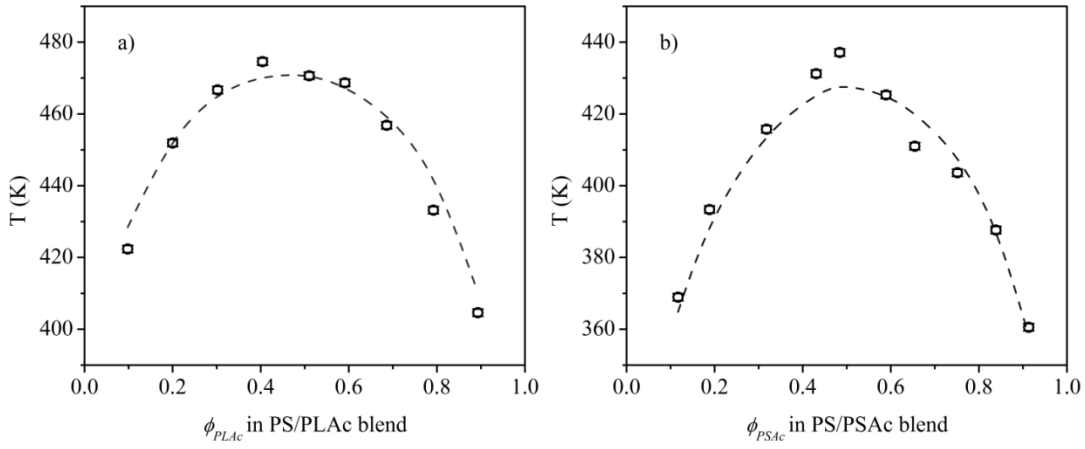

Figure 4.2: Cloud point temperatures (symbols) of a) PS/PLAc blends and b) PS/PSAc blends. The dashed curves represent the Flory-Huggins theory prediction of the location of the binodal curve.

Table 4.2: PS/PLAc blend characteristics and results of cloud point measurements[a]

	ϕ_{PLAc} in blend (at T_{cp})	T_{cp} (K), upon cooling	$N_{w,PS}$ (at T_{cp})	$N_{w,PLAc}$ (at T_{cp})	χ	Error in χ
1	0.098	422.3	58.4	83.8	0.0376	0.0007
2	0.200	451.9	59.3	85.3	0.0316	0.0006
3	0.302	466.7	59.7	86.1	0.0291	0.0006
4	0.404	474.6	59.9	86.5	0.0283	0.0006
5	0.510	470.6	59.8	86.3	0.0280	0.0006
6	0.591	468.7	59.8	86.2	0.0288	0.0006
7	0.686	456.8	59.4	85.6	0.0305	0.0006
8	0.792	433.2	58.7	84.3	0.0342	0.0007
9	0.893	404.6	57.9	82.8	0.0418	0.0008

[a]χ and N are based on a reference volume of 100 Å^3, T_{cp} is the cloud point temperature

Table 4.3: PS/PSAc blend characteristics and results of cloud point measurements[a]

	ϕ_{PSAc} in blend (at T_{cp})	T_{cp} (K), upon cooling	$N_{w,PS}$ (at T_{cp})	$N_{w,PSAc}$ (at T_{cp})	χ	Error in χ
1	0.117	368.9	55.7	49.8	0.0495	0.0011
2	0.188	393.4	56.4	50.5	0.0431	0.0009
3	0.318	415.7	57.0	51.2	0.0378	0.0008
4	0.430	431.2	57.5	51.7	0.0358	0.0008
5	0.484	437.1	57.7	51.8	0.0352	0.0008
6	0.589	425.3	57.3	51.5	0.0358	0.0008
7	0.654	411.0	56.9	51.1	0.0368	0.0008
8	0.751	403.6	56.7	50.8	0.0391	0.0008
9	0.839	387.7	56.2	50.4	0.0434	0.0009
10	0.913	360.6	55.5	49.6	0.0513	0.0011

[a] χ and N are based on a reference volume of 100 Å^3, T_{cp} is the cloud point temperature

The theoretical binadol curves for PS/PLAc and PS/PSAc blends are shown in Figure 4.3.

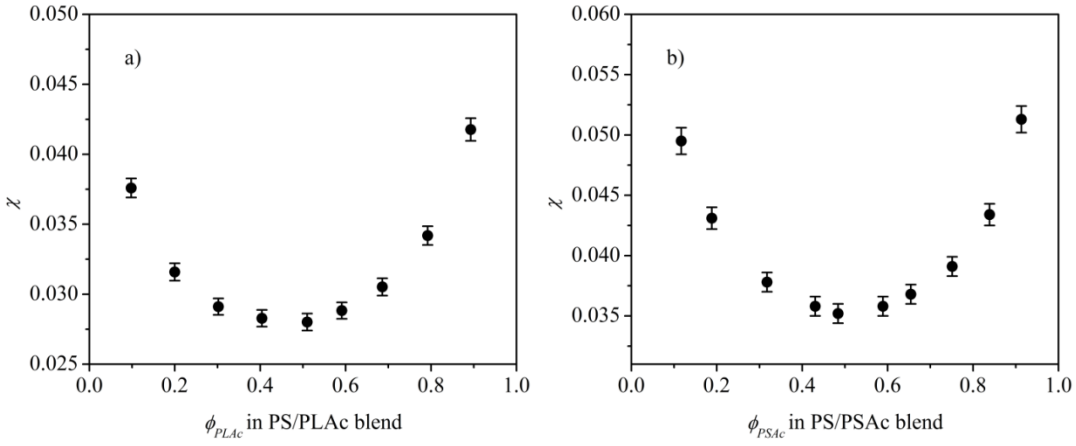

Figure 4.3: Binodal curve determined from Flory-Huggins theory for a) PS/PLAc blends and b) PS/PSAc blends.

A comparison of the cloud point data (Figure 4.2) and the theoretical binodal curve (Figure 4.3) gives the relationship between χ and T, reported in Figure 4.4. The data have been fit to a linear equation (dashed line): $\chi = \frac{34.6}{T} - 0.0451$.

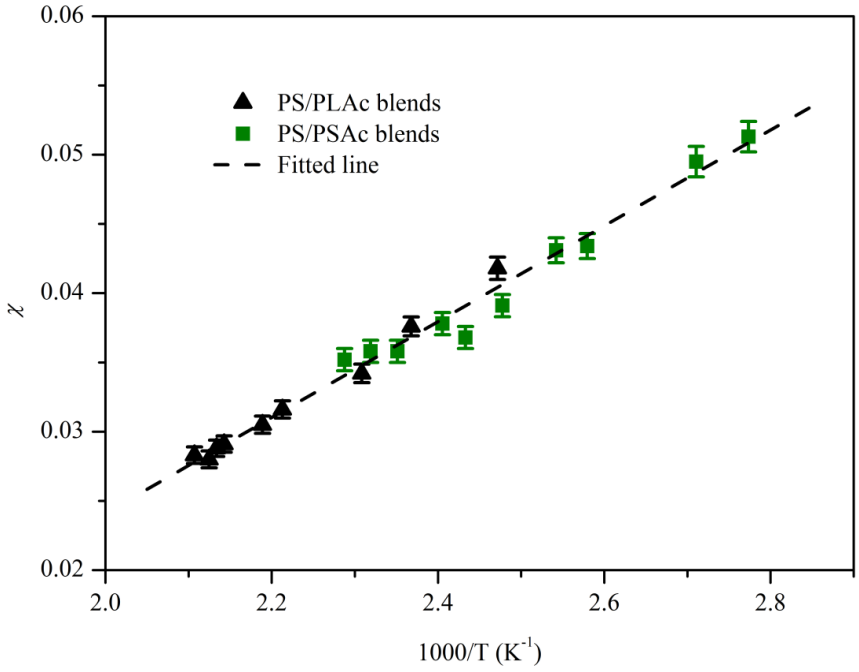

Figure 4.4: χ as a function of inverse temperature for PS/polyacrylate blends from cloud point measurements. χ is based on a reference volume of 100 Å^3. The error bars are included and in many cases are smaller than the data points.

There are three categories of errors to consider in this measurement of χ: 1) error in the molecular weight measurement from GPC; 2) error in the cloud point measurement; 3) error in the thermal expansion coefficient. For the GPC measurement, the error has been found to be within ±2% by multiple measurements. The error in cloud point measurement was within ±1 ºC for all experiments. In this study, we do not quantify the error in the thermal expansion coefficient, which was taken from a literature source. The cumulative error is summarized in Tables 4.2 and 4.3 and shown as error bars in Figure

4.4. The $\chi(T)$ curves for both polyacrylates are consistent with one another, indicating the behavior of $\chi(T)$ is independent on the side chain length of polyacrylates.

4.3. Determination of the χ parameter from the order-disorder transition (ODT) of SAS triblock copolymers

Five series of triblock copolymers were investigated, with the polymer characteristics given in Table 2.1 in chapter 2.

Figure 4.5 shows a representative plot of G' versus T and the T_{ODT} was determined as the intersection of the two extrapolated lines [170].

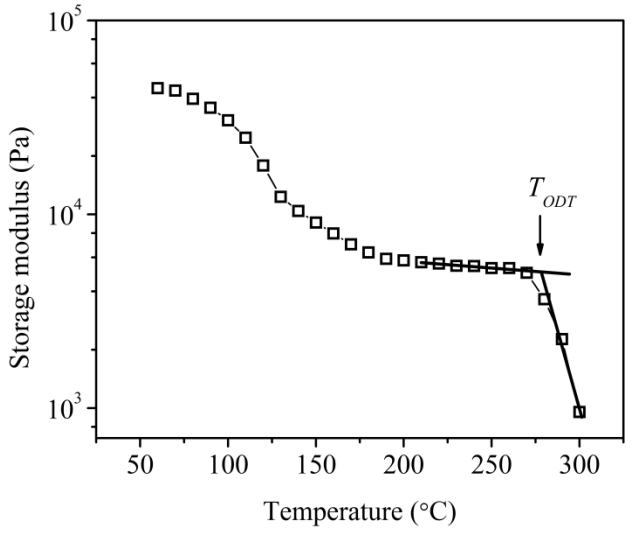

Figure 4.5: Storage modulus as a function of temperature of triblock copolymer.

The theoretical ODT of a triblock copolymer is defined by the composition (volume fraction of each block), and the thermodynamic parameter χN, where N is the number of total repeat units on the triblock copolymer (taken to be N_n in this study) [67]. With knowledge of the triblock copolymer N_n and composition, the predicted χ value at the order-disorder transition for each SAS triblock copolymer was calculated (Table 4.4).

Using the χ value at the ODT and experimental T_{ODT} values, the relationship between T_{ODT} and χ was constructed.

Table 4.4: Summary of χ determined from rheology measurements on SAS

Polymer	T_{ODT} (ºC)[a]	ϕ_{PS} at T_{ODT}[b]	N_n[c,d]	Theoretical χN_n at T_{ODT}[e]	χ at T_{ODT}[b,d]	Error in χb
SAS2-100-23	220.8	0.222	1477.9	35.64	0.0241	0.0011
SAS3-100-17	154.5	0.166	1324.9	50.22	0.0379	0.0019
SAS4-100-18	78.6	0.176	873.5	46.76	0.0535	0.0024
SAS2-76-24	233.7	0.230	1528.3	34.40	0.0225	0.0009
SAS3-76-18	156.9	0.174	1360.9	47.24	0.0347	0.0015
SAS4-73-18	82.8	0.175	881.1	47.22	0.0536	0.0022
SAS2-61-23	219.3	0.219	1491.1	36.12	0.0242	0.0006
SAS3-61-18	161.4	0.173	1358.0	47.84	0.0352	0.0017
SAS4-62-18	83.1	0.174	883.9	47.36	0.0536	0.0024
SAS5-0-24	279.2	0.226	1686.1	34.96	0.0207	0.0009
SAS5-0-21	138.5	0.157	1431.5	54.36	0.0380	0.0018
SAS5-0-17	126.5	0.195	919.5	41.50	0.0451	0.0020
SAS5-0-14	103.5	0.133	1361.8	66.66	0.0490	0.0022
SAS5-0-12	85.3	0.114	1319.1	78.64	0.0596	0.0026

[a] Determined with rheology
[b] Procedure is described in the main text
[c] N_n is the number-average degree of polymerization of the triblock copolymer
[d] Based on a reference volume of 100 Å^3
[e] Determined from theoretical phase diagram given in ref. [67].

There are still many open questions regarding the effects of dispersity on the block copolymer phase diagram [58, 59, 145, 171-174]. We have chosen to compare χ parameters calculated using two different theoretical triblock copolymer phase diagrams determined from self-consistent field theory: 1) the standard phase diagram of a

monodipserse triblock copolymer, described in ref. [67], and 2) the phase diagram for a triblock copolymer containing monodisperse end-blocks and a disperse midblock (Đ = 1.5), described in ref. [172]. Neither theoretical phase diagram is directly applicable to our SAS triblock copolymers, in which the polyacrylate midblock Đ ~ 1.2-1.3, the outerblock PS Đ ~ 1.1 (based upon characterization of PS homopolymers synthesized using the same methods), and the triblock copolymer molecular weight distribution is trimodal.

Figure 4.6 and Table 4.4 show χ versus 1/T for SAS of different midblock compositions (varying the wt % LAc in the midblock), using the theoretical phase diagram of a monodisperse triblock copolymer, taken from ref. [67]. The data have been fit to a linear equation (dashed line): $\chi = \frac{37.4}{T} - 0.0503$.

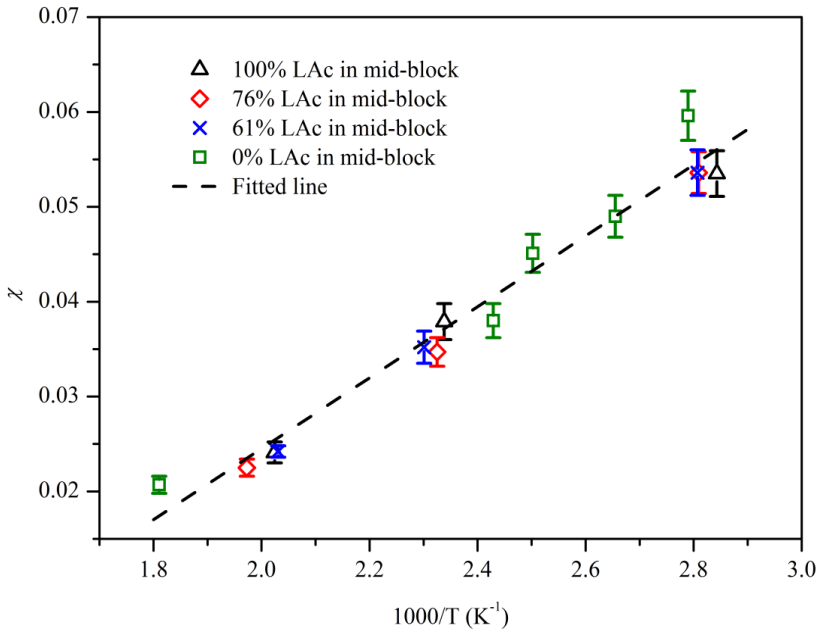

Figure 4.6: χ as a function of inverse temperature determined from ODT measurements on SAS triblock copolymers (based on theoretical phase diagram in ref. [67]).

The calculated χ versus 1/T using the phase diagram for a triblock copolymer containing a disperse midblock (Đ= 1.5), described in ref. [172], is included in Figure 4.7 and Table 4.5.

Table 4.5: Summary of χ determined from rheology measurements on SAS

Polymer	T_{ODT} (ºC)[a]	ϕ_{PS} at T_{ODT} [b]	N_n [c,d]	Theoretical χN_n at T_{ODT} [e]	χ at T_{ODT} [b,d]	Error in χb
SAS2-100-23	220.8	0.222	1477.9	28.82	0.0195	0.00068
SAS3-100-17	154.5	0.166	1324.9	37.14	0.0280	0.00110
SAS4-100-18	78.6	0.176	873.5	35.20	0.0403	0.00158
SAS2-76-24	233.7	0.230	1528.3	28.00	0.0183	0.00070
SAS3-76-18	156.9	0.174	1360.9	35.54	0.0261	0.00096
SAS4-73-18	82.8	0.175	881.1	35.38	0.0402	0.00167
SAS2-61-23	219.3	0.219	1491.1	29.16	0.0196	0.00061
SAS3-61-18	161.4	0.173	1358.0	35.70	0.0263	0.00113
SAS4-62-18	83.1	0.174	883.9	35.54	0.0402	0.00158
SAS5-0-24	279.2	0.226	1686.1	28.50	0.0169	0.00055
SAS5-0-21	138.5	0.157	1431.5	39.00	0.0273	0.00086
SAS5-0-17	126.5	0.195	919.5	32.10	0.0350	0.00137
SAS5-0-14	103.5	0.133	1361.8	44.64	0.0328	0.00126
SAS5-0-12	85.3	0.114	1319.1	49.68	0.0377	0.00142

[a] Determined with rheology
[b] Procedure is described in the main text
[c] N_n is the number-average degree of polymerization of the triblock copolymer
[d] Based on a reference volume of 100 $Å^3$
[e] Determined from theoretical phase diagram given in ref. [172].

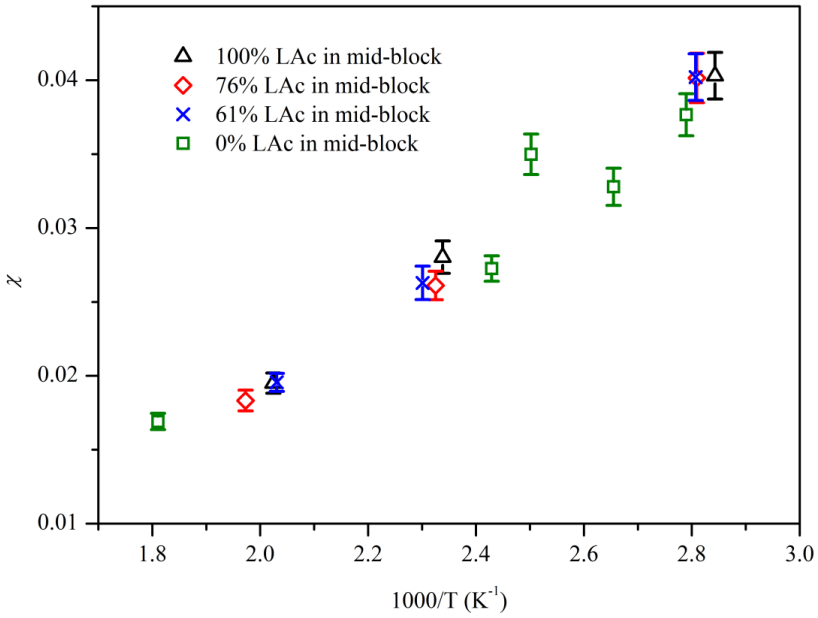

Figure 4.7: χ as a function of inverse temperature determined from ODT measurements on SAS triblock copolymers (based on theoretical phase diagram in ref. [172]).

Regardless of the theoretical phase diagram used in calculation of the χ parameters, it is clear that the $\chi(T)$ curves for all of the triblock copolymers are consistent with one another. The behavior of $\chi(T)$ is thus independent of the midblock composition of the triblock copolymer.

The error in the χ measurement was also evaluated and can be divided into four categories: 1) error in T_{ODT} from the rheology measurement; 2) error in molecular weight and volume fraction measurement from GPC and NMR; and 3) error in the thermal expansion coefficient of each component and 4) error in determining the theoretical χN_n. Multiple measurements of T_{ODT} have been taken on the same sample, and the error in T_{ODT} was within ±1 ºC. Multiple measurements of molecular weight and volume fraction were also performed and the errors for both were within ±2%. We are not able to evaluate the third category in this study, as we are drawing from the literature for the values the

thermal expansion coefficient. The uncertainty in determining χN_n from the theoretical phase diagram is potentially significant, and we have not attempted to quantify this error. The results from the first three categories of errors are summarized in Tables 4.4 and 4.5 and shown as error bars in Figures 4.6 and 4.7.

4.4. Discussion

Figure 4.4 and Figure 4.6 represent the temperature-dependent χ parameters measured for PS and long-chain poly(*n*-alkyl acrylates). The poly(*n*-alkyl acrylates) included in this study are PLAc, PSAc, and poly(LAc-*co*-SAc) random copolymers. Importantly, the poly(*n*-alkyl acrylates) differ in the length of the side-chain on each repeat unit (12 and 18 carbon atoms for PSAc and PLAc, respectively). χ parameters determined from cloud point measurements on binary blends and ODT measurements on triblock copolymers lie on one line in Figures 4.4 and 4.6 (within the error of the χ measurement). This indicates that the length of the side-chain (*n*) of the polyacrylate has little effect on the thermodynamic interactions between PS and the poly(*n*-alkyl acrylates) at large values of *n*.

To explore the side-chain length-dependence of the χ parameter, we have employed group contribution methods to calculate the solubility parameters (δ) of poly(*n*-alkyl acrylates) as a function of the side-chain length, *n*, shown in Figure 4.8. We have followed similar procedures to that described in ref. [151] (using the van Krevelen parameters in ref. [175]). The results of our calculations are in good agreement with refs. [167] and [151], which included side-chain lengths up to $n = 10$. Our calculations indicate that at higher values of n (> 10), the solubility parameter continues to decrease slightly

with increasing *n*. Additionally, we have calculated δ of PS using the same methods (δ = 9.3).

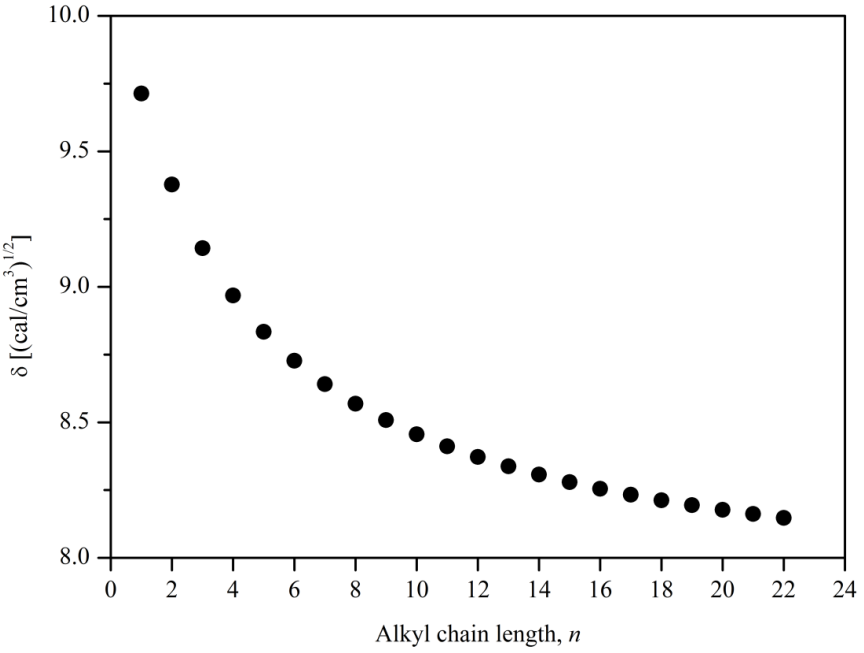

Figure 4.8: Solubility parameter (δ) of poly(*n*-alkyl acrylates) as a function of alkyl chain length (*n*)

The χ parameter was calculated using

$$\chi = \frac{v_{ref}}{kT}(\delta_1 - \delta_2)^2, \qquad \text{(eq. 4.2)}$$

where δ_1 and δ_2 are the solubility parameters of components 1 and 2, the reference volume was chosen to be 100 Å^3, and *k* is the Boltzmann constant.

Figure 4.9 compares the χ parameter at 120 °C for PS and poly(*n*-alkyl acrylates) as a function of the alkyl side-chain length, *n*. We have included χ parameters in Figure 4.9 from three different sources: 1) calculated from the solubility parameters given in Figure 4.8 (using eq. 4.2), 2) experimentally measured for short-chain poly(*n*-alkyl acrylates), reported in ref. [151] (we have calculated the χ parameter using the binary

interaction energy density reported in ref. [151], and a reference volume of 100 Å^3), and 3) experimentally measured for long-chain poly(*n*-alkyl acrylates) in our study (i.e., Figures 4.4 and 4.6).

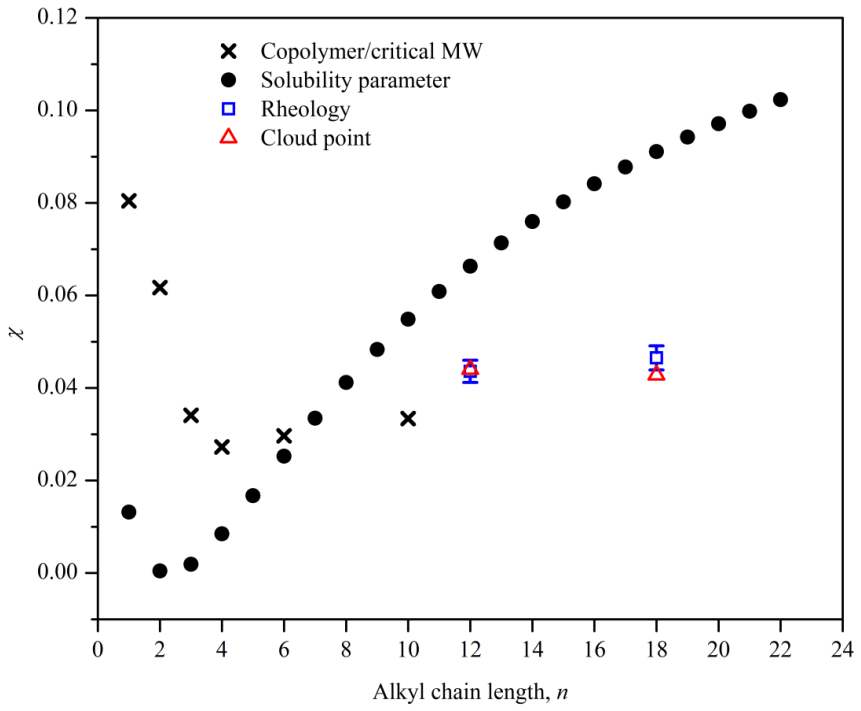

Figure 4.9: Effect of alkyl chain length on χ of PS and poly(*n*-alkyl acrylates) (v_{ref} = 100 Å^3).

It is clear that there are strong deviations between the χ parameters calculated using solubility parameter theory and the experimentally measured values, consistent with the conclusions of ref. [151] for poly(*n*-alkyl acrylates) with $n \leq 10$. Other studies have compared the solubility parameters for a variety of polymers determined experimentally (i.e., through PVT measurements, scattering, cloud point experiments, inverse gas chromatography, among other methods) with those predicted from group contribution methods. In some cases there is good agreement [175-178], and in other cases there are significant deviations between theory and experiment [175, 179-181]. We

also note that prediction of the χ parameter from solubility parameter theory (regardless of the source of the solubility parameter) does not always agree with direct measurement of the χ parameter, most notably in systems with a negative χ parameter [182, 183]. The results of our study indicate that group contribution methods, combined with solubility parameter theory, do not capture the thermodynamic behavior in blends of polystyrene and long-chain polyacrylates.

The experimentally measured χ parameters reported here are effective χ parameters, which do not strictly follow the Flory-Huggins definition of χ, but are fitting parameters that also account for additional contributions to the free energy of mixing not described by Flory-Huggins Theory. Oftentimes the empirical equation used in our study to describe the temperature-dependence of χ ($\chi = A/T + B$) is thought of in terms of an enthalpic contribution (i.e., A/T) and an entropic contribution (i.e., B). It may be more appropriate to directly compare the experimental enthalpic A/T term to the predictions from solubility parameter theory (i.e., eq. 4.2). If we consider only the enthalpic A/T portion of our experimentally measured $\chi(T)$ equations, we obtain similar values at 120 °C for polyacrylates with n = 12 and 18 (A/T = 0.095 and 0.090 for PLAc and PSAc, respectively; Figure 4.10).

Though these values are closer in magnitude to the χ parameters predicted by the group contribution methods for n = 12 and 18 (0.066 and 0.091 for PLAc and PSAc, respectively), there is still an important disconnect between the theory and experiment: the group contribution method predicts that χ increases with increasing n (at high n), whereas the experimental measurement (even when only considering the enthalpic A/T term) shows that χ is independent of n (at high n). Furthermore, the observation of a non-

negligible B term is oftentimes associated with the presence of additional contributions to the entropy of mixing, such as differences in molecular packing of the pure component and mixed states. These effects may be important in these systems, but the magnitude of the B term in the χ(T) equation is similar for polyacrylates with n = 12 and 18 (B = -0.051 and -0.047 for PLAc and PSAc, respectively).

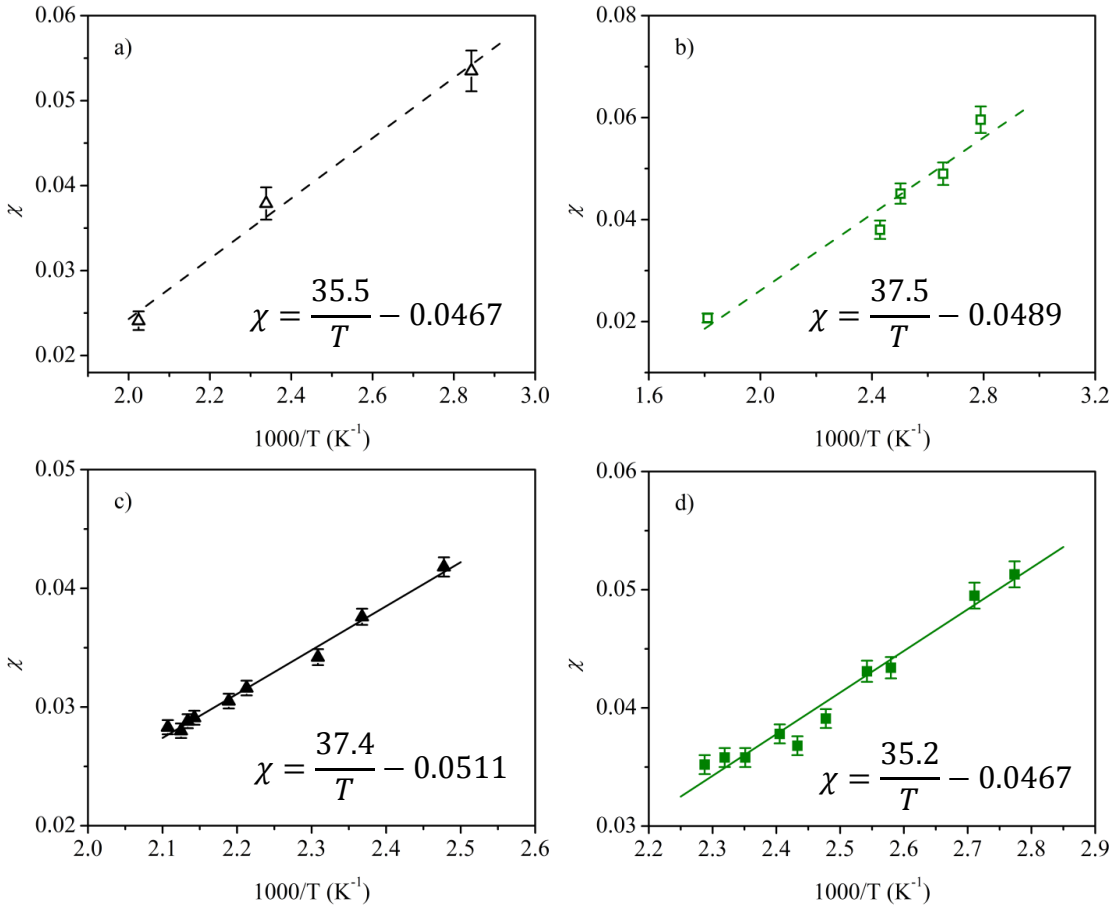

Figure 4.10: Linear fit of $\chi(T)$. a) PS/PLAc using ODT measurements on SAS; b) PS/PSAc using ODT measurements on SAS; c) PS/PLAc using cloud point measurements; and d) PS/PSAc using cloud point measurements.

The χ parameters determined from binary blend and block copolymers are quite similar to one another, though the level of quantitative agreement between them depends on the choice of theoretical phase diagram for the triblock copolymers (i.e., compare

Figures 4.6 and 4.7). The ability to generate a linear curve describing the temperature-dependence of χ (i.e., χ = A/T + B), as shown in Figures 4.4 and 4.6, through measurements on blends and block copolymers of varying composition, which contain polymers of varying molecular weight, indicates that these χ parameters are relatively insensitive to molecular weight and composition effects.

4.5. Concluding remarks

Two independent methods were employed to calculate the Flory-Huggins interaction parameter (χ) between polystyrene (PS) and long-chain poly(*n*-alkyl acrylates) (PLAc and PSAc): cloud point measurements on binary blends and characterization of the order-disorder transition of triblock copolymers. Importantly, the poly(*n*-alkyl acrylates) differ in the length of the alkyl side-chain on each repeat unit (12 and 18 carbon atoms for PSAc and PLAc, respectively). The χ parameter was found to be independent of the alkyl side-chain length (*n*) for large values of *n*. This behavior is in stark contrast to the *n*-dependence of the χ parameter predicted from solubility parameter theory. To our knowledge, this is the first study to explore the thermodynamic interactions between PS and long-chain poly(*n*-alkyl acrylates) with $n > 10$. In addition, the χ parameter appears to be relatively insensitive to polymer chain architecture, molecular weight, and composition in this system, as the temperature-dependence of the χ parameter was extracted from blends and block copolymers in which all of these parameters were varying. This work lays the foundation for future studies to examine blends or block copolymers consisting of long-chain polyacrylates and various other constituents, including the examination of systems containing multiple components with long side-chains. The implementation of polymers derived from fatty acids and vegetable

oils in multicomponent materials, such as blends and copolymers, will rely upon a detailed understanding of the thermodynamic interactions in such systems.

The characterization of the Flory-Huggins interaction parameter is an essential first step to the design of microstructured or nanostructured materials in multicomponent systems, guided by predictions of theories such as Self-Consistent Field Theory [184-186]. Also our work highlights the necessity for alternative theories to understand the origins of the behavior in this class of materials.

In Chapter 3, we have demonstrated that the SAS triblock copolymers have tunable properties including melting temperature of the midblock, viscosity of the midblock and melt viscosity of triblock copolymers, and the tensile properties. And in Chapter 4, the investigation of the thermodynamic interactions between PS and PA has revealed that side chain length in PLAc and PSAc doesn't affect the χ parameter with PS. Thus the side chain length could be utilized as an efficient route to tailor the properties of the triblock copolymers without changing the interactions between the midblock and end blocks.

Chapter 5

Shear Alignment of Poly(styrene-*b*-(lauryl-*co*-stearyl acrylate)-*b*-styrene) Triblock Copolymers

Block copolymers with well-resolved morphologies are quite important in industry; however, their spontaneously self-assembled nanostructures contain randomly oriented ordered grains that do not usually exhibit long-range order. From a macroscopic perspective, the material is isotropic. By applying external forces, i.e., shear (steady shear or large amplitude oscillatory shear (LAOS)), electrical fields [76, 77], magnetic fields [78], or surface patterns [79] could lead to the desired alignment of the BCPs. Control of morphology is the key to manipulating the properties of the multi-component and multi-phase polymer systems.

In this study, we will demonstrate the alignment of a triblock copolymer melt derived from fatty acids under LAOS. The morphology and orientation will be probed through small-angle X-ray scattering (SAXS). The effect of temperature, shear frequency and shear strain will be investigated.

5.1. Morphology of the triblock copolymer prior to shearing

The characteristics of the triblock copolymer (SAS2-76-24) in this study were summarized in Table 2.1 in chapter 2. The order-disorder transition of this polymer is 233.7 °C. The morphology of the compression molded polymer sample (prior to shearing) was investigated by both SAXS and TEM. Figure 5.1 shows the 2D SAXS pattern and the isotropic scattering indicates the random placement of the grains. The 1D SAXS profile is shown in Figure 5.2 and we have included the predictions (arrows) of the higher

order peak locations for FCC, HCP, BCC, cylinders and lamellae along with the 1D date. It can be seen that it is not consistent with any of the common single morphology.

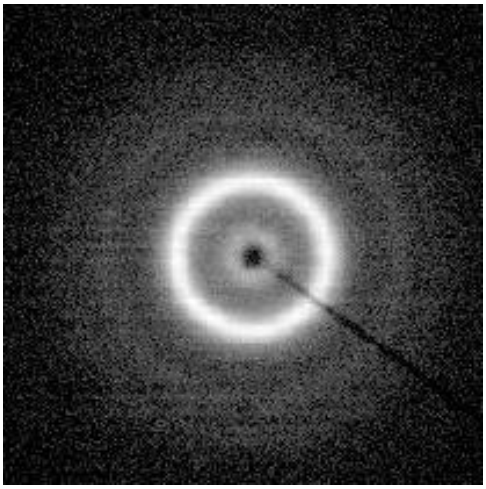

Figure 5.1: 2D SAXS scattering pattern for sample prior to shearing.

The TEM micrograph in Figure 5.2 reveals PS spheres in a PA matrix which lack short or long-range order.

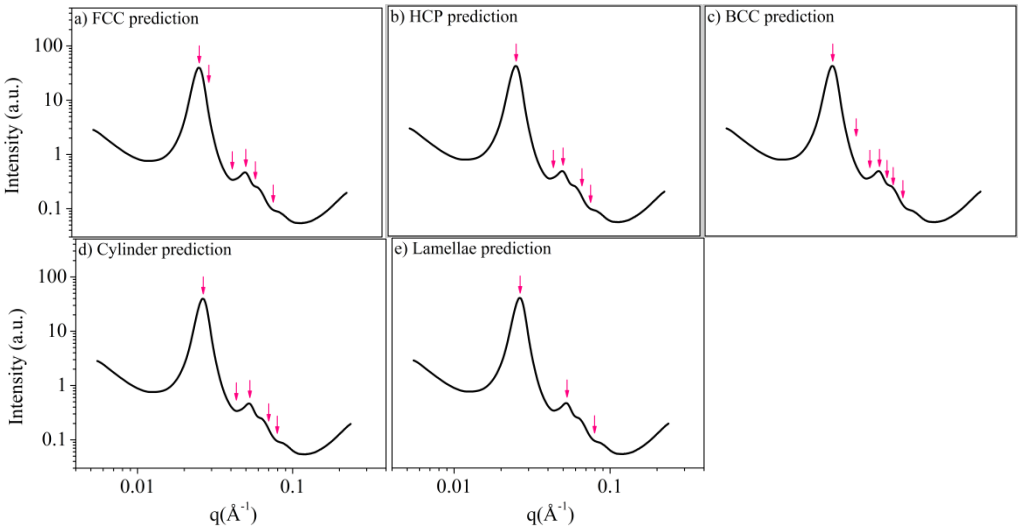

Figure 5.2: 1D SAXS pattern for sample prior to shearing. Arrows in a-e shows the prediction of intensity peak locations from structure of FCC spheres (a), HCP spheres (b), BCC spheres (c), HCP cylinders (d), and lamellae (e).

The TEM micrograph in Figure 5.3 reveals PS spheres in a PA matrix which lack short or long-range order.

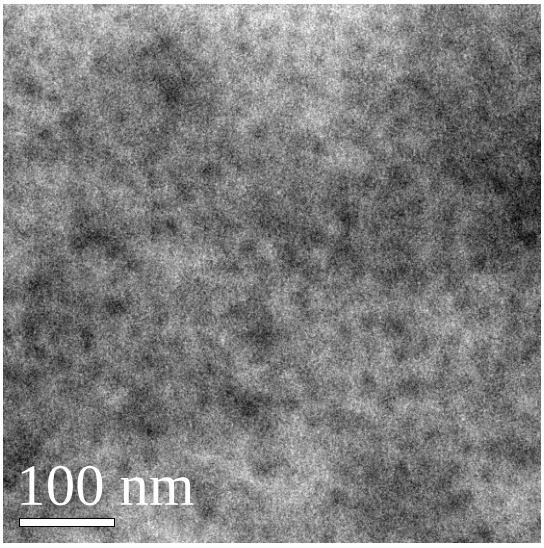

Figure 5.3: TEM image for SAS triblock copolymer at room temperature prior to LAOS.

5.2. Influence of frequency and temperature on the shear alignment

Many studies have shown that shear rate (or frequency) is a very important parameter in changing the orientation of the grains [74, 85-87]. Three oscillatory frequencies, 1 rad/s, 10 rad/s and 100 rad/s, were employed to investigate the influence of the frequency on the alignment behavior. On the sample disk, three samples were taken at shear strains of 0%, 50% and 90%.

The 2D SAXS diffraction patterns are summarized in Figure 5.4. The sample at the center was not aligned because no local shear was applied (γ=0%). The samples at 50% and 90% shear strain showed anisotropic hexagonal patterns. Thus, we can conclude that the orientation is similar in the range of shear frequency studied.

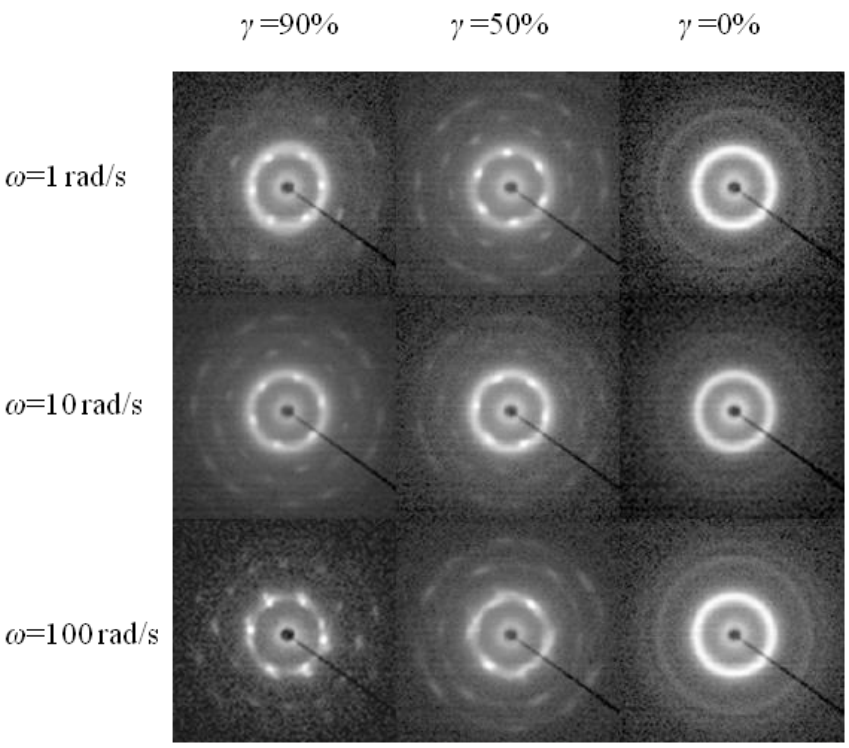

Figure 5.4: Representative 2D SAXS images obtained after LAOS at 180 ºC with an applied strain of 100%. The X-ray beam is in the velocity gradient direction.

Temperature is another important parameter governing the orientation in shear-aligned block copolymers [85, 103-105]. LAOS at 210 ºC was performed at three different frequencies; all samples remained unaligned. The results are presented in Figure 5.5. The alignment temperature of 210 ºC is very close to the ODT of this polymer (233.7 °C), and therefore LAOS is not efficient in aligning the grains under these conditions.

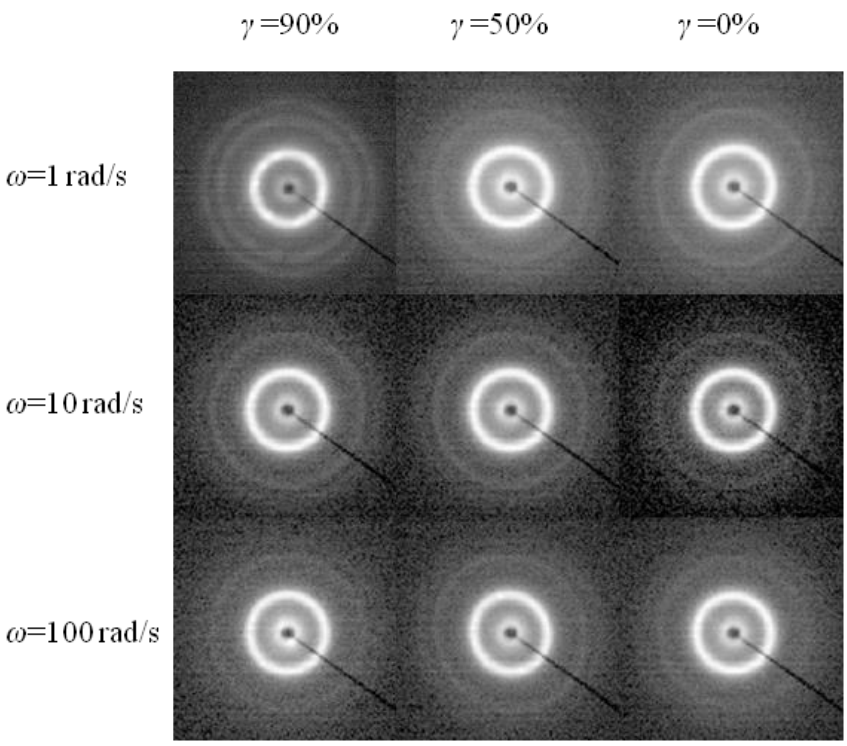

Figure 5.5: Representative 2D SAXS images obtained after LAOS at 210 ºC with an applied strain of 100%. The X-ray beam is in the velocity gradient direction.

Shear frequency has little effect on the alignment behavior and temperature places a significant role in the ordering. Detailed analysis of the shear alignment will be discussed in the next section. We have chosen a shear frequency of 1 rad/s and temperature of 180 ºC.

5.3. Analysis of data obtained in the velocity gradient, velocity, and vorticity directions

LAOS was performed at 180 ºC (53.7 ºC below T_{ODT}), with a strain of 100% and frequency of 1 rad/s. On the sample disk, five samples were taken and subject to measurement with SAXS beam in the velocity gradient, vorticity and velocity directions (Figure 5.6).

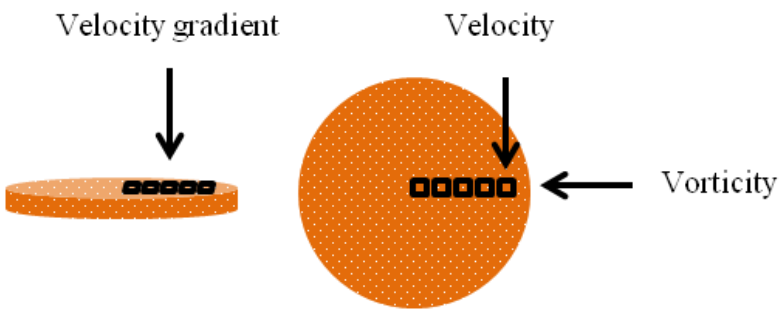

Figure 5.6: Schematic for sample location and x-ray beam direction.

The local shear strain of the three positions were calculated as

$$\gamma = \frac{r}{R} \times 100\%, \qquad \text{(eq. 5.1)}$$

where r is the distance from the center, R is the radius of the sample disc and 100% is the shear rate at the edge of the sample disc. The shear strains at the five locations were: 16%, 32%, 48%, 64% and 80%.

The 2D SAXS diffraction patterns are summarized in Figure 5.7. A strain of 16% was not sufficient to produce a well-aligned structure. When the shear rate increased, the sample became well-aligned, showing anisotropic diffraction patterns in all three shear directions (velocity gradient, velocity and vorticity directions). There are few differences in the scattering patterns obtained under different shear strains (in the range of 32-80% strain) and therefore we are going to present the determination of the morphology and orientation using the data obtained at a shear strain of 48% as a representative sample.

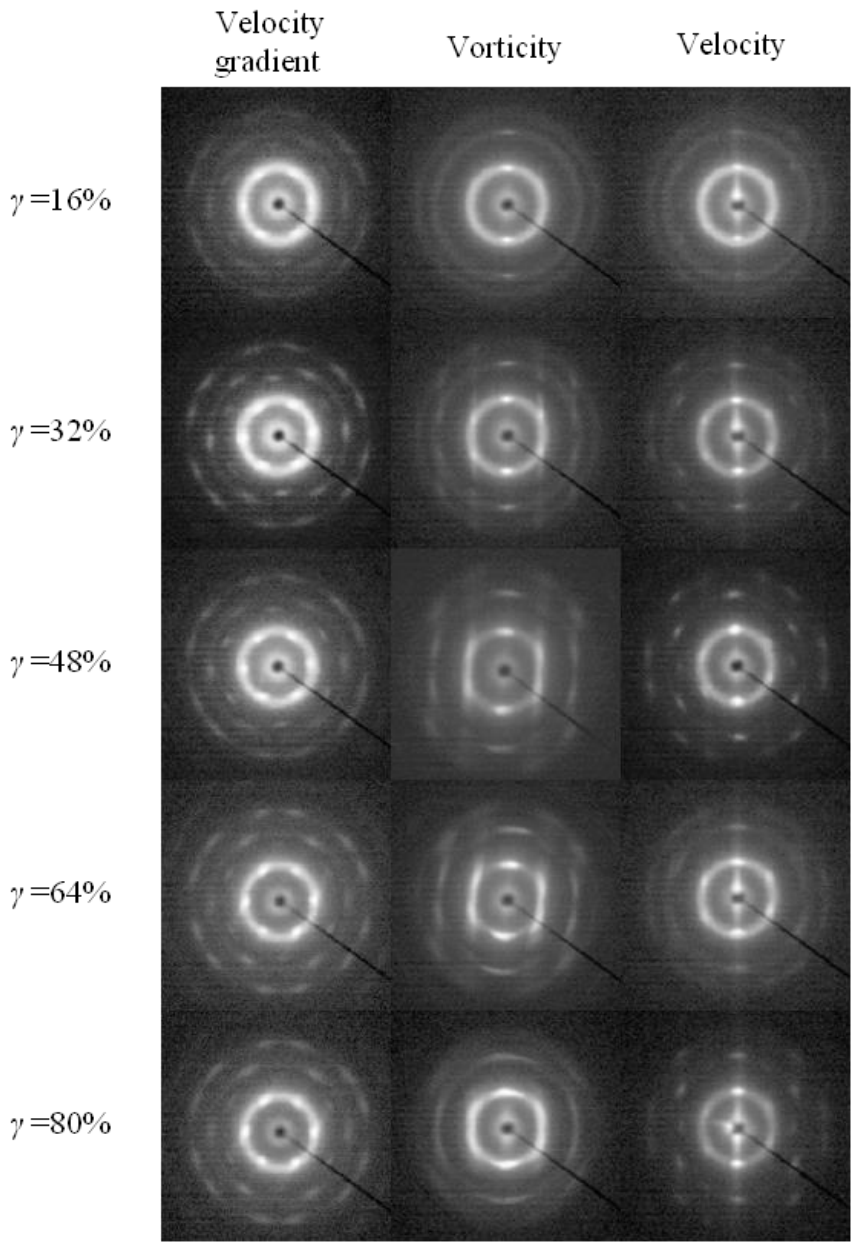

Figure 5.7: 2D SAXS data obtained after LAOS was applied to SAS2-76-24 at 180 ºC with an applied strain of 100%. The shear strain indicated on the left denotes the local strain at each sample position.

We will first discuss the data obtained from SAS2-76-24 in the velocity gradient direction, shown again in Figure 5.8a (at a local strain of 48%).

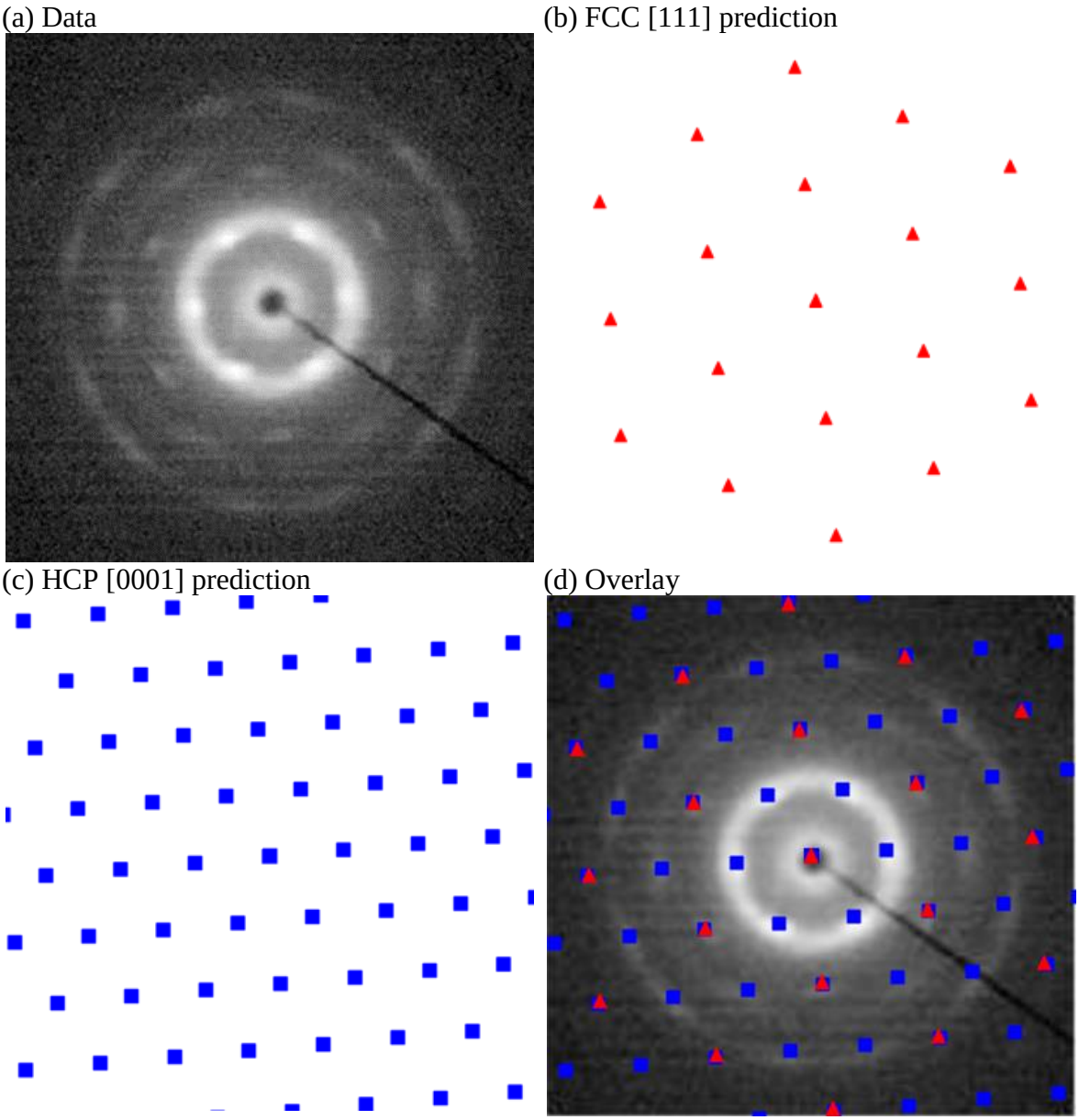

Figure 5.8: 2D SAXS data obtained along the velocity gradient direction. SAS2-76-24 sheared at 180 °C and the local strain is 48%.

A clear hexagonal symmetry extending up to 4-5 orders was observed. This scattering pattern has been observed in shear-oriented colloidal or micellar solution systems and has been assigned to the coexistence of the close-packed face-centered cubic, FCC, {111} planes and the hexagonally close packed, HCP, {0001} planes, aligned in the

shear plane [103, 104, 106-108]. The inner six spots were attributed to the HCP structure and the second order spots were attributed to a combination of HCP and FCC structures. Figure 5.8b gives the prediction of the interference pattern obtained from an FCC unit cell viewed in the [111] direction and Figure 5.8c presents the prediction of the interference pattern obtained from the HCP unit cell viewed in the [0001] direction. Both predictions are overlaid with our data in Figure 5.8d. The azimuthal angle dependence of the first-order diffraction maximum is shown in Figure 5.9 (obtained from the 2D data shown in Figure 5.8a), and it can be seen that the angular spacing is 60° between peak maxima and the intensities of the six spots are comparable, as expected for hexagonal packing.

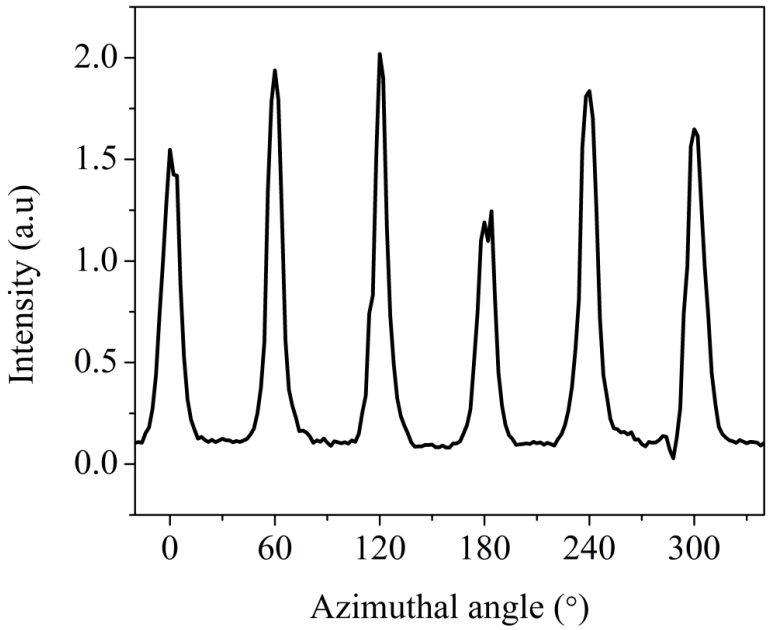

Figure 5.9: Representative azimuthal angle dependence of the first-order diffraction maxima in the velocity gradient direction. SAS2-76-24 sheared at 180 °C and the local strain is 48%.

Figure 5.10 illustrates the determination of structure and orientation viewed in the vorticity direction. The data obtained from SAS2-76-24, at a local strain of 48%, are shown in Figure 5.10a. Previous studies on shear-aligned spherical block copolymer micellar solutions have reported the presence of coexisting FCC and HCP structures (viewed along the $[11\bar{2}]$ and $[10\bar{1}0]$ directions in the vorticity direction, for FCC and HCP unit cells, respectively), for which the interference patterns are identical [103, 104, 106]. In Figure 5.10b, a superposition of these two unit cell orientations on our data are shown. However, these unit cell orientations alone do not fully represent the data taken in the vorticity direction, as shown in Figure 5.10a. In the inner ring, there are four additional spots, also observed in previous studies, and attributed to the presence of a tilted FCC {110} structure [103, 104, 106]. Figure 5.10d provides an overlay of the predictions from all three planes with the data obtained in the vorticity direction (also shown in Figure 5.10a), showing good agreement. It is important to note that the intensity of the spots obtained from the FCC unit cell viewed along the [110] are quite low compared to that obtained from the FCC unit cell viewed along the $[11\bar{2}]$ direction and the HCP unit cell viewed along the $[10\bar{1}0]$ direction, which was also observed in refs. [103, 104, 106]. The azimuthal angular dependence of the first-order diffraction maximum is shown in Figure 5.11 and it can be seen that the relative intensities of the peaks attributed to the FCC unit cell viewed along the [110] direction are about 6% of those attributed to the HCP and FCC unit cells (viewed along the $[10\bar{1}0]$ and FCC $[11\bar{2}]$ directions, respectively).

(a) Data

(b) FCC [$11\bar{2}$] prediction (red triangle)
HCP [$10\bar{1}0$] prediction (blue square)

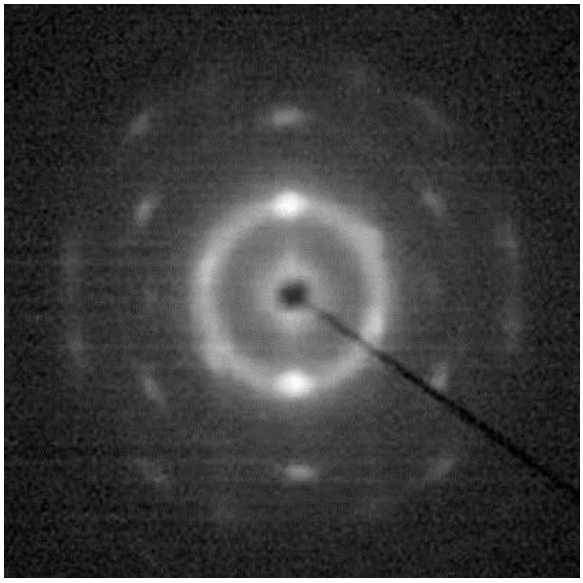

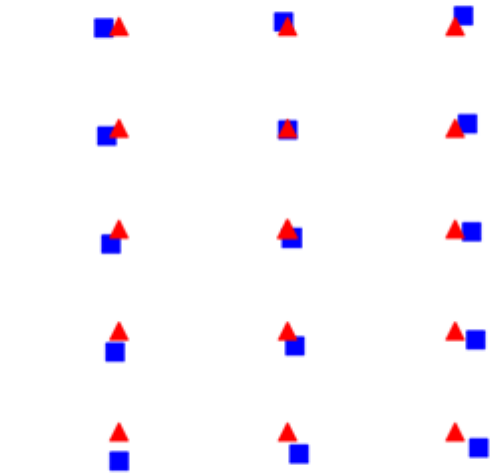

(c) FCC [110] prediction

(d) Overlay

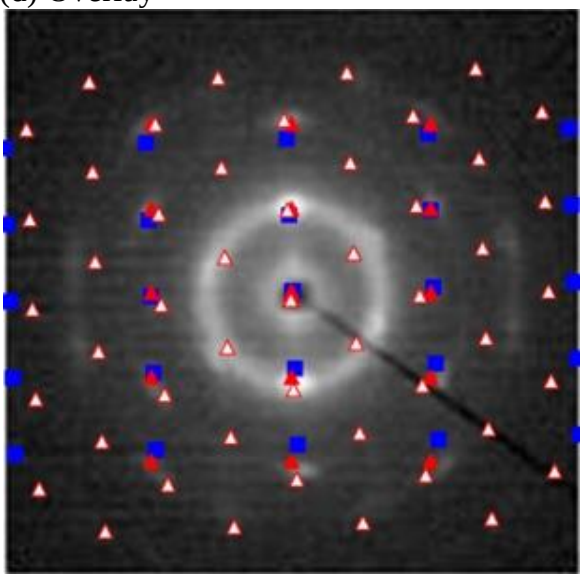

Figure 5.10: 2D SAXS data obtained along the vorticity direction. SAS2-76-24 sheared at 180 °C and the local strain is 48%.

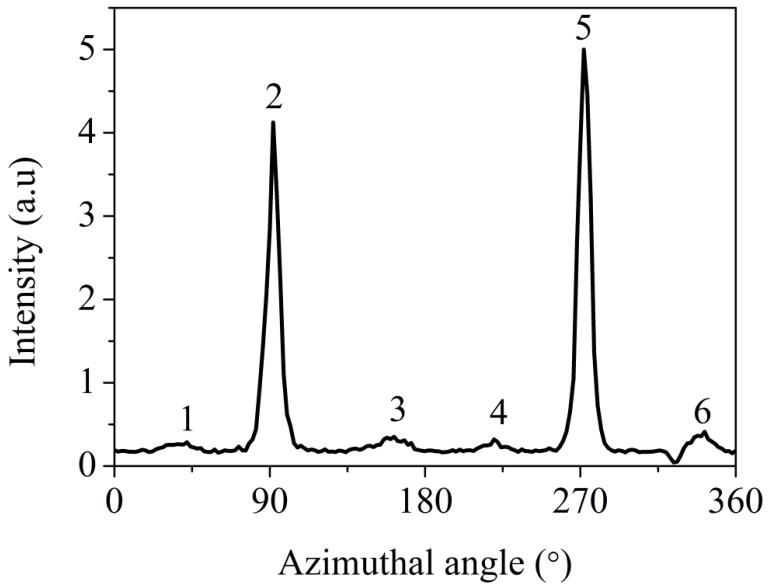

Figure 5.11: Azimuthal angle dependence of the first-order diffraction maxima in the vorticity direction. SAS2-76-24 sheared at 180 °C and the local strain is 48%. Peaks 1, 3, 4, and 6 are from FCC [110]; peaks 2 and 5 are from FCC [$11\bar{2}$] and HCP [$10\bar{1}0$].

Thus far, our data and analysis are quite consistent with that reported in refs. [103, 104, 106] for spherical block copolymer micellar solutions. In the previous studies, the presence of the FCC structure with {111} planes aligned in the shear direction could not be distinguished from that of the HCP structure with {0001} planes aligned in the shear direction: the data and analysis shown for these two unit cell orientations in Figures 5.8 and 5.10 (i.e., blue squares and red triangles) are almost identical to one another. (Note that the presence of the additional tilted FCC structure with the FCC {110} plane viewed in the vorticity direction was required to explain the additional spots observed in the vorticity direction). In prior studies, data were obtained in the velocity gradient and vorticity directions on block copolymer micellar solutions using a combination of two carefully designed shear cells [103, 104, 106]. In our study on triblock copolymer TPE melts, it is possible to take SAXS measurements in all three directions after removing the

solid sample from rheometer, which provides a more comprehensive analysis of the identification and orientation of the structures.

We will now discuss data obtained in the velocity direction, which has not been reported in prior studies. The SAXS data obtained in the velocity direction are presented in Figure 5.8. We will first discuss the predictions in the velocity direction for the case where the FCC {111} planes and the HCP {0001} planes are aligned along the shear plane, i.e consistent with the analysis previously. In this case, the FCC unit cell is viewed in the velocity direction along the $[1\bar{1}0]$ direction and the HCP unit cell is viewed along the $[\bar{2}110]$ direction (these two directions are chosen as they are perpendicular to the shear gradient and vorticity directions identified in Figure 5.8 b and c and Figure 5.10b). The resulting predicted SAXS patterns are shown for the velocity direction in Figure 5.12b and Figure 5.12c for FCC and HCP, respectively.

We must also consider the tilted FCC structure that was identified in the vorticity direction (i.e., the {110} plane is viewed in the vorticity direction, as discussed before), following ref. [103, 104, 106]. In this case, the appropriate direction to view the FCC unit cell in the velocity direction is also the $[1\bar{1}0]$ direction. Therefore, both FCC orientations will show the $\{1\bar{1}0\}$ planes aligned in the velocity direction. The predicted SAXS pattern is shown in Figure 5.12c for both FCC orientations.

The comparison of the predictions and data are shown in Figure 5.12d. It is apparent that the HCP unit cell viewed along the $[\bar{2}110]$ direction matches the scattering data shown in Figure 5.12a, but the predictions for the FCC unit cell viewed in the $[1\bar{1}0]$ directions are quite different from the data. We note that we have also considered the presence of twinned FCC structures, such as those proposed for soft colloidal crystal

systems by Forster et al. with the velocity gradient direction viewed along the FCC [111] axis and the velocity direction viewed along the FCC [$1\bar{1}0$] axis [187]. However, the predicted diffraction patterns reported in ref. [187] are not consistent with our data.

(a) Velocity

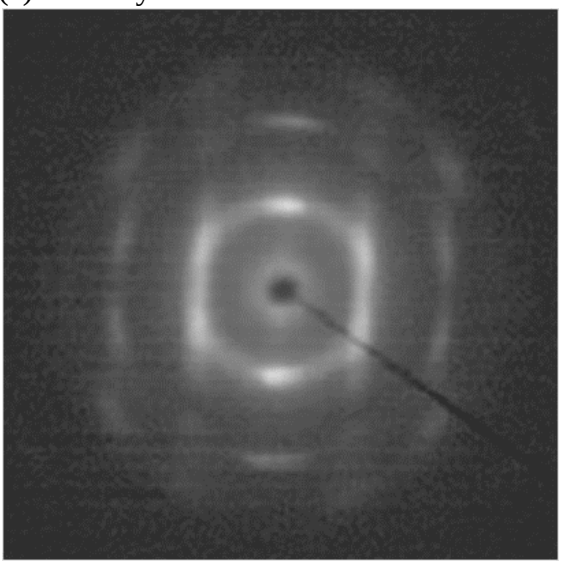

(b) FCC [$1\bar{1}0$] prediction

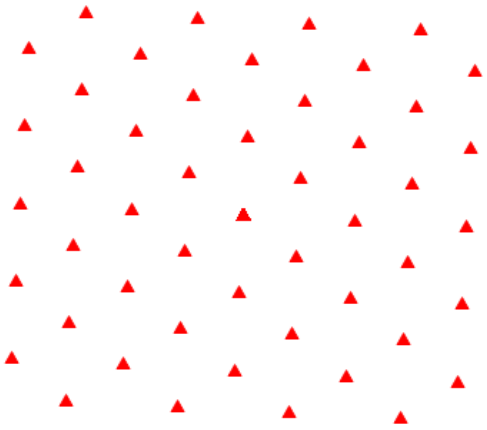

(c)
HCP [$\bar{2}110$] prediction

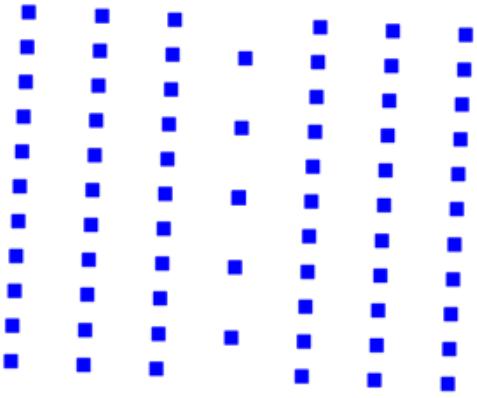

(d) Overlay

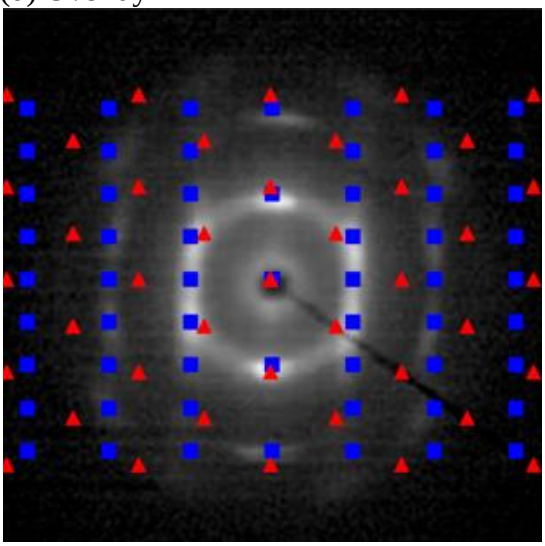

Figure 5.12: 2D SAXS data obtained along the velocity direction. SAS2-76-24 sheared at 180 °C and the local strain is 48%.

Viewing the overlay of the data and predictions for the HCP unit cell in the three directions, it can be seen that both the velocity gradient and velocity directions could be explained solely by the presence of the HCP structure. The only issue lies in the vorticity direction where the four additional spots in the primary diffraction ring cannot be attributed to the HCP structure viewed along the $[10\bar{1}0]$ direction. The additional presence of the tilted FCC unit cell viewed along the [110] axis fully explains the data presented in Figure 5.10 for the vorticity direction. The question remaining is, which directions of the tilted FCC unit cell should be viewed in the velocity gradient and velocity directions? In the discussion above, following prior studies, we discussed the implications of the FCC unit cell viewed in the $[1\bar{1}0]$ direction for the data obtained in the velocity direction, which were not consistent with one another. However, if we simply rotate the unit cell by 90°, the agreement between the data and prediction are much improved, with the velocity gradient direction viewing the FCC unit cell in the $[1\bar{1}0]$ direction and the velocity direction viewing the FCC unit cell in the [001] direction. Figures 5.13, 5.14, and 5.15 show the comparison of the data in all three directions with the predictions of the FCC and HCP structures, oriented with the $\{1\bar{1}0\}$ FCC planes and {0001} HCP planes aligned in the shear plane.

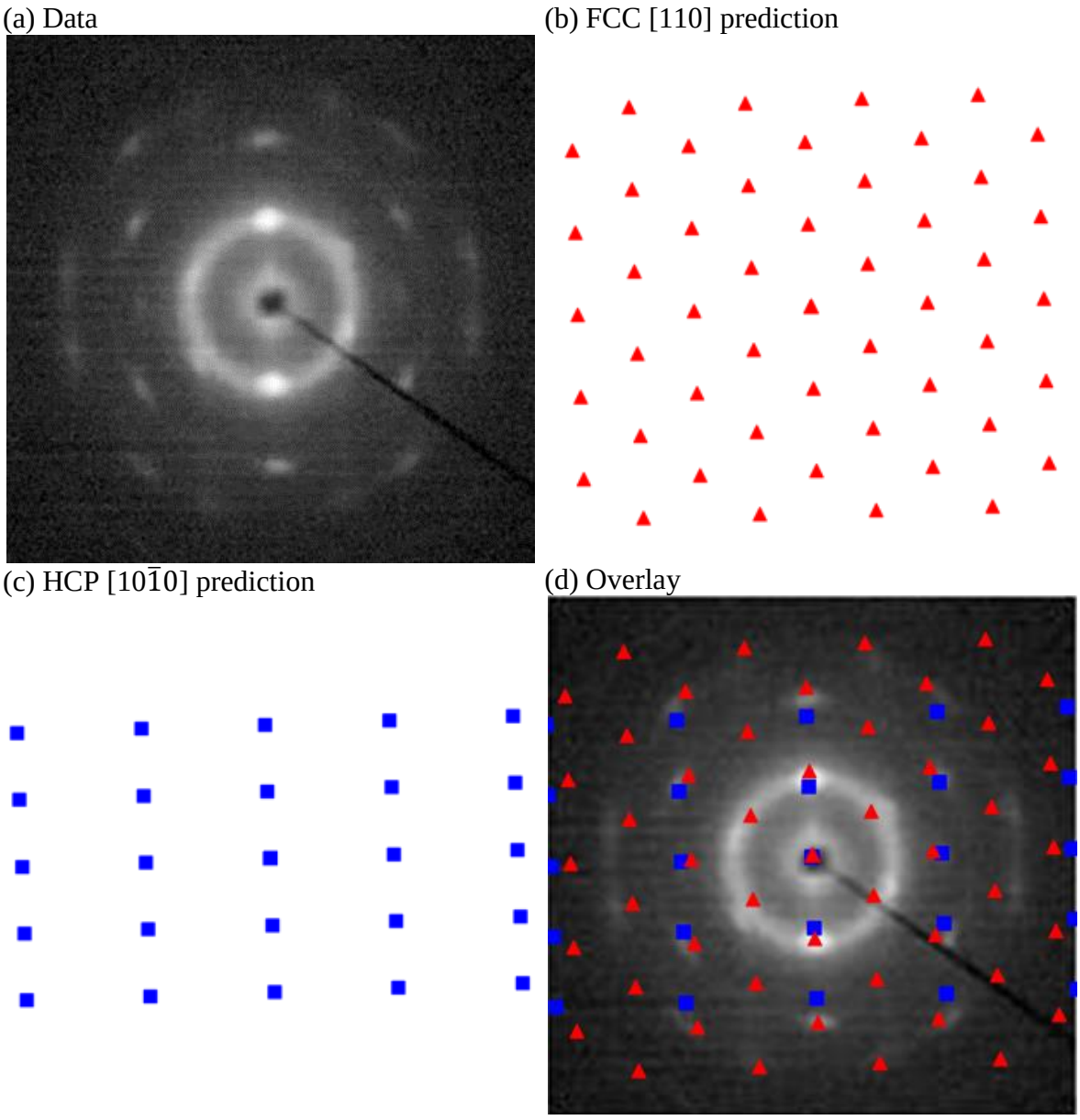

Figure 5.13: 2D SAXS data obtained along the vorticity direction. SAS2-76-24 sheared at 180 °C and the local strain is 48%.

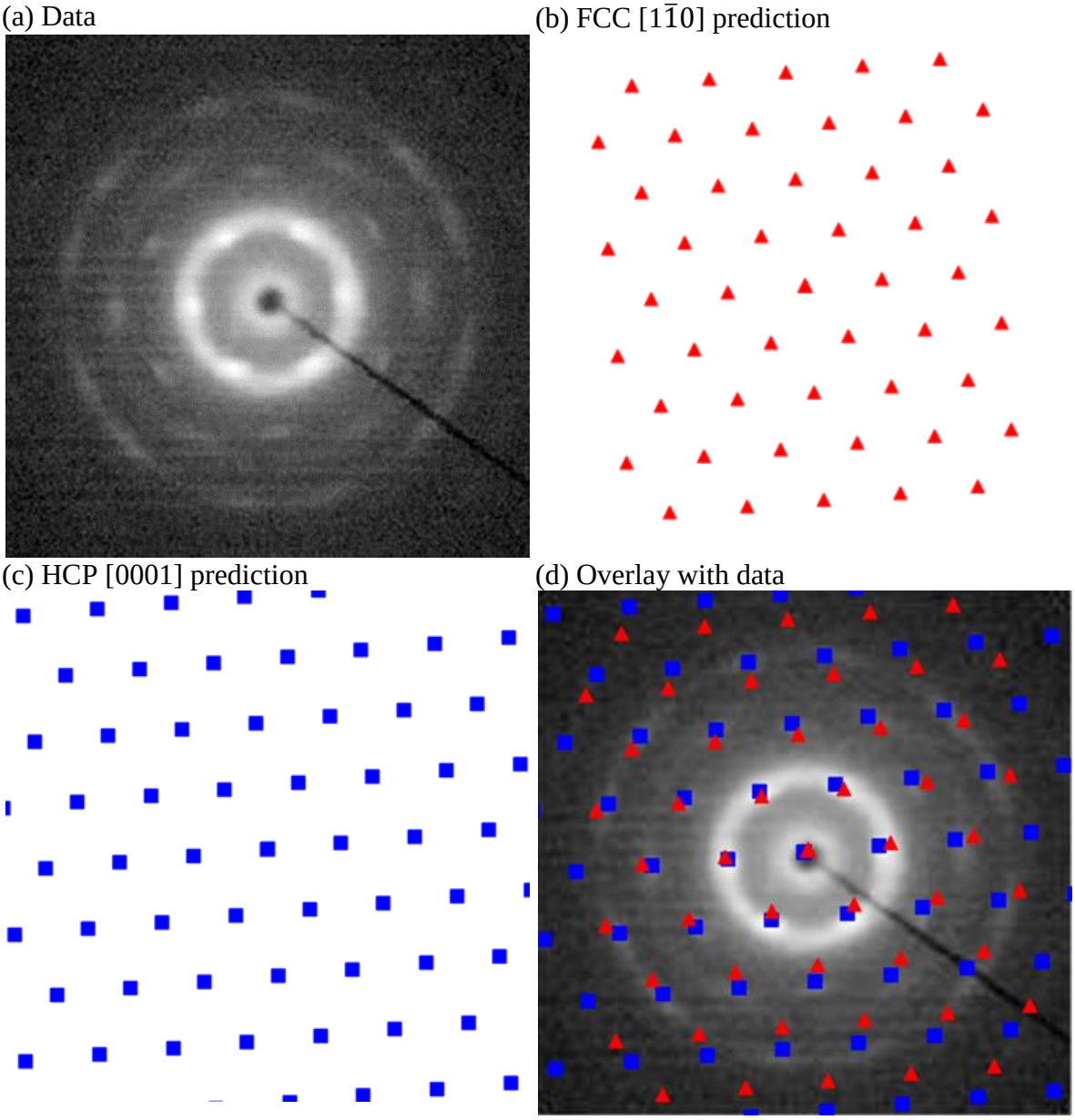

Figure 5.14: 2D SAXS data obtained along the velocity gradient direction. SAS2-76-24 sheared at 180 °C and the local strain is 48%.

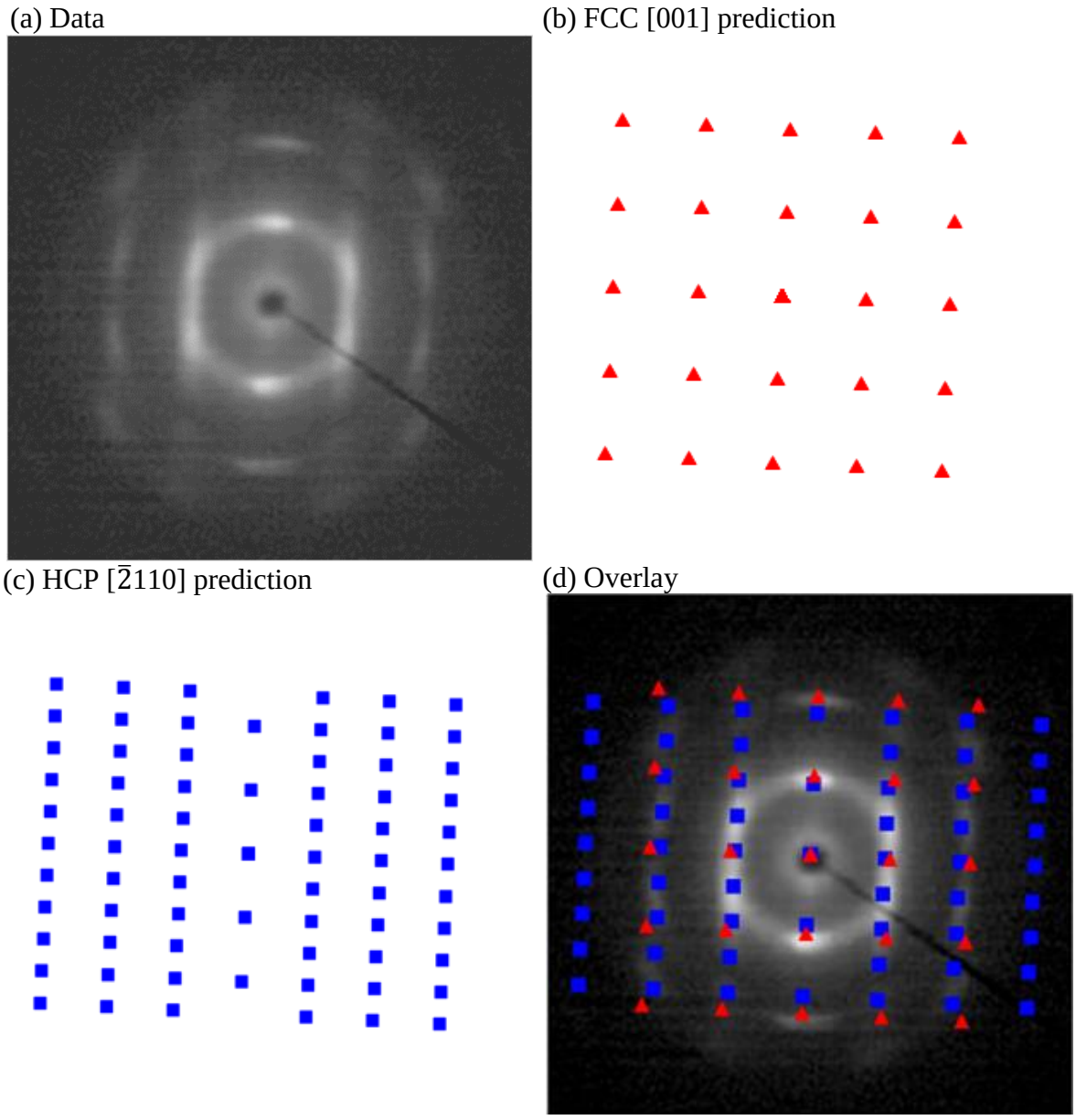

Figure 5.15: 2D SAXS data obtained along the velocity direction. SAS2-76-24 sheared at 180 °C and the local strain is 48%.

We note that the existence of the FCC unit cell aligned with close packed {111} planes in the shear plane can be eliminated as the prediction for this unit cell orientation does not match the scattering data obtained in the velocity direction, as shown in Figure

5.8. Furthermore, this FCC unit cell orientation is not required to explain the data obtained in the velocity gradient and vorticity direction. Though this FCC unit cell orientation has been reported in previous studies, which showed 2D scattering patterns in the velocity gradient and vorticity directions that are very similar to those reported in this study, the prior studies did not obtain data in the velocity direction.

We conclude that the shear aligned SAS triblock copolymer melt is a coexistence of HCP and FCC structures, containing a small population of FCC. The predominant orientation of the unit cells are such that the HCP {0001} and FCC $\{1\bar{1}0\}$ planes are parallel to the shear plane, the HCP $\{10\bar{1}0\}$ and FCC {110} planes are normal to the vorticity direction, and the HCP $\{\bar{2}110\}$ and FCC {001} planes are normal to the velocity direction. Data obtained from the triblock copolymer at other positions along the sample disc, with local strains of 32%, 64% and 80%, were also consistent with these conclusions. A comparison of the data and predictions for these three local strains are summarized in Figures 5.16, 5.17 and 5.18.

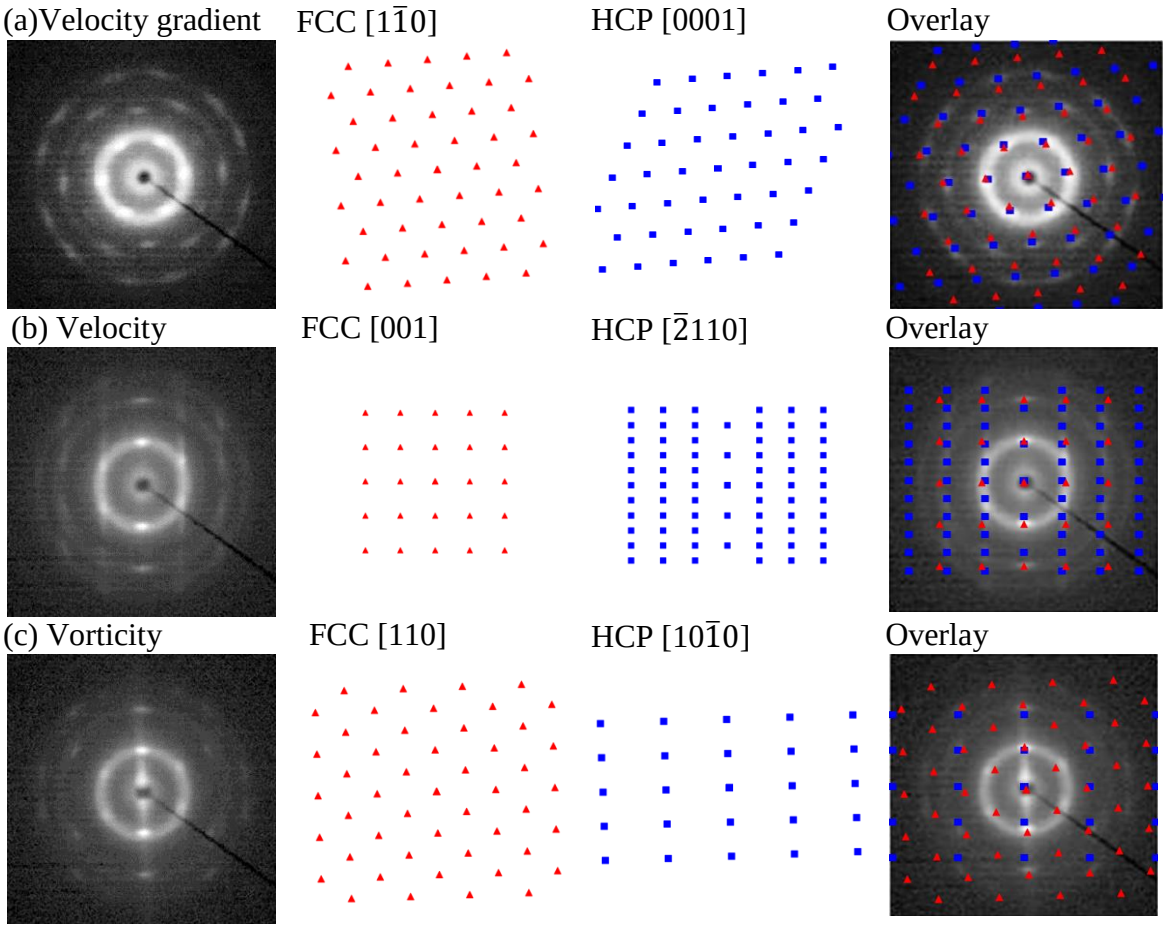

Figure 5.16: Overlay of prediction and data at shear strain of 32% in the a): velocity gradient direction; b) velocity direction; c) vorticity direction.

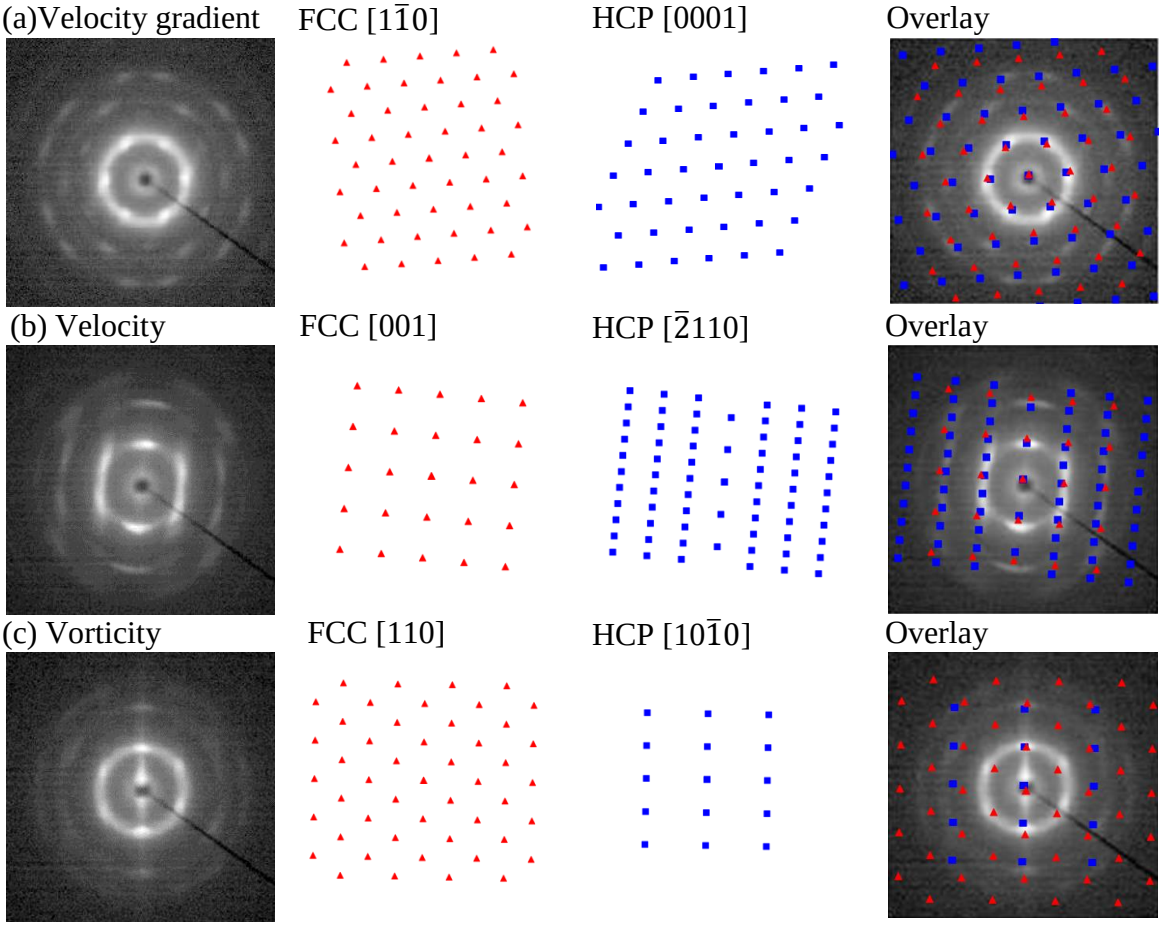

Figure 5.17: Overlay of prediction and data at shear strain of 64% in the a): velocity gradient direction; b) velocity direction; c) vorticity direction.

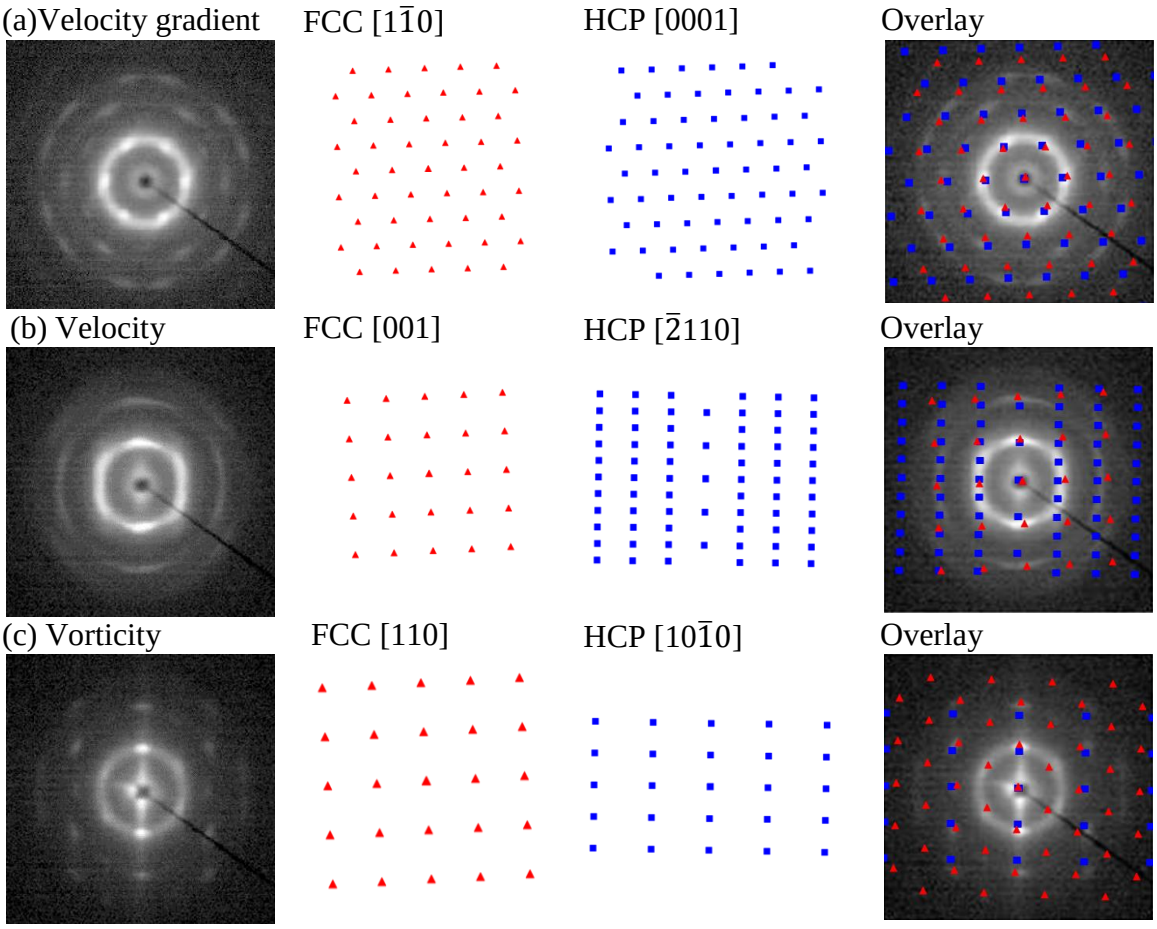

Figure 5.18: Overlay of prediction and data at shear strain of 80% in the a): velocity gradient direction; b) velocity direction; c) vorticity direction.

TEM was also utilized to characterize the morphology of the SAS2-76-24 triblock copolymer after LAOS and the result is displayed in Figure 5.19. Comparing to the TEM micrograph for the same sample prior to LAOS (Figure 5.3), it is clear that after LAOS, the grains of the sample was well aligned and the regularity increased drastically. Note here, the hexagonal packing was not observed from TEM which was expected in the velocity gradient direction from SAXS. The microtomed section may not be perfectly parallel to the velocity gradient direction and microtoming procedure may have altered

the morphology. Electron tomography will be conducted in the future to probe the three-dimensional morphology, which will provide comprehensive information on the orientation.

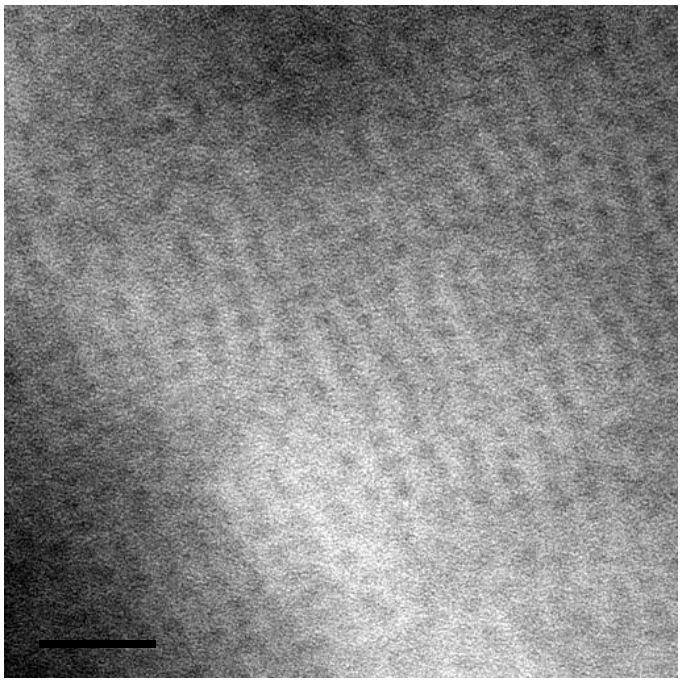

Figure 5.19: TEM image for SAS2-76-24 at room temperature after LAOS, viewed in the velocity gradient direction.

5.4. Concluding remarks

Large amplitude oscillatory shear (LAOS) was performed to align poly(styrene-*b*-(lauryl-*co*-stearyl)-*b*-styrene) (SAS) triblock copolymers. Different samples at different shear strain were characterized by SAXS in velocity gradient, velocity and vorticity directions. High shear strain is required for the alignment. The existence of hexagonally closed packed (HCP) and face-centered cubic (FCC) spheres were obtained from a randomly arranged FCC structure with a small population of FCC structure.

The predominant orientation is the HCP {0001} and FCC $\{1\bar{1}0\}$ planes parallel to the shear plane, HCP $\{10\bar{1}0\}$ and FCC {110} normal to the vorticity direction and HCP $\{\bar{2}110\}$ and FCC {001} planes normal to the velocity direction.

The shear alignment was not dependent on shear frequency and temperature close to the order-disorder transition is not sufficient for orientation.

Relatively few studies have shown the occurrence of the close packed sphere (CPS) structures in polymer melts, though from theoretical prediction there is a narrow stable region on the phase diagram [63, 112]. In this study we have demonstrated a close packed structure for the SAS triblock copolymers under LAOS. The mechanism and stability of this CPS structure will be investigated in the future.

Chapter 6

Sustainable Thermoplastic Elastomers from Fatty Acids and Salicylic Acid

In the previous chapters, we have demonstrated that partially sustainable triblock copolymers with midblocks derived from fatty acids are processable and exhibit elastomeric properties. In this chapter, we discuss the design and development of fully sustainable thermoplastic elastomers with fatty acid-based midblock and salicylic acid-derived endblocks. Salicylic acid is abundant in plant and food product. The hydroxyl and carboxylic acid groups are easily functionalized to a methacrylate group, which is appropriate for controlled radical polymerization [54, 117]. The synthesis, morphology, thermal and mechanical properties of this triblock copolymer were investigated.

6.1. Synthesis of acetylsalicylic ethyl methacrylate (ASEMA)

ASEMA was functionalized from acetylsalicylic acid (ASA). ASA was first converted to acyl chloride using oxalyl chloride followed by an esterification reaction with hydroxyethyl methacrylate. The structure was characterized by ^{1}H-NMR (Figure 6.1). The relative ratio of peak area at a, b, c, d, and e is 2:3:4:4:3.

6.2. Synthesis and characterization of poly(ASEMA-*b*-LMA-*b*-ASEMA) (ALA)

Poly(ASEMA) was synthesized using RAFT polymerization with a difunctional chain transfer agent, 1,4-bis(2-thiobenzoylthio)prop-2-yl)benzene BTBTPB (Scheme 2.7 in Chapter 2). The polymerization proceeded in a controlled manner with a relatively low dispersity ($Đ$=1.24, M_n=30.4 kg/mol). The ^{1}H-NMR spectra from PASEMA is presented in Figure 6.2. The characteristic signals of vinyl protons from ASEMA monomer at 5.6 and 6.1 ppm disappeared upon polymerization, replaced by emergence of broad peaks at 0.9-2 ppm corresponding to $–CH_2$-CH- protons from the polymer backbone. All other

peaks associated with the side groups were broader and shifted slightly compared to those from the ASEMA monomer. Figure 6.3 shows the GPC trace for PASEMA.

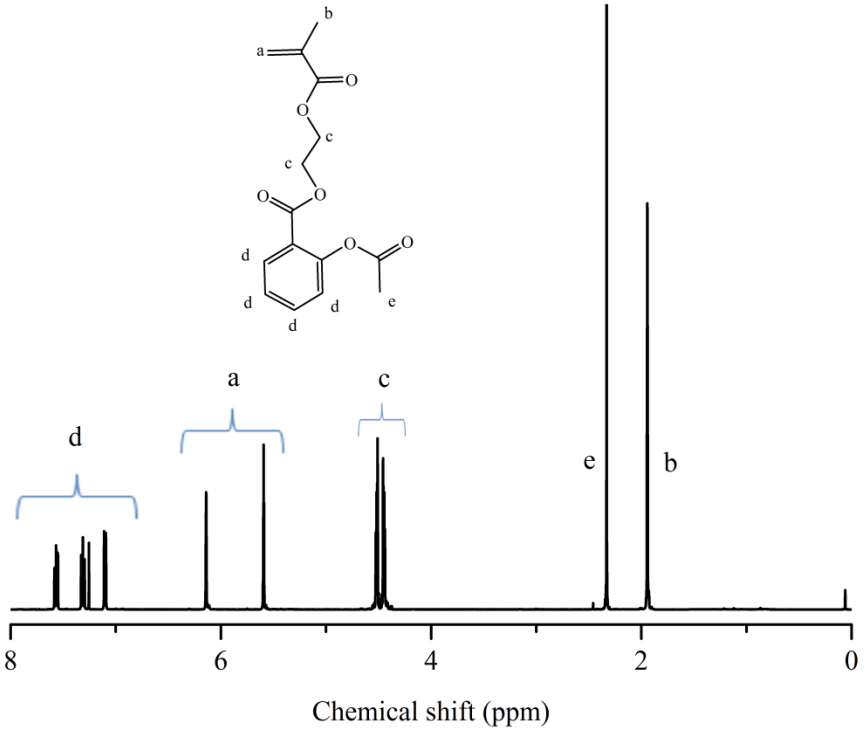

Figure 6.1: ^{1}H-NMR spectra obtained from ASEMA monomer.

The glass transition temperature (T_g) of PASEMA was measured by DSC and a distinct T_g was observed at around 53.0 °C. For TPE applications, the endblock should have a glass transition temperature higher than the service temperature (usually room temperature [31]). Thus ASEMA could be a good candidate as the source for the development of sustainable TPEs.

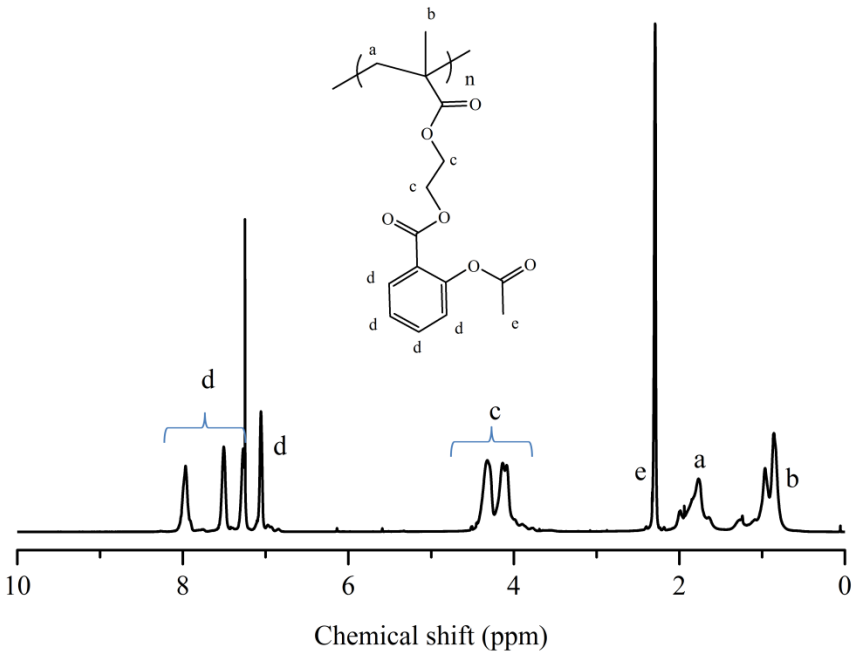

Figure 6.2: ^{1}H-NMR from PASEMA.

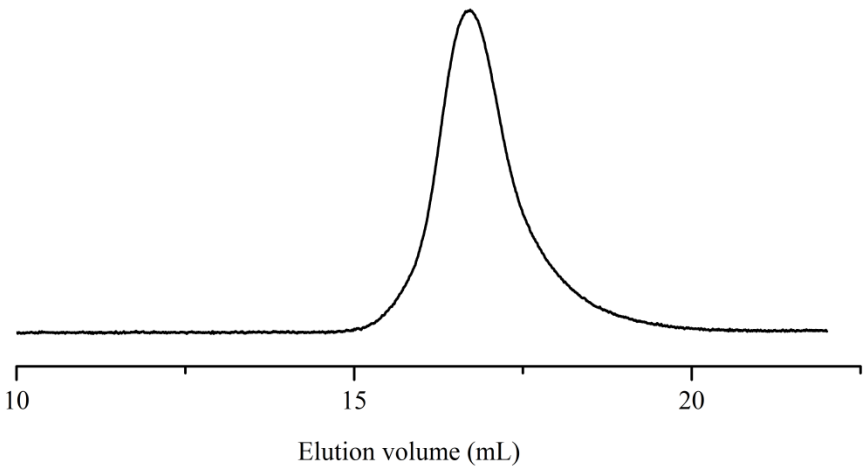

Figure 6.3: GPC trace of PASEMA.

Poly(ASEMA-*b*-LMA-*b*-ASEMA) (ALA) triblock copolymer was prepared in a two step reaction with a symmetric difunctional RAFT chain transfer agent. Poly(lauryl methacrylate) (PLMA) was first made as the midblock. The polymerization proceeded in

a controlled manner. 84% conversion was achieved after 24 hr and the $Đ$ for PLMA was 1.21 with M_n of 87.6 kg/mol.

The ^{1}H-NMR from PLMA was shown in Figure 6.4. The characteristic signals of vinyl protons from LMA monomer at 5.6 and 6.1 ppm disappeared upon polymerization, accompanied by the appearance of broad peaks at 0.9-2 ppm corresponding to $–CH_2$-CH- protons from the polymer backbone. The characteristic signals from the RAFT agent were also retained from 6.9-8.1 ppm, allowing for chain extension from PLMA to form triblock copolymers.

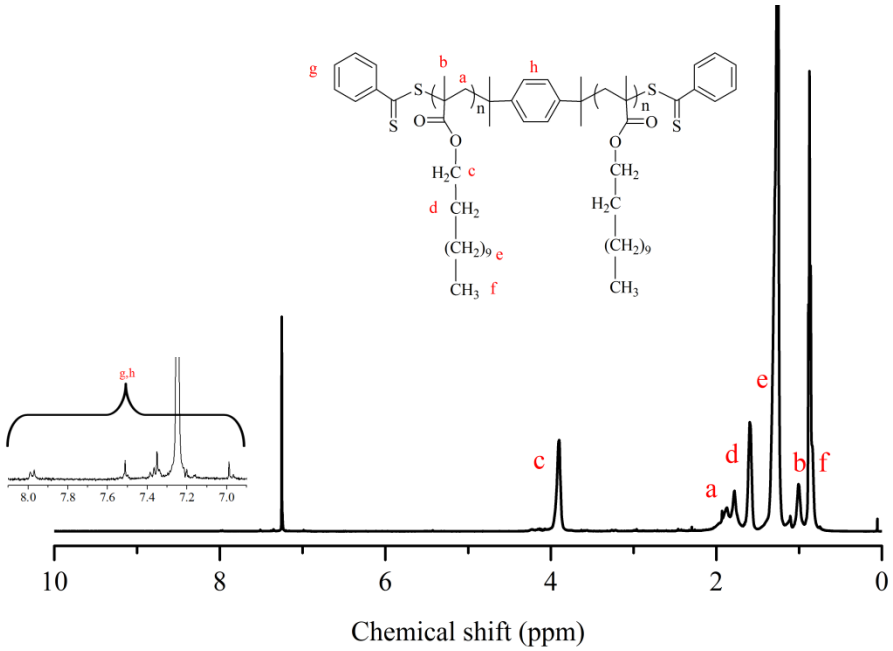

Figure 6.4: ^{1}H-NMR from PLMA.

PLMA was used as the macro-CTA for the preparation of ALA triblock copolymers. The incorporation of ASEMA blocks were confirmed by both NMR and GPC. Figure 6.5 shows the ^{1}H-NMR from ALA. Compared to Figure 6.4, the peaks at 7.0-8.0 ppm, 4.0-4.25 ppm and 2.2 ppm are from the ASEMA repeat units. The GPC

traces show a distinct shift to the left in the data when comparing the PLMA and ALA triblock copolymer (Figure 6.6).

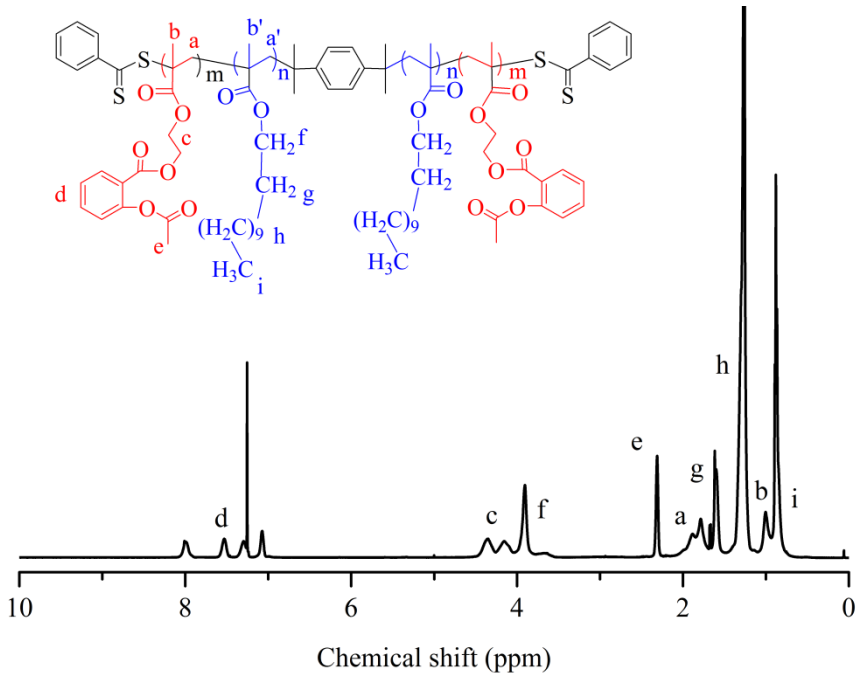

Figure 6.5: ^{1}H-NMR from ALA.

The GPC data for the ALA exhibit trimodal distributions which was also observed in the SAS triblock copolymers discussed in chapter 3. The shoulder to the right of the primary peak may indicate the presence of PLMA that were not chain extended or diblock copolymer. The trimodal nature of the GPC data is similar to that observed in ref. [144], in which the largest size mode (to the left of the primary peak) was attributed to chain branching. The weight fraction of PASEMA in the triblock copolymer was calculated based on NMR, to be 31%, and the M_n and $Đ$ from GPC were 130.5 kg/mol and 1.62.

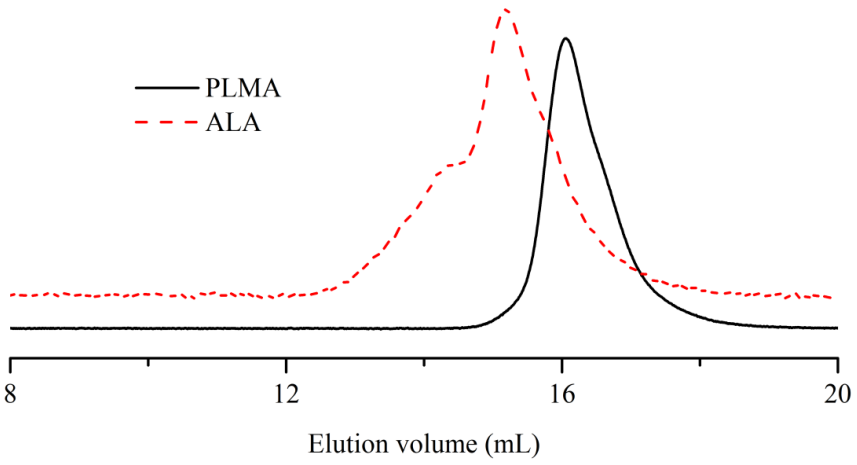

Figure 6.6: GPC traces for PLMA and ALA.

The T_g's of the midblock and end-blocks of ALA were measured by DSC and are presented in Figure 6.7. Two distinct transitions were observed, indicating the incompatibility of the two components, PLMA and PASEMA. The transitions of PLMA and PASEMA homopolymers are also included in Figure 6.7 and it can be seen that the two transition temperatures observed in ALA (-47.4 °C for the PLMA block and 55.8 °C for the PASEMA block) are nearly same as those from the corresponding homopolymers (-46.2 °C for PLMA and 53.0 °C for PASEMA). The incompatibility of the two components in ALA is crucial for TPEs applications, since the TPEs require micro-phase separation to form segregated sphere or cylinder domains of the hard block and the bridging of the rubbery block [31].

The thermal stability of PLMA, PASEMA and ALA were characterized by TGA. Figure 6.8 shows the TGA data and it can be seen that ALA triblock copolymer has a high thermal stability, with a onset degradation temperature higher than 250 °C and maximum degradation temperature higher than 350 °C.

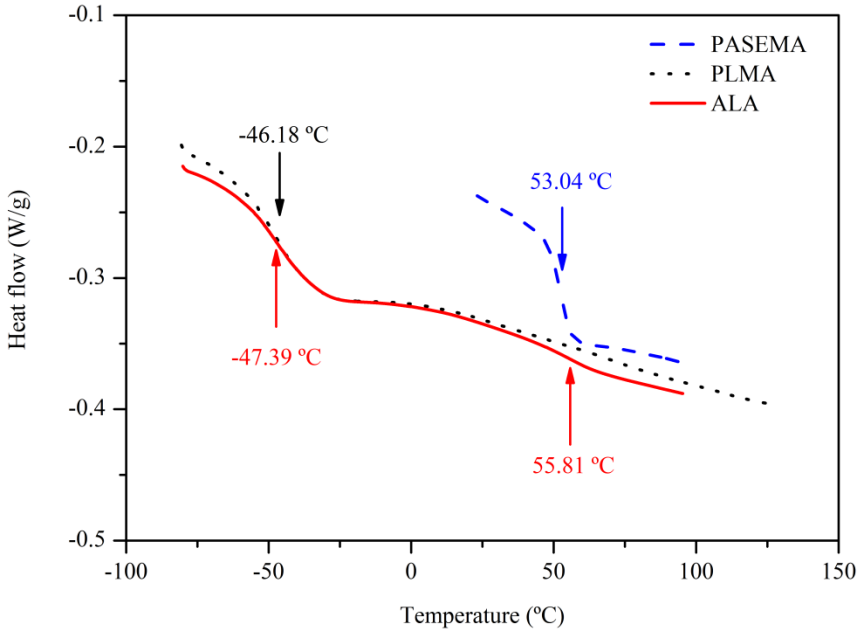

Figure 6.7: DSC data showing the T_g's of PLMA homopolymer (dotted black line), PASEMA homopolymer (dashed blue line) and ALA triblock copolymer (solid red line).

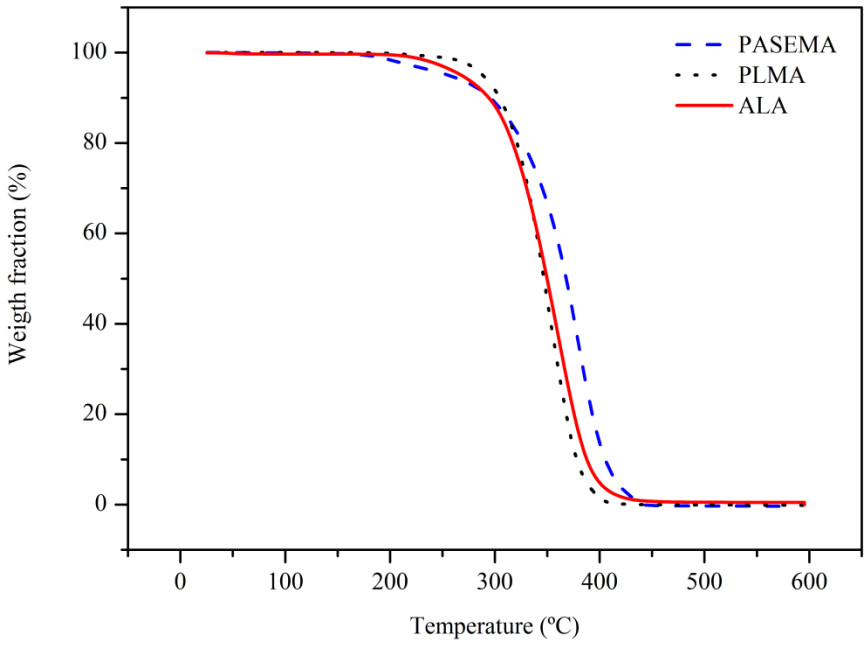

Figure 6.8: TGA data for PLMA homopolymer (black dotted line), PASEMA homopolymer (blue dashed line) and ALA triblock copolymer (red solid line).

To locate the order-disorder transition (ODT) of the ALA triblock copolymer, the dynamic storage modulus (G') was measured as a function of temperature using rheology (Figure 6.9). It is apparent that G' decreases abruptly at around 228.7 ºC. At a temperature higher than the ODT, ALA can be processed by injection molding, compression molding or extrusion to be remolded for targeted applications [31].

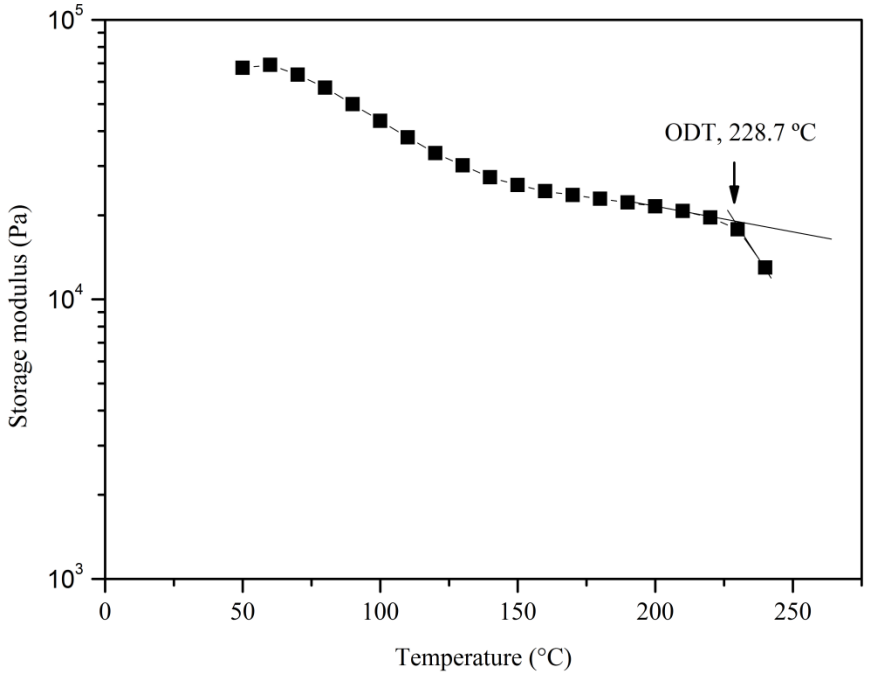

Figure 6.9: Determination of ODT of ALA triblock copolymers.

The morphology of ALA was probed by small angle x-ray scattering. The 2D SAXS pattern is presented in Figure 6.10 and the isotropic concentric rings indicate the random orientation of the nanostructures. The 1D integration is also shown in Figure 6.11. The higher order scattering rings in the 2D image indicate the microphase separation of the triblock copolymer. The relative location for the higher order scattering is not consistent with any known structures. There is possibly that the structure is a coexisting of different unit cells. However, the broadness of the peaks makes it very difficult to

resolve the morphology and further identification of the morphology is required, with the help of transmission electron microscope.

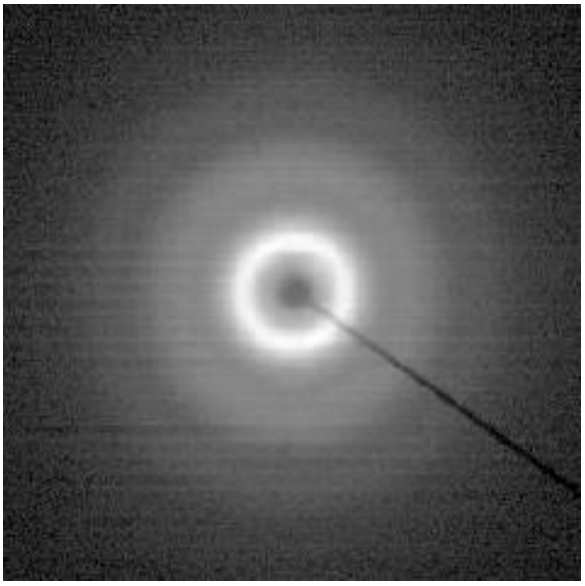

Figure 6.10: 2D SAXS pattern for as-mold ALA triblock copolymer.

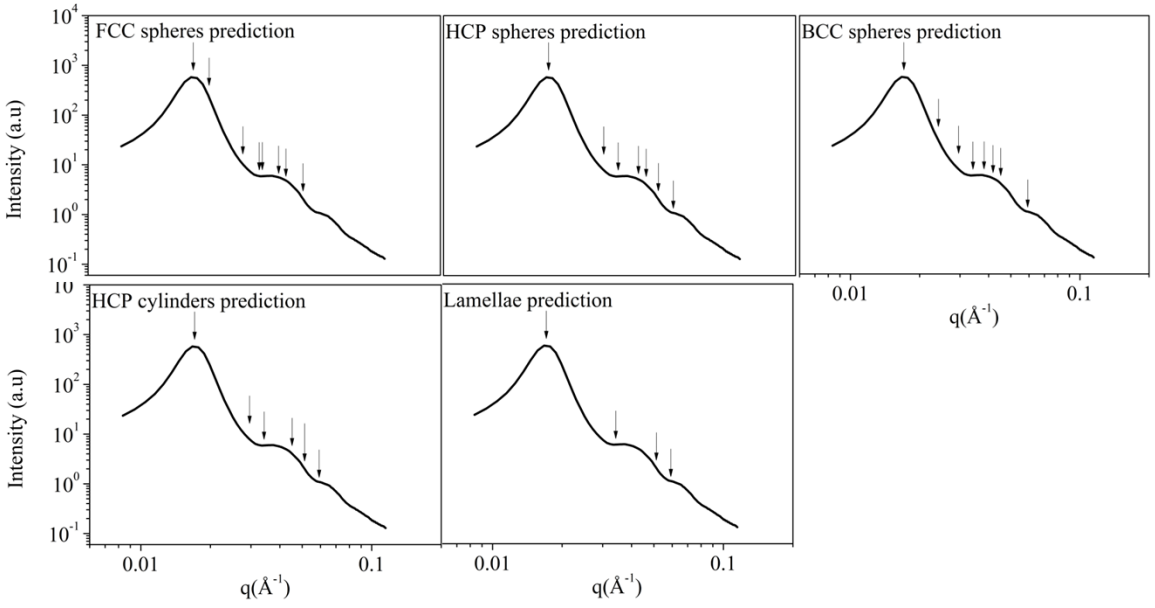

Figure 6.11: 1D SAXS reflection pattern for as-mold ALA triblock copolymer.

The mechanical properties of the ALA triblock copolymer were investigated with tensile testing. Five dogbone shaped specimen were prepared using compression molding and subjected to extensional force. The stress-strain behavior is shown in Figure 6.12. The elongation at break for ALA is 250±48%, and the tensile strength is 0.44±0.07 MPa. The elongation and tensile strength for all tested samples are summarized in Table 6.1.

Table 6.1: The elongation at break and tensile strength for ALA tested

	1	2	3	4	5
Elongation at break (%)	215	202	233	285	314
Tensile strength (MPa)	0.38	0.36	0.44	0.50	0.53

It is apparent that this triblock copolymer derived from long alkyl chain fatty acid and salicylic acid shows relatively low tensile strength compared to commercial styrene and butadiene (or isoprene) based TPEs. In chapter 3 we have discussed the mechanical properties of fatty acid based TPEs and we attribute the low strength to the very high entanglement molecular weight. In order to obtain high tensile strength, the rubbery matrix needs to be entangled, requiring M_n of the mid-block to be 2-3 times larger than M_e (the exact relationship between the critical molecular weight, M_c, and M_e depends on the polymer structure [146]). In the commercial SBS and SIS triblock copolymers, the M_e for poly(butadiene) and poly(isoprene) are 1.7 kg/mol and 6.1 kg/mol, respectively [147, 148]. Polymethacrylates have higher M_e's and as the alkyl chain length increases, M_e increases substantially. The M_e for PLMA has been reported to be 225 kg/mol [34],

thus the ALA in this study (PLMA midblock has a molecular weight of 87.6 kg/mol) is not entangled.

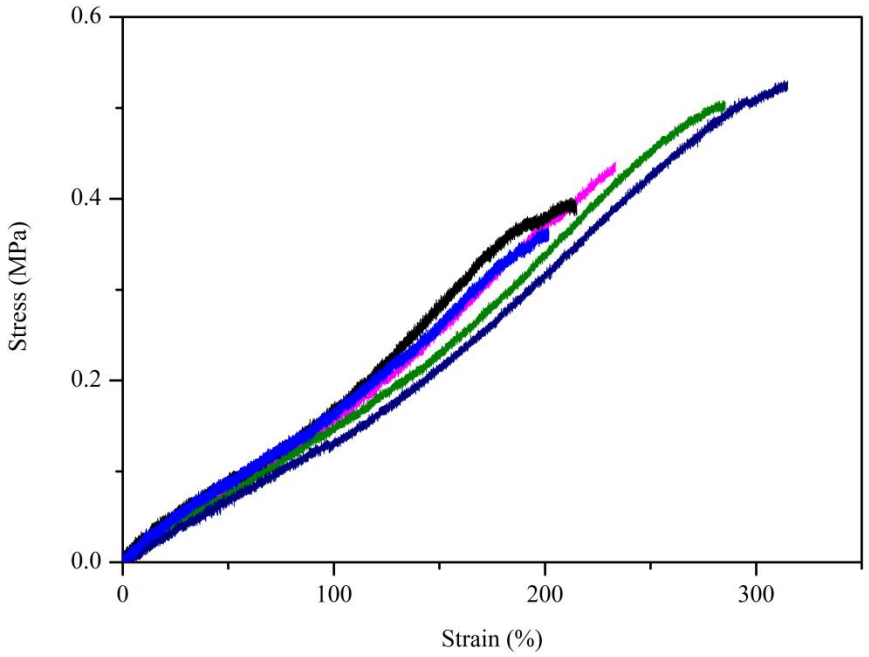

Figure 6.12: Tensile stress versus strain for ALA

The low tensile strength from long alkyl chain fatty acids derived triblock copolymers may be a disadvantage for some TPE applications, however, a soft matrix may be an advantage in pressure sensitive adhesives or applications employing oil-extended TPEs [31].

6.3. Concluding remarks

Fully sustainable triblock copolymers were prepared containing a fatty acid-derived midblock and salicylic acid-derived endblock, using reversible addition fragmentation chain transfer polymerization. The homopolymerization of LMA and ASEMA proceed in a controlled manner, with resulting dispersities lower than 1.3.

The ALA triblock copolymer showed two distinct glass transitions, which are nearly similar to those from the corresponding homopolymers. PLMA block has a glass

transition temperature well below room temperature and PASEMA block has a glass transition temperature about 30 °C above the room temperature, and the resulting triblock copolymer contains a rubbery midblock and a glassy endblock. The microphase separation was also probed by SAXS and it was reveled that the morphology was consistent with cylindrical structures.

The ALA triblock copolymer shows processability at high temperature and elastomeric properties at room temperature. However, the tensile strength is relatively low due to the large entanglement molecular weight. Future work should focus on enhancing the mechanical properties to enlarge the application scopes of these sustainable TPEs.

Chapter 7

Summary and Future Work

7.1. Conclusions of this work

Synthetic strategies using reversible addition chain transfer (RAFT) polymerization with a symmetric chain transfer agent were established for the synthesis of long chain polymeth(acrylate)s derived from fatty acids and a salicylic acid-based polymethacrylate. The polymerizations of the sustainable monomers were well-controlled with relatively low values of the dispersity (around 1.3).

Poly(styrene-*b*-(lauryl acrylate-*co*-stearyl acrylate)-*b*-styrene) (SAS) triblock copolymers were successfully synthesized using RAFT polymerization. The midblock was a random copolymer of lauryl (LAc) and stearyl acryalte (SAc) and the resulting triblock copolymers differed in the composition of the midblock, containing a mixture of poly(stearyl acrylate) (PSAc) and poly(lauryl acrylate) (PLAc) (the length of the alkyl side-chain on each repeat unit is 12 and 18 carbon atoms for PSAc and PLAc, respectively). Small-angle X-ray scattering (SAXS) and transmission electron microscopy revealed the microphase separation of the SAS triblock copolymers, likely a spherical morphology without strong long range order. The physical properties of the polymers were readily tuned by varying the acrylate midblock composition, including the melting temperature, viscosity, and triblock copolymer tensile properties. Mechanical testing revealed the thermoplastic elastomeric behavior of the triblock copolymers.

The Flory-Huggins interaction parameter (χ) between polystyrene (PS) and long-chain poly(*n*-alkyl acrylates) (i.e., PLAc and PSAc) was calculated by two independent methods: cloud point measurements on binary blends and characterization of the order-

disorder transition of triblock copolymers. The χ parameter was found to be independent of the alkyl side-chain length (*n*) for large values of *n*. This indicates that the acrylate composition can be used as a tool to manipulate the physical properties of the triblock copolymers without affecting the order-disorder transition temperature, or processing temperature, of the TPEs. This work lays the foundation for future studies to examine blends or block copolymers consisting of long-chain polyacrylates and various other constituents, including the examination of blends or block copolymers containing multiple components with long side-chains. The implementation of polymers derived from fatty acids and vegetable oils in multicomponent materials, such as blends and copolymers, will rely upon a detailed understanding of the thermodynamic interactions in such systems

Large amplitude oscillatory shear was employed to study the alignment behavior of SAS triblock copolymer melts under shear. SAXS was utilized to characterize the morphology and orientation of the microstructures in all three perpendicular directions, velocity gradient, velocity and vorticity directions. Well-aligned structures were obtained and the predominant of orientation was determined to hexagonally close-packed spheres with {0001} planes aligned in the shear plane, $\{10\bar{1}0\}$ planes normal to the vorticity direction and $\{\bar{2}110\}$ planes normal to the velocity direction, coexisting with a small population of face-centered cubic spheres with the $\{1\bar{1}0\}$ planes parallel to the shear plane, {110} planes normal to the vorticity direction and {001} planes normal to the velocity direction.

Fully sustainable triblock copolymers containing a fatty acid-derived polymethacrylate as the rubbery midblock and salicylic acid-derived polymethacrylate as

the glassy endblock were prepared using RAFT polymerization. The triblock copolymer showed two distinct glass transitions which were similar to the glass transition temperatures of the corresponding homopolymers. The phase separation was confirmed by SAXS, and the isotropic pattern indicated the random orientation of the macrostructures. The salicylic acid-based polymethacrylate was found to be suitable replacement for polystyrene in the endblocks of the triblock copolymer, with elevated glass transition temperatures (above room temperature).

7.2. On-going project

The thermodynamic interaction between the components of ALA triblock copolymers will be characterized, which will guide the future design of LMA and ASEMA based multicomponents polymer systems. The entanglement molecular weight of PASEMA and PLMA will be investigated, which will lead to more precise design of the triblock copolymer structure and molecular weight. The morphology of ALA has not been well studied and large amplitude oscillatory shear will be utilized to align the polymer and SAXS, TEM and electron tomography will be used to determine the equilibrium morphology of the triblock copolymers.

The shear alignment of the SAS triblock copolymer resulted in close-packed spheres structures, which was scarcely observed in block copolymer melts. The preference of close packed structures over BCC requires in-depth investigation in the molecular level and the mechanism needs to be studied. Shear alignment at different conditions with different SAS triblock copolymer characteristics will be probed. And electron tomography will be applied to better determine the morphology with SAXS.

7.3. Outlook and future challenges

The mechanical properties of triblock copolymer with fatty acid based long alkyl chain poly(meth)acrylates are relatively low comparing to the commercial polybutadiene and polyisoprene based TPEs, due to the fact that the entanglement molecular weight of the long alkyl chain poly(meth)acrylates are much higher than those of polybutadiene and polyisoprene. Future work should focus on the enhancement of the mechanical properties of the triblock copolymers with long alkyl chain poly(meth)acrylates to expand the applications of those sustainable polymers, by overcoming the high entanglement molecular weight.

Targeted application for TPEs with soft matrix could be explored, including pressure sensitive adhesives and shape memory polymers.

Other sustainable sources could also be investigated as the building materials for TPEs, especially, polymers with lower entanglement molecular weight.

References

1 Hiemenz, P.C., Lodge, T.P. (2007). *Polymer chemistry*. 2nd edn. CRC Press, Boca Raton, FL.

2 Weisz, P.B. (2004). Basic choices and constraints on long-term energy supplies. *Physics today* **57**, 47-51.

3 Okkerse, C., van Bekkum, H. (1999). From fossil to green. *Green Chemistry* **1**, 107-114.

4 Ragauskas, A.J., Williams, C.K., Davison, B.H., Britovsek, G., Cairney, J., Eckert, C.A., Frederick, W.J., Hallett, J.P., Leak, D.J., Liotta, C.L., Mielenz, J.R., Murphy, R., Templer, R., Tschaplinski, T. (2006). The path forward for biofuels and biomaterials. *Science* **311**, 484-489.

5 Alonso, D.M., Bond, J.Q., Dumesic, J.A. (2010). Catalytic conversion of biomass to biofuels. *Green Chemistry* **12**, 1493-1513.

6 Meier, M.A.R., Metzger, J.O., Schubert, U.S. (2007). Plant oil renewable resources as green alternatives in polymer science. *Chemical Society Reviews* **36**, 1788-1802.

7 Xia, Y., Larock, R.C. (2010). Vegetable oil-based polymeric materials: Synthesis, properties, and applications. *Greem Chemistry* **12**, 1893-1909.

8 Bhardwaj, R., Mohanty, A.K. (2007). Advances in the properties of polylactides based materials: A review. *J Biobased Mater Bio* **1**, 191-209.

9 Gallezot, P. (2007). Process options for converting renewable feedstocks to bioproducts. *Greem Chemistry* **9**, 295-302.

10 Wondraczek, H., Kotiaho, A., Fardim, P., Heinze, T. (2011). Photoactive polysaccharides. *Carbohydrate Polymers* **83**, 1048-1061.

11 Wilbon, P.A., Chu, F., Tang, C. (2013). Progress in renewable polymers from natural terpenes, terpenoids, and rosin. *Macromolecular Rapid Communications* **34**, 8-37.

12 Saito, T., Brown, R.H., Hunt, M.A., Pickel, D.L., Pickel, J.M., Messman, J.M., Baker, F.S., Keller, M., Naskar, A.K. (2012). Turning renewable resources into value-added polymer: Development of lignin-based thermoplastic. *Green Chemistry* **14**, 3295-3303.

13 Bolton, J.M., Hillmyer, M.A., Hoye, T.R. (2014). Sustainable thermoplastic elastomers from terpene-derived monomers. *ACS Macro Letters* **3**, 717-720.

14 Liu, Y., Yao, K., Chen, X., Wang, J., Wang, Z., Ploehn, H.J., Wang, C., Chu, F., Tang, C. (2014). Sustainable thermoplastic elastomers derived from renewable cellulose, rosin and fatty acids. *Polymer Chemistry* **5**, 3170-3181.

15 Harvey, B.G., Guenthner, A.J., Meylemans, H.A., Haines, S.R.L., Lamison, K.R., Groshens, T.J., Cambrea, L.R., Davis, M.C., Lai, W.W. (2015). Renewable thermosetting resins and thermoplastics from vanillin. *Green Chemistry* **17**, 1249-1258.

16 Agirre, A., de las Heras-Alarcon, C., Wang, T., Keddie, J.L., Asua, J.M. (2010). Waterborne, semicrystalline, pressure-sensitive adhesives with temperature-responsiveness and optimum properties. *Acs Applied Materials & Interfaces* **2**, 443-451.

17 Agirre, A., Nase, J., Degrandi, E., Creton, C., Asua, J.M. (2010). Improving adhesion of acrylic waterborne psas to low surface energy materials: Introduction of stearyl acrylate. *Journal of Polymer Science Part a-Polymer Chemistry* **48**, 5030-5039.

18 Öztürk, E., Turan, E., Caykara, T. (2010). Fabrication of ultrahydrophobic poly(lauryl acrylate) brushes on silicon wafer via surface-initiated atom transfer radical polymerization. *Applied Surface Science* **257**, 1015-1020.

19 Fei, P., Cavicchi, K.A. (2010). Synthesis and characterization of a poly(styrene-block-methylacrylate-random-octadecylacrylate-block-styrene) shape memory aba triblock copolymer. *Acs Applied Materials & Interfaces* **2**, 2797-2803.

20 Ronda, J.C., Lligadas, G., Galià, M., Cádiz, V. (2011). Vegetable oils as platform chemicals for polymer synthesis. *European Journal of Lipid Science and Technology* **113**, 46-58.

21 Lu, Y., Larock, R. (2009). Novel polymeric materials from vegetable oils and vinyl monomers: Preparation, properties, and applications. *ChemSusChem* **2**, 136-147.

22 Metzger, J.O., Bornscheuer, U. (2006). Lipids as renewable resources: Current state of chemical and biotechnological conversion and diversification. *Applied Microbiology and Biotechnology* **71**, 13-22.

23 Warwel, S., Klaas, M.R.G. (1995). Chemo-enzymatic epoxidation of unsaturated carboxylic acids. *Journal of Molecular Catalysis B: Enzymatic* **1**, 29-35.

24 Gupta, A.P., Ahmad, S., Dev, A. (2011). Modification of novel bio-based resin-epoxidized soybean oil by conventional epoxy resin. *Polymer Engineering and Science* **51**, 1087-1091.

25 Lligadas, G., Ronda, J.C., Galia, M., Biermann, U., Metzger, J.O. (2006). Synthesis and characterization of polyurethanes from epoxidized methyl oleate based polyether polyols as renewable resources. *Journal of Polymer Science Part A: Polymer Chemistry* **44**, 634-645.

26 Campanella, A., La Scala, J.J., Wool, R.P. (2009). The use of acrylated fatty acid methyl esters as styrene replacements in triglyceride-based thermosetting polymers. *Polymer Engineering and Science* **49**, 2384-2392.

27 Henna, P., Larock, R.C. (2009). Novel thermosets obtained by the ring-opening metathesis polymerization of a functionalized vegetable oil and dicyclopentadiene. *Journal of Applied Polymer Science* **112**, 1788-1797.

28 Takeda, Y., Nakagawa, Y., Tomishige, K. (2012). Selective hydrogenation of higher saturated carboxylic acids to alcohols using a reox-pd/sio$_2$ catalyst. *Catal Sci Eng* **2**, 2221-2223.

29 Toba, M., Tanaka, S., Niwa, S., Mizukami, F., Koppány, Z., Guczi, L., Cheah, K.Y., Tang, T.S. (1999). Synthesis of alcohols and diols by hydrogenation of carboxylic acids and esters over ru–sn–al$_2$o$_3$ catalysts. *Applied Catalysis A* **189**, 243-250.

30 Dutta, P., Gogoi, B., Dass, N.N., Sen Sarma, N. (2013). Efficient organic solvent and oil sorbent co-polyesters: Poly-9-octadecenylacrylate/methacrylate with 1-hexene. *Reactive and Functional Polymers* **73**, 457-464.

31 Holden, G., Legge, N.R., Quirk, R., Schroeder, H.E. (1996). *Thermoplastic elastomers*. 2nd edn. Hanser Gardner Pubns, Cincinnati, OH.

32 Xu, J., Zhang, A., Zhou, T., Cao, X., Xie, Z. (2007). A study on thermal oxidation mechanism of styrene–butadiene–styrene block copolymer (sbs). *Polymer Degradation and Stability* **92**, 1682-1691.

33 Singh, R.P., Desai, S.M., Solanky, S.S., Thanki, P.N. (2000). Photodegradation and stabilization of styrene–butadiene–styrene rubber. *Journal of Applied Polymer Science* **75**, 1103-1114.

34 Chatterjee, D.P., Mandal, B.M. (2006). Triblock thermoplastic elastomers with poly(lauryl methacrylate) as the center block and poly(methyl methacrylate) or poly(tert-butyl methacrylate) as end blocks. Morphology and thermomechanical properties. *Macromolecules* **39**, 9192-9200.

35 Jeusette, M., Leclère, P., Lazzaroni, R., Simal, F., Vaneecke, J., Lardot, T., Roose, P. (2007). New "all-acrylate" block copolymers: Synthesis and influence of the architecture on the morphology and the mechanical properties. *Macromolecules* **40**, 1055-1065.

36 Olsén, P., Borke, T., Odelius, K., Albertsson, A.-C. (2013). E-decalactone: A thermoresilient and toughening comonomer to poly(l-lactide). *Biomacromolecules* **14**, 2883-2890.

37 Martello, M.T., Burns, A., Hillmyer, M. (2012). Bulk ring-opening transesterification polymerization of the renewable δ-decalactone using an organocatalyst. *ACS Macro Letters* **1**, 131-135.

38 Wanamaker, C.L., Bluemle, M.J., Pitet, L.M., O'Leary, L.E., Tolman, W.B., Hillmyer, M.A. (2009). Consequences of polylactide stereochemistry on the properties of polylactide-polymenthide-polylactide thermoplastic elastomers. *Biomacromolecules* **10**, 2904-2911.

39 Wanamaker, C.L., O'Leary, L.E., Lynd, N.A., Hillmyer, M.A., Tolman, W.B. (2007). Renewable-resource thermoplastic elastomers based on polylactide and polymenthide. *Biomacromolecules* **8**, 3634-3640.

40 Coelho, J.F.J., Carvalho, E.Y., Marques, D.S., Popov, A.V., Goncalves, P.M., Gil, M.H. (2007). Synthesis of poly(lauryl acrylate) by single-electron transfer/degenerative chain

transfer living radical polymerization catalyzed by $na_2s_2o_4$ in water. *Macromolecular Chemistry and Physics* **208**, 1218-1227.

41 Jordan, E.F. (1971). Side-chain crystallinity. III. Influence of side-chain crystallinity on the glass transition temperatures of selected copolymers incorporating n-octadecyl acrylate or vinyl stearate. *Journal of Polymer Science Part A-1: Polymer Chemistry* **9**, 3367-3378.

42 Floudas, G., Placke, P., Stepanek, P., Brown, W., Fytas, G., Ngai, K.L. (1995). Dynamics of the "strong" polymer of n-lauryl methacrylate below and above the glass transition. *Macromolecules* **28**, 6799-6807.

43 Konaganti, V.K., Madras, G. (2009). Photocatalytic and thermal degradation of poly(methyl methacrylate), poly(butyl acrylate), and their copolymers. *Industrial and Engineering Chemistry Research* **48**, 1712-1718.

44 Mahalik, J.P., Madras, G. (2005). Effect of alkyl group substituents, temperature, and solvents on the ultrasonic degradation of poly(n-alkyl acrylates). *Industrial and Engineering Chemistry Research* **44**, 6572-6577.

45 Mosnáček, J., Yoon, J.A., Juhari, A., Koynov, K., Matyjaszewski, K. (2009). Synthesis, morphology and mechanical properties of linear triblock copolymers based on poly(α-methylene-γ-butyrolactone). *Polymer* **50**, 2087-2094.

46 Juhari, A., Mosnáček, J., Yoon, J.A., Nese, A., Koynov, K., Kowalewski, T., Matyjaszewski, K. (2010). Star-like poly (n-butyl acrylate)-b-poly (α-methylene-γ-butyrolactone) block copolymers for high temperature thermoplastic elastomers applications. *Polymer* **51**, 4806-4813.

47 Frick, E.M., Zalusky, A.S., Hillmyer, M.A. (2003). Characterization of polylactide-b-polyisoprene-b-polylactide thermoplastic elastomers. *Biomacromolecules* **4**, 216-223.

48 Shin, J., Martello, M.T., Shrestha, M., Wissinger, J.E., Tolman, W.B., Hillmyer, M.A. (2011). Pressure-sensitive adhesives from renewable triblock copolymers. *Macromolecules* **44**, 87-94.

49 Martello, M.T., Schneiderman, D.K., Hillmyer, M.A. (2014). Synthesis and melt processing of sustainable poly(ε-decalactone)-block-poly(lactide) multiblock thermoplastic elastomers. *ACS Sustainable Chemistry & Engineering* **2**, 2519-2526.

50 Holmberg, A.L., Stanzione, J.F., Wool, R.P., Epps, T.H. (2014). A facile method for generating designer block copolymers from functionalized lignin model compounds. *ACS Sustainable Chemistry & Engineering* **2**, 569-573.

51 Russell, W.R., Labat, A., Scobbie, L., Duncan, G.J., Duthie, G.G. (2009). Phenolic acid content of fruits commonly consumed and locally produced in scotland. *Food Chemistry* **115**, 100-104.

52 Haminiuk, C.W.I., Maciel, G.M., Plata-Oviedo, M.S.V., Peralta, R.M. (2012). Phenolic compounds in fruits – an overview. *International Journal of Food Science & Technology* **47**, 2023-2044.

53 Englis, D.T., Burnett, B.B., Schreiber, R.A., Miles, J.W. (1955). Food analysis, determination of benzoic and salicylic acids in food products. *Journal of Agricultural and Food Chemistry* **3**, 964-969.

54 Zheng, Y., Yao, K., Lee, J., Chandler, D., Wang, J., Wang, C., Chu, F., Tang, C. (2010). Well-defined renewable polymers derived from gum rosin. *Macromolecules* **43**, 5922-5924.

55 Bates, F.S., Fredrickson, G.H. (1999). Block copolymers--designer soft materials. *Physics today* **52**, 32.

56 Nagpal, U., Detcheverry, F.o.A., Nealey, P.F., de Pablo, J.J. (2011). Morphologies of linear triblock copolymers from monte carlo simulations. *Macromolecules* **44**, 5490-5497.

57 Matsen, M.W., Thompson, R.B. (1999). Equilibrium behavior of symmetric aba triblock copolymer melts. *Journal of Chemical Physics* **111**, 7139-7146.

58 Lynd, N.A., Hillmyer, M.A. (2005). Influence of polydispersity on the self-assembly of diblock copolymers. *Macromolecules* **38**, 8803-8810.

59 Lynd, N.A., Meuler, A.J., Hillmyer, M.A. (2008). Polydispersity and block copolymer self-assembly. *Progress in Polymer Science* **33**, 875-893.

60 Ruzette, A.V., Tencé-Girault, S., Leibler, L., Chauvin, F., Bertin, D., Guerret, O., Gérard, P. (2006). Molecular disorder and mesoscopic order in polydisperse acrylic block copolymers prepared by controlled radical polymerization. *Macromolecules* **39**, 5804-5814.

61 Moad, G., Rizzardo, E., Thang, S.H. (2008). Toward living radical polymerization. *Accounts of Chemical Research* **41**, 1133-1142.

62 Matsen, M.W., Bates, F.S. (1997). Block copolymer microstructures in the intermediate-segregation regime. *Journal of Chemical Physics* **106**, 2436.

63 Matsen, M.W., Bates, F.S. (1996). Unifying weak- and strong-segregation block copolymer theories. *Macromolecules* **29**, 1091-1098.

64 Matsen, M.W., Bates, F.S. (1997). Block copolymer microstructures in the intermediate-segregation regime. *The Journal of Chemical Physics* **106**, 2436-2448.

65 Leibler, L. (1980). Theory of microphase separation in block copolymers. *Macromolecules* **13**, 1602-1617.

66 Matsen, M.W., Thompson, R.B. (1999). Equilibrium behavior of symmetric aba triblock copolymer melts. *The Journal of Chemical Physics* **111**, 7139-7146.

67 Matsen, M.W. (2012). Effect of architecture on the phase behavior of ab-type block copolymer melts. *Macromolecules* **45**, 2161-2165.

68 Flory, P.J. (1942). Thermodynamics of high polymer solutions. *The Journal of Chemical Physics* **10**, 51-61.

69 Huggins, M.L. (1942). Some properties of solutions of long-chain compounds. *The Journal of Physical Chemistry* **46**, 151-158.

70 Travis, H.R., Brian, J.E., Bamin, K. (2014). Characterization of the flory-huggins interaction parameter of polymer thermodynamics. *EPL (Europhysics Letters)* **108**, 66003.

71 Chremos, A., Nikoubashman, A., Panagiotopoulos, A.Z. (2014). Flory-huggins parameter χ, from binary mixtures of lennard-jones particles to block copolymer melts. *The Journal of Chemical Physics* **140**, 054909.

72 Petri, H.-M., Schuld, N., Wolf, B.A. (1995). Hitherto ignored effects of chain length on the flory-huggins interaction parameters in concentrated polymer solutions. *Macromolecules* **28**, 4975-4980.

73 Angelescu, D.E., Waller, J.H., Adamson, D.H., Deshpande, P., Chou, S.Y., Register, R.A., Chaikin, P.M. (2004). Macroscopic orientation of block copolymer cylinders in single-layer films by shearing. *Advanced Materials* **16**, 1736-1740.

74 Koppi, K.A., Tirrell, M., Bates, F.S., Almdal, K., Colby, R.H. (1992). Lamellae orientation in dynamically sheared diblock copolymer melts. *J Phys II France* **2**, 1941-1959.

75 Koppi, K.A., Tirrell, M., Bates, F.S., Almdal, K., Mortensen, K. (1994). Epitaxial growth and shearing of the body centered cubic phase in diblock copolymer melts. *Journal of Rheology (1978-present)* **38**, 999-1027.

76 Amundson, K., Helfand, E., Quan, X., Hudson, S.D., Smith, S.D. (1994). Alignment of lamellar block copolymer microstructure in an electric field. 2. Mechanisms of alignment. *Macromolecules* **27**, 6559-6570.

77 Pinna, M., Schreier, L., Zvelindovsky, A.V. (2009). Mechanisms of electric-field-induced alignment of block copolymer lamellae. *Soft Matter* **5**, 970-973.

78 Majewski, P.W., Gopinadhan, M., Osuji, C.O. (2012). Magnetic field alignment of block copolymers and polymer nanocomposites: Scalable microstructure control in functional soft materials. *Journal of Polymer Science Part B: Polymer Physics* **50**, 2-8.

79 Li, M., Ober, C.K. (2006). Block copolymer patterns and templates. *Materials Today* **9**, 30-39.

80 Luo, K., Yang, Y. (2001). Chain stretching effect on the morphology and kinetics of microphase separation of diblock copolymer under simple shear flow. *The Journal of Chemical Physics* **115**, 2818-2826.

81 Lísal, M., Brennan, J.K. (2007). Alignment of lamellar diblock copolymer phases under shear: Insight from dissipative particle dynamics simulations. *Langmuir* **23**, 4809-4818.

82 Peters, B.L., Ramírez-Hernández, A., Pike, D.Q., Müller, M., de Pablo, J.J. (2012). Nonequilibrium simulations of lamellae forming block copolymers under steady shear: A comparison of dissipative particle dynamics and brownian dynamics. *Macromolecules* **45**, 8109-8116.

83 Wiesner, U. (1997). Lamellar diblock copolymers under large amplitude oscillatory shear flow: Order and dynamics. *Macromolecular Chemistry and Physics* **198**, 3319-3352.

84 Nikoubashman, A., Register, R.A., Panagiotopoulos, A.Z. (2013). Simulations of shear-induced morphological transitions in block copolymers. *Soft Matter* **9**, 9960-9971.

85 Gupta, V.K., Krishnamoorti, R., Chen, Z.R., Kornfield, J.A., Smith, S.D., Satkowski, M.M., Grothaus, J.T. (1996). Dynamics of shear alignment in a lamellar diblock copolymer: Interplay of frequency, strain amplitude, and temperature. *Macromolecules* **29**, 875-884.

86 Gupta, V.K., Krishnamoorti, R., Kornfield, J.A., Smith, S.D. (1995). Evolution of microstructure during shear alignment in a polystyrene-polyisoprene lamellar diblock copolymer. *Macromolecules* **28**, 4464-4474.

87 Kannan, R.M., Kornfield, J.A. (1994). Evolution of microstructure and viscoelasticity during flow alignment of a lamellar diblock copolymer. *Macromolecules* **27**, 1177-1186.

88 Scott, D.B., Waddon, A.J., Lin, Y.G., Karasz, F.E., Winter, H.H. (1992). Shear-induced orientation transitions in triblock copolymer styrene-butadiene-styrene with cylindrical domain morphology. *Macromolecules* **25**, 4175-4181.

89 Winter, H.H., Scott, D.B., Gronski, W., Okamoto, S., Hashimoto, T. (1993). Ordering by flow near the disorder-order transition of a triblock copolymer styrene-isoprene-styrene. *Macromolecules* **26**, 7236-7244.

90 Morrison, F.A., Winter, H.H. (1989). The effect of unidirectional shear on the structure of triblock copolymers. I. Polystyrene-polybutadiene-polystyrene. *Macromolecules* **22**, 3533-3540.

91 Morrison, F.A., Winter, H.H., Gronski, W., Barnes, J.D. (1990). Effect of unidirectional shear on the structure of triblock copolymers. 2. Polystyrene-polyisoprene-polystyrene. *Macromolecules* **23**, 4200-4205.

92 Lee, J.Y., Park, M.S., Yang, H.C., Cho, K., Kim, J.K. (2003). Alignment and orientational proliferation of hex cylinders in a polystyrene-block-polyisoprene-block-polystyrene copolymer in the presence of clay. *Polymer* **44**, 1705-1710.

93 Bondzic, S., Polushkin, E., Schouten, A.J., Ikkala, O., ten Brinke, G. (2007). The influence of grain size on the alignment of hexagonally ordered cylinders of self-assembled diblock copolymer-based supramolecules. *Polymer* **48**, 4723-4732.

94 Osuji, C., Zhang, Y., Mao, G., Ober, C.K., Thomas, E.L. (1999). Transverse cylindrical microdomain orientation in an lc diblock copolymer under oscillatory shear. *Macromolecules* **32**, 7703-7706.

95 Osuji, C.O., Chen, J.T., Mao, G., Ober, C.K., Thomas, E.L. (2000). Understanding and controlling the morphology of styrene–isoprene side-group liquid crystalline diblock copolymers. *Polymer* **41**, 8897-8907.

96 Angelescu, D.E., Waller, J.H., Register, R.A., Chaikin, P.M. (2005). Shear-induced alignment in thin films of spherical nanodomains. *Advanced Materials* **17**, 1878-1881.

97 Hong, Y.-R., Adamson, D.H., Chaikin, P.M., Register, R.A. (2009). Shear-induced sphere-to-cylinder transition in diblock copolymer thin films. *Soft Matter* **5**, 1687-1691.

98 Marencic, A.P., Adamson, D.H., Chaikin, P.M., Register, R.A. (2010). Shear alignment and realignment of sphere-forming and cylinder-forming block-copolymer thin films. *Physical Review E* **81**, 011503.

99 Pinna, M., Zvelindovsky, A.V.M., Guo, X., Stokes, C.L. (2011). Diblock copolymer sphere morphology in ultra thin films under shear. *Soft Matter* **7**, 6991-6997.

100 Marencic, A.P., Wu, M.W., Register, R.A., Chaikin, P.M. (2007). Orientational order in sphere-forming block copolymer thin films aligned under shear. *Macromolecules* **40**, 7299-7305.

101 Wu, M.W., Register, R.A., Chaikin, P.M. (2006). Shear alignment of sphere-morphology block copolymer thin films with viscous fluid flow. *Physical Review E* **74**.

102 Zvelindovsky, A.V.M., Sevink, G.J.A. (2003). Sphere morphology of block copolymer systems under shear. *EPL (Europhysics Letters)* **62**, 370.

103 Bang, J., Lodge, T.P. (2003). Mechanisms and epitaxial relationships between close-packed and bcc lattices in block copolymer solutions. *The Journal of Physical Chemistry B* **107**, 12071-12081.

104 Bang, J., Lodge, T.P., Wang, X., Brinker, K.L., Burghardt, W.R. (2002). Thermoreversible, epitaxial fcc↔bcc transitions in block copolymer solutions. *Physical Review Letters* **89**, 215505.

105 Hamley, I.W., Daniel, C., Mingvanish, W., Mai, S.-M., Booth, C., Messe, L., Ryan, A.J. (2000). From hard spheres to soft spheres: The effect of copolymer composition on the structure of micellar cubic phases formed by diblock copolymers in aqueous solution. *Langmuir* **16**, 2508-2514.

106 Park, M.J., Bang, J., Harada, T., Char, K., Lodge, T.P. (2004). Epitaxial transitions among fcc, hcp, bcc, and cylinder phases in a block copolymer solution. *Macromolecules* **37**, 9064-9075.

107 McConnell, G.A., Lin, M.Y., Gast, A.P. (1995). Long range order in polymeric micelles under steady shear. *Macromolecules* **28**, 6754-6764.

108 McConnell, G.A., Gast, A.P., Huang, J.S., Smith, S.D. (1993). Disorder-order transitions in soft sphere polymer micelles. *Physical Review Letters* **71**, 2102-2105.

109 Hamley, I.W., Pople, J.A., Fairclough, J.P.A., Terrill, N.J., Ryan, A.J., Booth, C., Yu, G.-E., Diat, O., Almdal, K., Mortensen, K., Vigild, M. (1998). Effect of shear on cubic phases in gels of a diblock copolymer. *The Journal of Chemical Physics* **108**, 6929-6936.

110 Hanley, K.J., Lodge, T.P., Huang, C.-I. (2000). Phase behavior of a block copolymer in solvents of varying selectivity. *Macromolecules* **33**, 5918-5931.

111 Watzlawek, M., Likos, C.N., Löwen, H. (1999). Phase diagram of star polymer solutions. *Physical Review Letters* **82**, 5289-5292.

112 Makiko, N. (2008). Stability of the fcc structure in block copolymer systems. *Journal of Physics: Condensed Matter* **20**, 465104.

113 Huang, Y.-Y., Chen, H.-L., Hashimoto, T. (2003). Face-centered cubic lattice of spherical micelles in block copolymer/homopolymer blends. *Macromolecules* **36**, 764-770.

114 Huang, Y.-Y., Hsu, J.-Y., Chen, H.-L., Hashimoto, T. (2007). Existence of fcc-packed spherical micelles in diblock copolymer melt. *Macromolecules* **40**, 406-409.

115 Imaizumi, K., Ono, T., Kota, T., Okamoto, S., Sakurai, S. (2003). Transformation of cubic symmetry for spherical microdomains from face-centred to body-centred cubic upon uniaxial elongation in an elastomeric triblock copolymerthis paper was presented at the xiith international conference on small-angle scattering, venice, italy, 25-29 august 2002. *Journal of Applied Crystallography* **36**, 976-981.

116 Kota, T., Imaizumi, K., Sasaki, S., Sakurai, S. (2011). Spontaneous enhancement of packing regularity of spherical microdomains in the body-centered cubic lattice upon uniaxial stretching of elastomeric triblock copolymers. *Polymers (20734360)* **3**, 36-50.

117 Chiefari, J., Chong, Y.K., Ercole, F., Krstina, J., Jeffery, J., Le, T.P.T., Mayadunne, R.T.A., Meijs, G.F., Moad, C.L., Moad, G., Rizzardo, E., Thang, S.H. (1998). Living free-radical polymerization by reversible addition−fragmentation chain transfer: The raft process. *Macromolecules* **31**, 5559-5562.

118 Moad, G., Rizzardo, E., Thang, S.H. (2005). Living radical polymerization by the raft process. *Australian Journal of Chemistry* **58**, 379-410.

119 Germack, D.S., Wooley, K.L. (2007). Raft-based synthesis and characterization of abc versus acb triblock copolymers containing tert-butyl acrylate, isoprene, and styrene blocks. *Macromolecular Chemistry and Physics* **208**, 2481-2491.

120 McCormick, C.L., Sumerlin, B.S., Lokitz, B.S., Stempka, J.E. (2008). Raft-synthesized diblock and triblock copolymers: Thermally-induced supramolecular assembly in aqueous media. *Soft Matter* **4**.

121 Yu, Y., Zhan, X., Zhang, Q., Chen, F. (2011). Synthesis of triblock copolymer having alternating structures and kinetics study on raft-mediated bulk, miniemulsion and seed miniemulsion polymerizations. *Polymer Engineering & Science* **51**, 1041-1050.

122 Strube, O.I., Schmidt-Naake, G. (2009). Synthesis of reactive triblock copolymers via reversible addition-fragmentation chain transfer (raft) polymerization. *Macromolecular Symposia* **275–276**, 13-23.

123 Barner-Kowollik, C., Davis, T.P., Stenzel, M.H. (2006). Synthesis of star polymers using raft polymerization: What is possible? *Australian Journal of Chemistry* **59**, 719-727.

124 Bernard, J., Lortie, F., Fenet, B. (2009). Design of heterocomplementary h-bonding raft agents – towards the generation of supramolecular star polymers. *Macromolecular Rapid Communications* **30**, 83-88.

125 Darcos, V., Dureault, A., Taton, D., Gnanou, Y., Marchand, P., Caminade, A.-M., Majoral, J.-P., Destarac, M., Leising, F. (2004). Synthesis of hybrid dendrimer-star polymers by the raft process. *Chemical Communications*.

126 Mayadunne, R.T.A., Jeffery, J., Moad, G., Rizzardo, E. (2003). Living free radical polymerization with reversible addition−fragmentation chain transfer (raft polymerization): Approaches to star polymers. *Macromolecules* **36**, 1505-1513.

127 Barner, L., Barner-Kowollik, C., Davis, T.P., Stenzel, M.H. (2004). Complex molecular architecture polymers via raft. *Australian Journal of Chemistry* **57**, 19-24.

128 Patton, D.L., Mullings, M., Fulghum, T., Advincula, R.C. (2005). A facile synthesis route to thiol-functionalized α,ω-telechelic polymers via reversible addition fragmentation chain transfer polymerization. *Macromolecules* **38**, 8597-8602.

129 Chong, Y.K., Krstina, J., Le, T.P.T., Moad, G., Postma, A., Rizzardo, E., Thang, S.H. (2003). Thiocarbonylthio compounds [sc(ph)s−r] in free radical polymerization with reversible addition-fragmentation chain transfer (raft polymerization). Role of the free-radical leaving group (r). *Macromolecules* **36**, 2256-2272.

130 Tabuchi, M., Kawauchi, T., Kitayama, T., Hatada, K. (2002). Living polymerization of primary alkyl acrylates with t-butyllithium/bulky aluminum lewis acids. *Polymer* **43**, 7185-7190.

131 Eitouni, H.B., Balsara, N.P. (2007). Thermodynamics of polymer blends. In *Physical Properties of Polymers Handbook, 2nd ed*. Mark, J. E., Ed. Springer, New York, NY.

132 Forster, S., Apostol, L., Bras, W. (2010). Scatter: Software for the analysis of nano- and mesoscale small-angle scattering. *Journal of Applied Crystallography* **43**, 639-646.

133 Förster, S., Timmann, A., Konrad, M., Schellbach, C., Meyer, A., Funari, S.S., Mulvaney, P., Knott, R. (2005). Scattering curves of ordered mesoscopic materials. *The Journal of Physical Chemistry B* **109**, 1347-1360.

134 Bae, S.-k., Lee, S.-Y., Hong, S.C. (2011). Thiol-terminated polystyrene through the reversible addition–fragmentation chain transfer technique for the preparation of gold nanoparticles and their application in organic memory devices. *Reactive and Functional Polymers* **71**, 187-194.

135 Jordan, E.F., Feldeise.Dw, Wrigley, A.N. (1971). Side-chain crystallinity .1. Heats of fusion and melting transitions on selected homopolymers having long side chains. *Journal of Polymer Science Part A-1: Polymer Chemistry* **9**, 1835.

136 O'Leary, K.A., Paul, D.R. (2006). Physical properties of poly(n-alkyl acrylate) copolymers. Part 1. Crystalline/crystalline combinations. *Polymer* **47**, 1226-1244.

137 Jordan, E.F., Artymyshyn, B., Speca, A., Wrigley, A.N. (1971). Side-chain crystallinity. II. Heats of fusion and melting transitions on selected copolymers incorporating n-octadecyl acrylate or vinyl stearate. *Journal of Polymer Science Part A-1: Polymer Chemistry* **9**, 3349-3365.

138 Lin, L.Y., Lee, N.S., Zhu, J., Nyström, A.M., Pochan, D.J., Dorshow, R.B., Wooley, K.L. (2011). Tuning core vs. Shell dimensions to adjust the performance of nanoscopic containers for the loading and release of doxorubicin. *Journal of Controlled Release* **152**, 37-48.

139 Theis, A., Feldermann, A., Charton, N., Davis, T.P., Stenzel, M.H., Barner-Kowollik, C. (2005). Living free radical polymerization (raft) of dodecyl acrylate: Chain length dependent termination, mid-chain radicals and monomer reaction order. *Polymer* **46**, 6797-6809.

140 Lovestead, T.M., Davis, T.P., Stenzel, M.H., Barner-Kowollik, C. (2007). Scope for accessing the chain length dependence of the termination rate coefficient for disparate length radicals in acrylate free radical polymerization. *Macromolecular Symposium* **248**, 82-93.

141 Beers, K.L., Matyjaszewski, K. (2001). The atom transfer radical polymerization of lauryl acrylate. *Journal of Macromolecular Science Pure and Applied Chemistry* **38**, 731-739.

142 O'Leary, K., Paul, D.R. (2004). Copolymers of poly(n-alkyl acrylates): Synthesis, characterization, and monomer reactivity ratios. *Polymer* **45**, 6575-6585.

143 Hsieh, H.W.S., Post, B., Morawetz, H. (1976). A crystallographic study of polymers exhibiting side-chain crystallization. *Journal of Polymer Science: Polymer Physics Edition* **14**, 1241-1255.

144 Legge, T.M., Slark, A.T., Perrier, S. (2007). Novel difunctional reversible addition fragmentation chain transfer (raft) agent for the synthesis of telechelic and aba triblock methacrylate and acrylate copolymers. *Macromolecules* **40**, 2318-2326.

145 Widin, J.M., Schmitt, A.K., Schmitt, A.L., Im, K., Mahanthappa, M.K. (2012). Unexpected consequences of block polydispersity on the self-assembly of aba triblock copolymers. *Journal of the American Chemical Society* **134**, 3834-3844.

146 Fetters, L.J., Lohse, D.J., Milner, S.T., Graessley, W.W. (1999). Packing length influence in linear polymer melts on the entanglement, critical, and reptation molecular weights. *Macromolecules* **32**, 6847-6851.

147 Roovers, J., Toporowski, P.M. (1990). Charcteristic ratio and plateau modulus of 1,2-polybutadiene-a comparison with other rubbers. *Rubber Chemistry and Technology* **63**, 734-746.

148 Gotro, J.T., Graessley, W.W. (1984). Model hydrocarbon polymers: Rheological properties of linear polyisoprenes and hydrogenated polyisoprenes. *Macromolecules* **17**, 2767-2775.

149 Tong, J.D., Leclère, P., Doneux, C., Brédas, J.L., Lazzaroni, R., Jérôme, R. (2001). Morphology and mechanical properties of poly(methylmethacrylate)-b-poly(alkylacrylate)-b-poly(methylmethacrylate). *Polymer* **42**, 3503-3514.

150 Tong, J.D., Jerôme, R. (2000). Synthesis of poly(methyl methacrylate)-b-poly(n-butyl acrylate)-b-poly(methyl methacrylate) triblocks and their potential as thermoplastic elastomers. *Polymer* **41**, 2499-2510.

151 Zhu, S., Paul, D.R. (2002). Binary interaction energy densities for blends of styrene/acrylonitrile copolymers with methyl methacrylate/n-alkyl acrylate copolymers. *Macromolecules* **35**, 8227-8238.

152 Chu, J.H., Paul, D.R. (1999). Interaction energies for blends of san with methyl methacrylate copolymers with ethyl acrylate and n-butyl acrylate. *Polymer* **40**, 2687-2698.

153 Men'shikov, E.A., Bol'shakova, A.V., Yaminskii, I.V. (2009). Determination of the flory-huggins parameter for a pair of polymer units from afm data for thin films of block copolymers. *Protection of Metals and Physical Chemistry of Surfaces* **45**, 295-299.

154 Somani, R.H., Shaw, M.T. (1981). Miscibility of acrylic polymers in polystyrene by melt titration. *Macromolecules* **14**, 1549-1554.

155 Sperling, L.H., Widmaier, J.M. (1983). A survey of dual phase continuity and miscibility in interpenetrating polymer networks, making use of selective decrosslinking and dissolution of one component: Poly(n-butyl acrylate)/polystyrene. *Polymer Engineering & Science* **23**, 693-696.

156 Callaghan, T.A., Paul, D.R. (1993). Interaction energies for blends of poly(methyl methacrylate), polystyrene, and poly(.Alpha.-methylstyrene) by the critical molecular weight method. *Macromolecules* **26**, 2439-2450.

157 Kressler, J., Higashida, N., Shimomai, K., Inoue, T., Ougizawa, T. (1994). Temperature dependence of the interaction parameter between polystyrene and poly(methyl methacrylate). *Macromolecules* **27**, 2448-2453.

158 Sato, T., Ikeda, M., Sugawara, A. (2004). Effect of monomer sequence on miscibility in statistical copolymer blends and estimation of segmental χ parameters from their miscibility. *Polymer International* **53**, 951-958.

159 Hammouda, B., Bauer, B.J., Russell, T.P. (1994). Small-angle neutron scattering from deuterated polystyrene/poly(butyl methacrylate) homopolymer blend mixtures. *Macromolecules* **27**, 2357-2359.

160 Russell, T.P., Hjelm, R.P., Seeger, P.A. (1990). Temperature dependence of the interaction parameter of polystyrene and poly(methyl methacrylate). *Macromolecules* **23**, 890-893.

161 Schubert, D.W., Abetz, V., Stamm, M., Hack, T., Siol, W. (1995). Composition and temperature dependence of the segmental interaction parameter in statistical copolymer/homopolymer blends. *Macromolecules* **28**, 2519-2525.

162 Siqueira, D.F., Schubert, D.W., Erb, V., Stamm, M., Amato, J.P. (1995). Interface thickness of the incompatible polymer system ps/pnbma as measured by neutron reflectometry and ellipsometry. *Colloid and Polymer Science* **273**, 1041-1048.

163 Fukuda, T., Inagaki, H. (1983). Interactions between unlike polymers versus dilute solution properties of copolymers. *Pure and Applied Chemistry* **55**, 1541-1551.

164 Durant, Y.G., Sundberg, D.C., Guillot, J. (1994). A comparison of methods for the estimation of polymer monomer interaction parameters - the polystyrene n-butyl methacrylate system. *Journal of Applied Polymer Science* **52**, 1823-1832.

165 Ahmadi, A., Freire, J.J. (2009). Molecular dynamics simulation of miscibility in several polymer blends. *Polymer* **50**, 4973-4978.

166 Mu, D., Li, J.Q., Zhou, Y.H. (2011). Modeling and analysis of the compatibility of polystyrene/poly(methyl methacrylate) blends with four inducing effects. *Journal of Molecular Modeling* **17**, 607-619.

167 Lewin, J.L., Maerzke, K.A., Schultz, N.E., Ross, R.B., Siepmann, J.I. (2010). Prediction of hildebrand solubility parameters of acrylate and methacrylate monomers and their mixtures by molecular simulation. *Journal of Applied Polymer Science* **116**, 1-9.

168 Quach, A., Simha, R. (1971). Pressure-volume-temperature properties and transitions of amorphous polymers: Polystyrene and poly (orthomethylstyrene). *Journal of Applied Physics* **42**, 4592-4606.

169 Rogers, S., Mandelkern, L. (1957). Glass transitions of the poly(n-alkyl methacrylates). *The Journal of Physical Chemistry* **61**, 985-991.

170 Lynd, N.A., Hillmyer, M.A. (2007). Effects of polydispersity on the order−disorder transition in block copolymer melts. *Macromolecules* **40**, 8050-8055.

171 Pandav, G., Ganesan, V. (2013). Fluctuation effects on the order-disorder transition in polydisperse copolymer melts. *The Journal of Chemical Physics* **139**, -.

172 Matsen, M.W. (2013). Comparison of a-block polydispersity effects on bab triblock and ab diblock copolymer melts. *The European Physical Journal E* **36**, 1-7.

173 Widin, J.M., Schmitt, A.K., Im, K., Schmitt, A.L., Mahanthappa, M.K. (2010). Polydispersity-induced stabilization of a disordered bicontinuous morphology in aba triblock copolymers. *Macromolecules* **43**, 7913-7915.

174 Beardsley, T.M., Matsen, M.W. (2011). Monte carlo phase diagram for a polydisperse diblock copolymer melt. *Macromolecules* **44**, 6209-6219.

175 Van Krevelen, D.W., Te Nijenhuis, K. (2009). Chapter 7 - cohesive properties and solubility. In *Properties of polymers (fourth edition)* (by, D.W.V.K., Nijenhuis, K.T., eds), pp. 189-227. Elsevier, Amsterdam.

176 D'Amelia, R.P., Tomic, J.C., Nirode, W.F. (2014). The determination of the solubility parameter (δ) and the mark-houwink constants (k &α) of food grade polyvinyl acetate (pvac). *Journal of Polymer and Biopolymer Physics Chemistry* **2**, 67-72.

177 Liu, Y., Shi, B.L. (2008). Determination of flory interaction parameters between polyimide and organic solvents by hsp theory and igc. *Polymer Bulletin* **61**, 501-509.

178 Bordes, C., Freville, V., Ruffin, E., Marote, P., Gauvrit, J.Y., Briancon, S., Lanteri, P. (2010). Determination of poly(epsilon-caprolactone) solubility parameters: Application to solvent substitution in a microencapsulation process. *International Journal of Pharmaceutics* **383**, 236-243.

179 Graessley, W.W., Krishnamoorti, R., Balsara, N.P., Fetters, L.J., Lohse, D.J., Schulz, D.N., Sissano, J.A. (1994). Deuteration effects and solubility parameter ordering in blends of saturated hydrocarbon polymers. *Macromolecules* **27**, 2574-2579.

180 Kim, S.D., Chakravarti, S., Tian, J., Bell, P. (2010). The phase behavior and the flory–huggins interaction parameter of blends containing amorphous poly(resorcinol phthalate-block-carbonate), poly(bisphenol-a carbonate) and poly(ethylene terephthalate). *Polymer* **51**, 2199-2206.

181 Cochran, E.W., Bates, F.S. (2002). Thermodynamic behavior of poly(cyclohexylethylene) in polyolefin diblock copolymers. *Macromolecules* **35**, 7368-7374.

182 Graessley, W.W., Krishnamoorti, R., Reichart, G.C., Balsara, N.P., Fetters, L.J., Lohse, D.J. (1995). Regular and irregular mixing in blends of saturated hydrocarbon polymers. *Macromolecules* **28**, 1260-1270.

183 Krishnamoorti, R., Graessley, W.W., Fetters, L.J., Garner, R.T., Lohse, D.J. (1995). Anomalous mixing behavior of polyisobutylene with other polyolefins. *Macromolecules* **28**, 1252-1259.

184 Helfand, E. (1975). Theory of inhomogeneous polymers: Fundamentals of the gaussian random- walk model. *The Journal of Chemical Physics* **62**, 999-1005.

185 Evers, O.A., Scheutjens, J.M.H.M., Fleer, G.J. (1990). Statistical thermodynamics of block copolymer adsorption. 1. Formulation of the model and results for the adsorbed layer structure. *Macromolecules* **23**, 5221-5233.

186 Matsen, M.W. (2002). The standard gaussian model for block copolymer melts. *Journal of Physics: Condensed Matter* **14**, R21.

187 Taheri, S.M., Rosenfeldt, S., Fischer, S., Bosecke, P., Narayanan, T., Lindner, P., Forster, S. (2013). Shear-induced macroscopic "siamese" twins in soft colloidal crystals. *Soft Matter* **9**, 8464-8475.